



# Balkan Journal of Electrical & Computer Engineering

An International Peer Reviewed, Referred, Indexed and Open Access Journal

[www.bajece.com](http://www.bajece.com)

Vol : 6  
No : 4  
Year : 2018  
ISSN : 2147 - 284X



It is abstracted and indexed in, Index Google Scholarship, the PSCR, Cross ref, DOAJ, Research Bible, Indian Open Access Journals (OAJ), Institutional Repositories (IR), J-Gate (Informatics India), Ulrich's, International Society of Universal Research in Sciences, DRJI, EyeSource, Cosmos Impact Factor, Cite Factor, SIS Scientific Indexing Service, IJIF, iiiiFactor. ULAKBİM-TR Dizin.

**General Publication Director & Editor-in-Chief**  
Musa Yılmaz, Batman University, Turkey.

**Vice Editor**  
Hamidreza Nazarpouya, University of California Riverside, USA

**Scientific Committee**  
Abhishek Shukla (India)  
Abraham Lomi (Indonesia)  
Aleksandar Georgiev (Bulgaria)  
Arunas Lipnickas (Lithuania)  
Audrius Senulis (Lithuania)  
Belle R. Upadhyaya (USA)  
Brijender Kahanwal (India)  
Chandar Kumar Chanda (India)  
Daniela Dzhonova-Atanasova (Bulgaria)  
Deris Stiawan (Indonesia)  
Emel Onal (Turkey)  
Emine Ayaz (Turkey)  
Enver Hatimi (Kosovo)  
Ferhat Sahin (USA)  
Gursel Alici (Australia)  
Hakan Temeltaş (Turkey)  
Ibrahim Akduman (Turkey)  
Jan Izykowski (Poland)  
Javier Bilbao Landatxe (Spain)  
Jelena Dikun (Lithuania)  
Karol Kyslan (Slovakia)  
Kunihiko Nabeshima (Japan)  
Lambros Ekonomou (Greece)  
Lazhar Rahmani (Algerie)  
Marcel Istrate (Romania)  
Marija Eidukeviciute (Lithuania)  
Milena Lazarova (Bulgaria)  
Muhammad Hadi (Australia)  
Muhamed Turkanović (Slovenia)  
Mourad Houabes (Algerie)  
Murari Mohan Saha (Sweden)  
Nick Papanikolaou (Greece)  
Okyay Kaynak (Turkey)  
Osman Nuri Ucan (Turkey)  
Ozgur E. Mustecaplioglu (Turkey)  
Padmanaban Sanjeevikumar (India)  
Ramazan Caglar (Turkey)  
Rumen Popov (Bulgaria)  
Tarek Bouktir (Algeria)  
Sead Berberovic (Croatia)  
Seta Bogosyan (USA)  
Savvas G. Vassiliadis (Greece)  
Suwarno (Indonesia)  
Tulay Adali (USA)  
Yogeshwarsing Calleecharan (Mauritius)  
YangQuan Chen (USA)  
Youcef Soufi (Algeria)

#### **Aim & Scope**

The journal publishes original papers in the extensive field of Electrical-Electronics and Computer engineering. It accepts contributions which are fundamental for the development of electrical engineering, computer engineering and its applications, including overlaps to physics. Manuscripts on both theoretical and experimental work are welcome. Review articles and letters to the editors are also included.

Application areas include (but are not limited to): Electrical & Electronics Engineering, Computer Engineering, Software Engineering, Biomedical Engineering, Electrical Power Engineering, Control Engineering, Signal and Image Processing, Communications & Networking, Sensors, Actuators, Remote Sensing, Consumer Electronics, Fiber-Optics, Radar and Sonar Systems, Artificial Intelligence and its applications, Expert Systems, Medical Imaging, Biomedical Analysis and its applications, Computer Vision, Pattern Recognition, Robotics, Industrial Automation.



ISSN: 2147- 284X  
Vol: 6  
No : 4  
Year: October 2018

#### **CONTENTS**

- A. Dumlu and M. R. Yildirim;** Real-Time Implementation of Continuous Model Based Sliding Mode Control Technique for Trajectory Tracking Control of Mobile Robot. ....**211-216**
- A. Askarova, S. Bolegenova, V. Maximov, S.Bolegenova, Z. Gabitova, A. Yergaliyeva, A. Nugymanova, M. Beketayeva, Sh. Ospanova;** Application of Overfire Air Technology on an Example of a Steam Boiler PK-39 of the Aksu TPP (Kazakhstan), ..... **217-223**
- B. B. Alagoz, H. Alisoy;** Estimation of Reduced Order Equivalent Circuit Model Parameters of Batteries from Noisy Current and Voltage Measurements, ..... **224-231**
- A. Mukhamedgali and Z. B. Rakisheva;** Design and Simulation of Uniform Magnetic Field, ..... **232-236**
- İ.Kiyak;** Harmonic Analysis of Electrospindle System with Wavelet Packet Transform, ..... **237-241**
- G. B. Nurpeissova, D. V. Panyukova, and A. T. Nurpeissov;** Smart Techniques' Implementation for Small Entities and Central Power Grid in Almaty, Kazakhstan: Challenges and Possibilities, ..... **242-246**
- N. Onat;** Trends in Power System Protection Researches: A Review of Fundamental Relays, ..... **247-256**
- N. S. Doszhan, G.E. Ibrayev and R.R. Pilpani;** Ultra-High Accurate Attitude Determination and Control of Microsatellite Formation Flight, ..... **257-261**
- S. B. Efe, B. Kocaman and D. Demir Aktas;** Implementation and Performance Analysis of a Switched Reluctance Motor Fed from Non-Energy Stored PV System, ..... **262-265**
- O. Aydin, B. Samanci and S. Ozoguz;** Characterization and Measurement of Cable Losses Using Fractional-order Circuit Model, ..... **266-270**

**BALKAN  
JOURNAL OF  
ELECTRICAL & COMPUTER ENGINEERING**  
(An International Peer Reviewed, Indexed and Open Access Journal)

**Contact**  
Batman University  
Department of Electrical-Electronics Engineering  
Bati Raman Campus Batman-Turkey

**Web:** <http://dergipark.gov.tr/bajece>  
<https://www.bajece.com>  
**e-mail:** [bajece@hotmail.com](mailto:bajece@hotmail.com)

# Real-Time Implementation of Continuous Model Based Sliding Mode Control Technique for Trajectory Tracking Control of Mobile Robot

A. Dumlu, and M. R. Yildirim

**Abstract**—In this study, real-time trajectory tracking control of an autonomous mobile robot has been designed, analyzed and studied. Two control techniques such as the proportional–integral–derivative (PID) control and model based sliding mode control (SMC) have been considered to increase the tracking performance of the mobile robot. Firstly, kinematic and dynamic analysis of the system have been obtained and then this dynamic model has been used for proposed sliding mode controller in order to increase trajectory tracking performance of the system. The experimental outcomes strongly verified that the proposed controller gives a quite well trajectory tracking response and smaller magnitude overshoot compared with the classical PID controller.

**Index Terms**—PID control, Robot control, Sliding mode control, Trajectory control.

## I. INTRODUCTION

THE PURPOSE of robotic systems used in today's modern industrial world is to improve the quality of products, industrial productivity, correctness, speed and flexibility. Although the requirements of industrial applications are complex and difficult, robotic systems are increasingly being used more and more in dangerous, tedious or repetitive industrial processes, where people do not want to work. More efficient and quality manufacturing is an important issue of the industry, and this demand has led to the development of more skilled and modern robotic systems. These skilled systems are usually autonomous and therefore require initial actions, such as calibration, trajectory planning in order to fulfill their assigned tasks. For this reason, it is a very important step to accurately and precisely control the system in the working environment in order to be able to fulfill the assigned tasks successfully.

**A. DUMLU**, is with Department of Electrical Engineering University of Erzurum Technical University, Erzurum, Turkey, (e-mail: [ahmetdumlu@erzurum.edu.tr](mailto:ahmetdumlu@erzurum.edu.tr)).

**M. R. YILDIRIM**, is with Company of Turk Telekom, Erzurum, Turkey, (e-mail: [mehmetrasimyildirim@gmail.com](mailto:mehmetrasimyildirim@gmail.com) ).

Manuscript received September 13, 2018; accepted October 24, 2018.  
DOI: [10.17694/bajece.459568](https://doi.org/10.17694/bajece.459568)

The main areas of research in the field of robotics systems can be summarized as system design, trajectory planning, trajectory optimization, and motion control.

Among these scientific research areas, the control of robotic systems has a crucial place to follow a precise and reliable trajectory between the initial and final position of the robot [1]. Accurate trajectory control is vital issue for the efficient operation of a given robotic application. For this reason, a large number of control methods have been applied in the literature for various types of robotic systems, such as, H infinity control [2], neural network control [3], [4], adaptive fuzzy control [5], [6] and fractional order control [7-9].

Another robust control technique used for trajectory tracking control of nonlinear system in literature is SMC method. SMC method is an effective and robust control technique and has a variable structure for the unknown dynamics of unknown loads and nonlinear systems. This control method is also used to simplify design, increase the trajectory tracking accuracy and reduce the model complexity [10]. The SMC technique provides a systematic approach that improves the system capability to eliminate the problem of stability preservation [11]. Therefore, due to the characteristics of the sliding mode controller, many researchers have used this control method to overcome the control problem in their systems [12-18].

In this study, a model based sliding mode control method is used for an autonomous mobile in order to get accurate trajectory tracking control approach. Motivated by the advantages of the SMC method, a model based sliding mode control method is proposed and performed on a real mobile robot. In order to illustrate the efficiency of SMC, the real time studies have been realized and compared to the classical PID controller. The main contributions of this study are given as follows; Model based sliding mode controller (SMC) is developed to obtain strong robustness, fast finite-time convergence, precision, and chatter-free control. SMC is utilized to compensate the unknown system dynamics where no knowledge relating to the nonlinear model is available a priori.

The rest of the paper is organized as follows. Section II presents system description of the mobile robot. The model based SMC method for the mobile robot has shown in section III. In section IV, the experimental outcomes have been demonstrated, followed by the conclusion in Section V.

## II. SYSTEM DESCRIPTION

Figure 1 shows the designed mobile robot. For the prototype design, only the outer casing and motors of the unmanned vehicle named KOBUKI produced by Turlebot firm were utilized. Instead of the control card, drives, sensors and software used by TurleBot, a unique design has been implemented in this work.

The system has two rear driving wheels and two free caster front wheels. Each driving wheel has been coupled to the shaft of the DC motor and each DC motor is fitted with gearhead and optical encoder. The power for the system is supplied by two 12 V batteries. Moreover, the system has a personal computer with a controller board for real time applications.



Fig.1. Designed mobile robot

### A. Inverse kinematic of mobile robot

For the mobile robot, inverse kinematics refers to the use of the kinematics equations of the system to determine the angular velocity of the left and the right wheels that provided the desired position or velocity of the wheelchair. Schematic top view of the mobile robot is shown in Fig. (2). The motion and the orientation of the wheelchair are achieved by independent actuators of the left and right wheels, and each wheel is independent and driven by a DC motor.

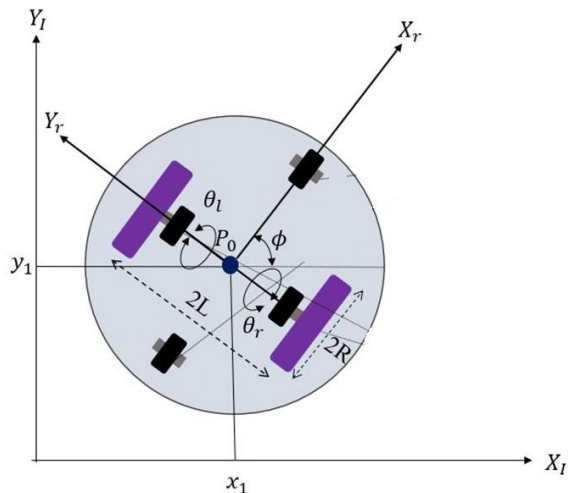


Fig.2. Schematic top view of the mobile robot

For the purpose of analysis, two coordinate systems are defined. The global coordinate system  $\{X_I, Y_I\}$  is fixed to the Cartesian workspace and the local coordinate system  $\{X_r, Y_r\}$  is attached to the base of mobile robot platform. The origin of the platform frame is defined to be the midpoint  $P_0$  on the axis between the wheels. The angular positions of the right and left wheel are given by  $\theta_r$  and  $\theta_l$ , respectively. The position of any point in the mobile robot can be defined using the transformation of the local coordinate system to the global coordinate system as follows;

$$X^I = R(\phi)X^r \quad (1)$$

where  $R(\phi)$  is the orthogonal rotation matrix;

$$R(\phi) = \begin{bmatrix} \cos(\phi) & -\sin(\phi) & 0 \\ \sin(\phi) & \cos(\phi) & 0 \\ 0 & 0 & 1 \end{bmatrix} \quad (2)$$

On the conditions of no lateral slip motion, we can write the following kinematic equations in velocity dimension and mobile robot frame;

$$v = \frac{v_r + v_l}{2} = R \frac{(\dot{\theta}_r + \dot{\theta}_l)}{2} \quad (3)$$

and the angular velocity of the mobile robot is;

$$\dot{\phi} = \frac{v_r - v_l}{2L} = R \frac{(\dot{\theta}_r - \dot{\theta}_l)}{2} \quad (4)$$

On the other hand, using the orthogonal rotation matrix mobile robot velocities can be obtained from the global coordinate system as follows;

$$\begin{bmatrix} \dot{x}_1 \\ \dot{x}_2 \\ \dot{\phi} \end{bmatrix} = \begin{bmatrix} \frac{R}{2} \cos(\phi) & \frac{R}{2} \cos(\phi) \\ \frac{R}{2} \sin(\phi) & \frac{R}{2} \sin(\phi) \\ \frac{R}{2L} & -\frac{R}{2L} \end{bmatrix} \begin{bmatrix} \dot{\theta}_r \\ \dot{\theta}_l \end{bmatrix} \quad (5)$$

### B. Constraint equations of mobile robot

The mobile robot is a class of benchmark non-holonomic system due to its kinematic constraints. The two main non-holonomic constraint equations related to generalized coordinates are obtained from the two main assumptions and choosing two redundant coordinates,  $x_1, x_2$  and two generalized coordinates,  $\theta_r, \theta_l$ . The first assumption is that mobile robot cannot move in a lateral direction. This means that in the robot frame, the velocity of the centre point  $P_0$  is zero along the lateral axis namely  $\dot{y}_r = 0$ . Using the orthogonal rotation matrix  $R(\phi)$ , the first non-holonomic constraint equations related to velocity in the global coordinate system gives;

$$\dot{x}_2 \cos(\phi) - \dot{x}_1 \sin(\phi) = 0 \quad (6)$$

The second assumption is that the two driving wheels pure rolling constraint. This means that each wheel maintains a one contact point  $P$  with the ground as shown in Fig. (3).

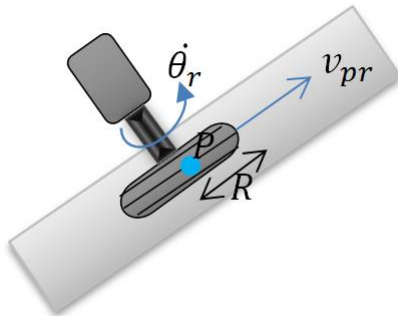


Fig.3. Pure rolling motion constraint

Using the rotation matrix  $R(\phi)$ , the rolling constraint equations are formulated as follows;

$$\dot{x}_1 \cos(\phi) + \dot{x}_2 \sin(\phi) + L\dot{\phi} = R\dot{\theta}_r \quad (7)$$

$$\dot{x}_1 \cos(\phi) + \dot{x}_2 \sin(\phi) - L\dot{\phi} = R\dot{\theta}_l \quad (8)$$

On the other hand, the mobile robot has a one holonomic constraint equation and to obtain it, first of all we subtract Eq. (7) from Eq. (8) and then integrating with choosing the initial condition;

$$2L\dot{\phi} = R(\dot{\theta}_r - \dot{\theta}_l) \quad (9)$$

$$\phi = c(\theta_r - \theta_l) \quad (10)$$

where  $c$  is equal to  $R/2L$ . For the obtain second non-holonomic constraint equations now we add the Eq. (7) and Eq. (8);

$$\dot{x}_1 \cos(\phi) + \dot{x}_2 \sin(\phi) = cL(\dot{\theta}_r + \dot{\theta}_l) \quad (11)$$

Hence we may write two non-holonomic constraint equations in matrix form;

$$A(q)\dot{q} = 0 \quad (12)$$

where;

$$q = \begin{bmatrix} q_1 \\ q_2 \\ q_3 \\ q_4 \end{bmatrix} = \begin{bmatrix} x_1 \\ x_2 \\ \theta_r \\ \theta_l \end{bmatrix}, A(q) = \begin{bmatrix} a_{11} & a_{12} & a_{13} & a_{14} \\ a_{21} & a_{22} & a_{23} & a_{24} \end{bmatrix} \quad (13)$$

$$= \begin{bmatrix} -\sin(\phi) & \cos(\phi) & 0 & 0 \\ -\cos(\phi) & -\sin(\phi) & cL & cL \end{bmatrix}$$

### C. Dynamic modelling of the mobile robot

The complete dynamic model of the mobile robot which describe the actuating motor torques are derived using Lagrangian approach. The first type of Lagrange's equations will be employed by using the generalized coordinates as  $q = [x_1, x_2, \theta_r, \theta_l]^T$ . For the examined robotic system case, the

Lagrangian equations of the first type can be written as given in Eq. 14.

$$\frac{d}{dt} \left( \frac{\partial L}{\partial \dot{q}_i} \right) - \frac{\partial L}{\partial q_i} = Q_i - a_{1i}\lambda_1 - a_{2i}\lambda_2 \quad \text{for } i = 1 \text{ to } 4 \quad (14)$$

where  $Q_i$  denotes the external Lagrange force,  $\lambda_1$  and  $\lambda_2$  are the Lagrangian multipliers and  $L$  is the Lagrangian function.

The total kinetic energy of the mobile robot platform and two wheels can be denoted as follows;

$$K = \frac{1}{2}(m_c + 2m_w)(\dot{x}_1^2 + \dot{x}_2^2) + m_c cL(\dot{\theta}_r - \dot{\theta}_l)(\dot{x}_2 \cos(\phi) - \dot{x}_1 \sin(\phi)) + \frac{1}{2}I_w(\dot{\theta}_r^2 + \dot{\theta}_l^2) + \frac{1}{2}(I_c + 2m_w L^2 + 2I_m)c^2(\dot{\theta}_r - \dot{\theta}_l)^2 \quad (15)$$

where,  $m_c$  is the mass of the mobile robot without the driving wheels and actuators (DC motors),  $m_w$  is the mass of each driving wheel (with actuator),  $I_c$  is the moment of inertia of the mobile robot about the vertical axis through the centre of mass,  $I_w$  is the moment of inertia of each driving wheel with a motor about the wheel axis, and  $I_m$  is the moment of inertia of each driving wheel with a motor about the wheel diameter. Using Eq. (15) along with the Lagrangian function,  $L = K$  the equations of motion of the mobile robot are given by;

$$(m_c + 2m_w)\ddot{x}_1 - m_c d(\ddot{\phi} \sin\phi + \dot{\phi}^2 \cos\phi) = \lambda_1 \sin\phi + \lambda_2 \cos\phi \quad (16)$$

$$(m_c + 2m_w)\ddot{x}_2 + m_c d(\ddot{\phi} \cos\phi - \dot{\phi}^2 \sin\phi) = -\lambda_1 \cos\phi + \lambda_2 \sin\phi \quad (17)$$

$$m_c c d(\ddot{x}_2 \cos\phi - \ddot{x}_1 \sin\phi) + (I_c + 2m_w L^2 + 2I_m)c^2 + I_w \ddot{\theta}_r - (I_c + 2m_w L^2 + 2I_m)c^2 \ddot{\theta}_l = \tau_1 - cL\lambda_2 \quad (18)$$

$$-m_c c d(\ddot{x}_2 \cos\phi - \ddot{x}_1 \sin\phi) - (I_c + 2m_w L^2 + 2I_m)c^2 \ddot{\theta}_r - (I_c + 2m_w L^2 + 2I_m)c^2 \ddot{\theta}_l = \tau_2 - cL\lambda_2 \quad (19)$$

Hence the actuator torques acting on the two wheels of mobile robot can be determined in the standard form as;

$$M(q)\ddot{q} + C(q, \dot{q})\dot{q} = E(q)\tau - A^T(q)\lambda \quad (20)$$

On the other hand, the system described by Eq. (20) is transformed into a state space representation which is more useful for the model based sliding mode control. For this purpose, a  $4 \times 2$   $S(q)$  matrix can be defined as shown in Eq. (21) and its columns are in the null space of  $A(q)$  matrix in the two non-holonomic constraint equations i.e.,  $A(q)S(q) = 0$ .

$$S(q) = \begin{bmatrix} cL\cos\phi & cL\cos\phi \\ cL\sin\phi & cL\sin\phi \\ 1 & 0 \\ 0 & 1 \end{bmatrix} \quad (21)$$

From the two non-holonomic constraint equations, the velocity  $\dot{q}$  must be in the null space of  $A(q)$ . Consequently a reduced smooth vector  $\eta = [\eta_1 \ \eta_2]^T$  can be defined with mathematical relation form in Eq. (22).

$$\dot{q} = S(q)\eta, \quad \ddot{q} = \dot{S}(q)\eta + S(q)\dot{\eta} \quad (22)$$

It's obviously the fact that, for the specific choice of  $S(q)$  matrix in Eq. (22), smooth vector  $\eta$  can be equal to two wheel velocities vector i.e.,  $\eta = \dot{\theta} = [\dot{\theta}_r \ \dot{\theta}_l]$ . To eliminate the constraint term  $A^T(q)\lambda$  in Eq. (20), this equation's both sides must multiply by  $S^T(q)$  matrix. Hence the new model can be written as follow;

$$S^T(q)M(q)\ddot{q} + S^T(q)C(q, \dot{q}) = \tau \quad (23)$$

Eq. (23) can be rewritten as in the standard form;

$$\tau = M(q)\ddot{q} + N(q, \dot{q}) + \tau_d \quad (24)$$

where,  $M(q)$  is the mass matrix,  $N(q, \dot{q})$  is the sum of the centrifugal, Coriolis and gravity terms,  $\tau_d$  is disturbance and friction component of directly related to mobile robot system using a complete dynamic model of systems, respectively. On the other hand Eq. (24) shows that the mobile robot dynamics are expressed as a function of the right and left wheel angular velocities  $\dot{\theta} = [\dot{\theta}_r \ \dot{\theta}_l]$ , and the driving motor torques  $\tau = [\tau_r \ \tau_l]^T$ . As it is seen from Eq. (24), the desired tracking control of the mobile robot can be achieved by changing or controlling the supply voltage of the DC motors.

If the both sides of Eq. 24 is multiplied by  $M(q)^{-1}$ ,  $\ddot{q}$  can be defined as follows;

$$\ddot{q}_{4x1} = f(q)_{4x1} + g(q)_{4x1}u(t)_{4x1} + \zeta(t, u(t))_{4x1} \quad (25)$$

where,  $f(q)_{4x1} = -M(q)^{-1}H(q, \dot{q})$ ,  $g(q)_{4x1} = M(q)^{-1}$ ,  $u(t)_{4x1} = \tau$  and  $\zeta(t, u(t))_{4x1}$  stands the bounded uncertainties of the system. The aim of the proposed control technique in this study is to control the system variables,  $q_{4x1}$ , accurately for the given reference trajectory,  $q_{d4x1}$ . In order to meet the accurate trajectory tracking, the tracking error  $e(t)_{4x1} = q_{d4x1} - q_{4x1}$  should be minimized as much as possible.

### III. MODEL BASED SLIDING MODE CONTROL TECHNIQUE

The model based sliding mode control method is a variable structure control and it has a robust structure against the uncertainties in the system and disturbance effects. The control signal used in the sliding mode control method consists of two components. The first component is the equivalent control component and it can be obtained using a sliding surface function with an approximate model of the system. The second

component is a switched control component it can be used to compensate the uncertainties affecting the system.

In this proposed method, a sliding surface  $s$  is selected as follows;

$$s = \lambda e + \dot{e} \quad (26)$$

where,  $\lambda$  is a positive constant matrix,  $e$  is a tracking error matrix and it can be given as  $e = [q_d - q]$ . Differentiating Eq. (26) with respect to time, the following equation is obtained

$$\dot{s} = \lambda \dot{e} + \ddot{e} \quad (27)$$

This can be further written as;

$$\dot{s} = \lambda \dot{e} + (\ddot{q}_d - \ddot{q}) \quad (28)$$

Substituting  $\ddot{q}$  from Eq. (25) into Eq. (28) yields;

$$\dot{s} = \lambda \dot{e} + \ddot{q}_d - f(q) - g(q)u \quad (29)$$

It is well known that, in the second order sliding surface condition, if,  $s(t)$  and  $\dot{s}(t)$  equal to null then the tracking error  $e$  reaches to zero. Hence, the reaching phase control law  $u_{eq}$  can be obtained by using the  $\dot{s}(t) = 0$  as follows;

$$u_{eq} = \frac{-f(q)}{g(q)} + \frac{\lambda \dot{e}}{g(q)} + \frac{\ddot{q}_d}{g(q)} \quad (30)$$

In addition to this, it is not appropriate to use only the reaching phase control law to control the system. As mentioned above, the effect of the uncertainties which are constrained but unknown, can be serious for system. Therefore, a switching control law,  $u_{sc}$ , in Eq. (31), should be added to control signal to ensure the robustness of system against the external or system disturbances.

$$u_{sc} = k_x \text{sgn}(s) \quad (31)$$

where,  $k_x$  is the switching gain matrix and  $\text{sgn}(s)$  can be expressed given as below.

$$\text{sgn}(s) = \begin{cases} 1 & \rightarrow s > 0 \\ 0 & \rightarrow s = 0 \\ -1 & \rightarrow s < 0 \end{cases} \quad (32)$$

Thus, the total feedback SMC control law ( $u$ ) for the system is written as follows;

$$u = u_{eq} + u_{sc} = \frac{-f(q)}{g(q)} + \frac{\lambda \dot{e}}{g(q)} + \frac{\ddot{q}_d}{g(q)} + k_x \text{sgn}(s) \quad (33)$$

Practically, the control law given in Eq. (33) can caused oscillations which is called chattering factor. To overcome the control-chattering during the implementation, the  $\text{sgn}$  (high-frequency switching function), can be approximated to the  $\text{sat}$  function, which is called the smooth limited function. The

model based SMC implementation block diagram is shown in Fig. (4).

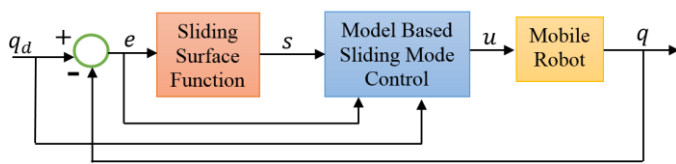


Fig.4. The block diagram of model based SMC

IV. EXPERIMENTAL RESULTS AND DISCUSSIONS

After modelling the wheeled mobile robot and the proposed SMC controllers, this test platform has simulated experimentally through two different case studies to verify the effectiveness and performance of the proposed methodology with respect to the classical PID control for given task. The controllers have been performed using SIMULINK 2014 from MathWorks. The Q8 USB data acquisition device from Quanser has been used to execute the experiments. In experimental study, the sampling time has been adjusted in 0.001 sec. The controller parameters have been adjust as  $k_p = 6, k_i = 2, k_d = 0,2$  and  $\lambda = 48,8664, k_x = 214$  for PID and sliding mode control, respectively.

The controller's performance is tested in the first experiment with an eight shape reference with radius  $R = 1\ m$  given by Eq. (34). Since this defined trajectory contains mathematically trigonometric functions, it is necessary for the mobile robot to keep pace with suddenly changing angular speed changes of the right and left wheels of the vehicle in order to be able to track this trajectory.

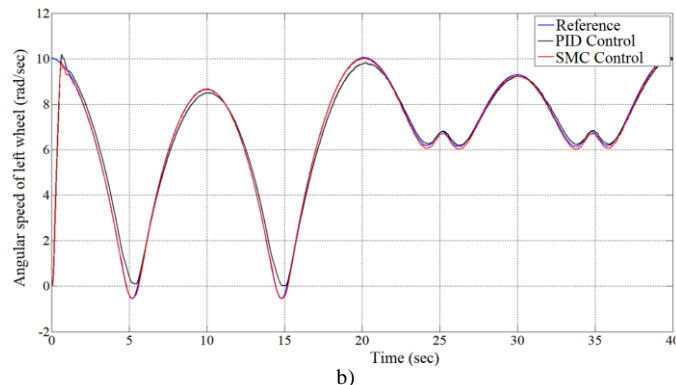
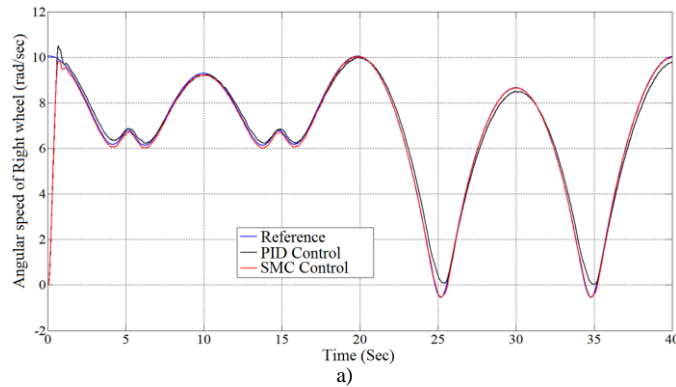


Fig.5. Trajectory tracking responses of right and left wheels

$$x_r = R * \sin\left(2 * \frac{\pi}{20} * t\right), y_r = R * \sin\left(\frac{\pi}{20} * t\right), \quad (34)$$

Using the kinematic equations obtained in Section II, the angular velocity changes that should be realized by the right and left wheels for mobile robot to follow this defined trajectory and the performances of the PID and SMC controllers have been shown in Fig. (5). And also, Fig. (6) presents the tracking errors of the both controllers.

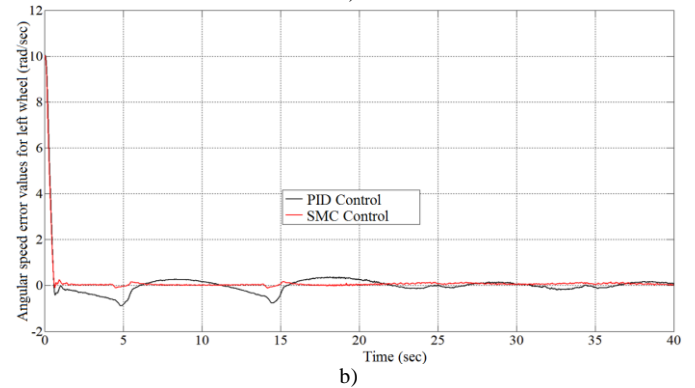
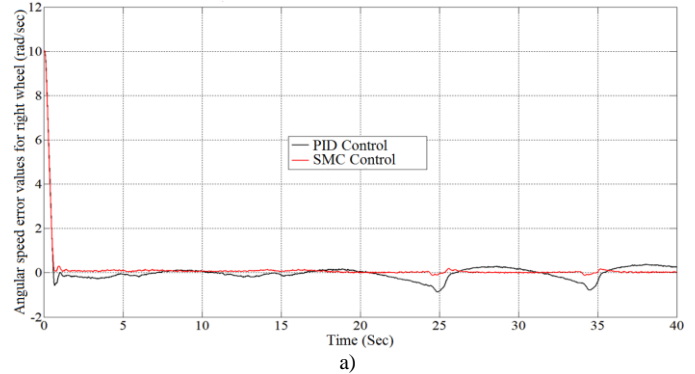


Fig.6. Angular speed error values of right and left wheels

As it can be seen from Figs. (5) and (6), the proposed SMC technique follows the reference trajectory more accurately than the PID control technique. According to the trajectory tracking response for both controllers in Figs. (5) and (6), PID controller causes overshoot values at the beginning of the motion. Meanwhile, with the robust control designs, the SMC improved the control performances with quite small tracking errors. By employing the system dynamic model to SMC controller, the controller makes the system more robust against the presence of uncertainties and disturbances in the feedback loop. However, as can be seen from figures, overshoot values are eliminated completely for the proposed SMC controller case due to the SMC technique is a robust and an efficient control technique for un-modelled dynamics and un-known loads of the robotic system. Also, both transient and steady-state error values are reduced by using the proposed SMC controller as shown in Figures.

V. CONCLUSION

In this study, the model based SMC has been proposed in order to control the uncertain nonlinear mobile robotic system. In order to get finite-time convergence, better tracking of

trajectory and chatter-free control, a model based SMC is developed. The experimental outcomes strongly verified that the proposed SMC provides a quite well trajectory tracking performance during the motion. Owing to the proposed algorithm, the SMC controller follows the reference with small error when it is compared with the responses of classical PID controller. For future work, the authors aim to design adaptive sliding mode control strategy by using the same model based method for the considered mobile robot system. Using the adaptive SMC in the proposed controller, it is expected that the trajectory tracking error value will be remarkably reduced.

#### REFERENCES

- [1] N. Uchiyama, T. Hashimoto, S. Sano and S. Takagi, "Model-Reference Control Approach to Obstacle Avoidance for a Human-Operated Mobile Robot," in *IEEE Transactions on Industrial Electronics*, vol. 56, no. 10, pp. 3892-3896, Oct. 2009.
- [2] M. Makarov, M. Grossard, P. Rodríguez-Ayerbe and D. Dumur, "Modeling and Preview Control Design for Motion Control of Elastic-Joint Robots With Uncertainties," in *IEEE Transactions on Industrial Electronics*, vol. 63, no. 10, pp. 6429-6438, Oct. 2016.
- [3] S. Li, Y. Zhang and L. Jin, "Kinematic Control of Redundant Manipulators Using Neural Networks," in *IEEE Transactions on Neural Networks and Learning Systems*, vol. 28, no. 10, pp. 2243-2254, Oct. 2017.
- [4] Y. Zhang, S. Chen, S. Li and Z. Zhang, "Adaptive Projection Neural Network for Kinematic Control of Redundant Manipulators With Unknown Physical Parameters," in *IEEE Transactions on Industrial Electronics*, vol. 65, no. 6, pp. 4909-4920, June 2018.
- [5] Z. Hou, A. Zou, L. Cheng and M. Tan, "Adaptive Control of an Electrically Driven Nonholonomic Mobile Robot via Backstepping and Fuzzy Approach," in *IEEE Transactions on Control Systems Technology*, vol. 17, no. 4, pp. 803-815, July 2009.
- [6] D. Chwa, "Fuzzy Adaptive Tracking Control of Wheeled Mobile Robots With State-Dependent Kinematic and Dynamic Disturbances," in *IEEE Transactions on Fuzzy Systems*, vol. 20, no. 3, pp. 587-593, June 2012.
- [7] A. Rojas-Moreno and G. Perez-Valenzuela, "Fractional order tracking control of a wheeled mobile robot," *2017 IEEE XXIV International Conference on Electronics, Electrical Engineering and Computing (INTERCON)*, Cusco, 2017, pp. 1-4.
- [8] Y. Zhao, N. Chen and Y. Tai, "Trajectory tracking control of wheeled mobile robot based on fractional order backstepping," *2016 Chinese Control and Decision Conference (CCDC)*, Yinchuan, 2016, pp. 6730-6734.
- [9] T. Chen, B. Dai, J. Song and L. Zhou, "On lateral fractional order controller in auto-parking system," *Proceedings of the 30th Chinese Control Conference*, Yantai, 2011, pp. 3429-3434.
- [10] V. Utkin, "Variable structure systems with sliding modes," in *IEEE Transactions on Automatic Control*, vol. 22, no. 2, pp. 212-222, April 1977.
- [11] C. - Su, T. - Leung and Y. Stepanenko, "Real-time implementation of regressor-based sliding mode control algorithm for robotic manipulators," in *IEEE Transactions on Industrial Electronics*, vol. 40, no. 1, pp. 71-79, Feb. 1993.
- [12] L. M. Capisani and A. Ferrara, "Trajectory Planning and Second-Order Sliding Mode Motion/Interaction Control for Robot Manipulators in Unknown Environments," in *IEEE Transactions on Industrial Electronics*, vol. 59, no. 8, pp. 3189-3198, Aug. 2012.
- [13] J. Baek, M. Jin and S. Han, "A New Adaptive Sliding-Mode Control Scheme for Application to Robot Manipulators," in *IEEE Transactions on Industrial Electronics*, vol. 63, no. 6, pp. 3628-3637, June 2016.
- [14] F. Zhang, "High-speed nonsingular terminal switched sliding mode control of robot manipulators," in *IEEE/CAA Journal of Automatica Sinica*, vol. 4, no. 4, pp. 775-781, 2017.
- [15] M. Van, S. S. Ge and H. Ren, "Finite Time Fault Tolerant Control for Robot Manipulators Using Time Delay Estimation and Continuous Nonsingular Fast Terminal Sliding Mode Control," in *IEEE Transactions on Cybernetics*, vol. 47, no. 7, pp. 1681-1693, July 2017.
- [16] J. Lee, P. H. Chang and M. Jin, "Adaptive Integral Sliding Mode Control With Time-Delay Estimation for Robot Manipulators," in *IEEE Transactions on Industrial Electronics*, vol. 64, no. 8, pp. 6796-6804, Aug. 2017.
- [17] G. P. Incremona, M. Rubagotti and A. Ferrara, "Sliding Mode Control of Constrained Nonlinear Systems," in *IEEE Transactions on Automatic Control*, vol. 62, no. 6, pp. 2965-2972, June 2017.
- [18] A. Ferrara and G. P. Incremona, "Design of an Integral Suboptimal Second-Order Sliding Mode Controller for the Robust Motion Control of Robot Manipulators," in *IEEE Transactions on Control Systems Technology*, vol. 23, no. 6, pp. 2316-2325, Nov. 2015.

#### BIOGRAPHIES



**AHMET DUMLU** was born in Erzurum, Turkey, in 1980. He received the B.S. degree in electronic engineering from Erziyes University, Kayseri, Turkey, in 2004, the M.S. degree in electrical & electronic engineering from Ataturk University, Erzurum, in 2009, and the Ph.D. degree in electrical engineering from Ataturk University, Erzurum, Turkey, in 2003. He is currently an Associate Professor with the Department of Electrical and Electronics Engineering, College of Engineering,

Erzurum Technical University, Erzurum. His work has focused on the development and application of control theory to a variety of mechatronic systems, with a focus on observation and estimation-based control. Much of his recent work has focused on the analysis and control of dynamical systems that arise in engineering applications. His areas of interest also include fuzzy logic and fuzzy control, neural networks, genetic algorithms, and their applications to dynamic systems and electrical engineering.



**MEHMET RASİM YILDIRIM** was born in Erzurum, Turkey, in 1990. He received the B.S. degree from Ataturk University, Erzurum, Turkey, in 2013 and he is currently working toward the M.S. degree. His research interests include the theory of mechatronic and robotic systems, with a focus on observation and estimation-based control.

# Application of Overfire Air Technology on an Example of a Steam Boiler PK-39 of the Aksu TPP (Kazakhstan)

A. Askarova, S. Bolegenova, V. Maximov, S.Bolegenova, Z. Gabitova, A. Yergaliyeva, A. Nugymanova, M. Beketayeva, Sh. Ospanova

**Abstract**— When burning any fossil fuels, one of the most harmful combustion products are nitrogen oxides NO<sub>x</sub>, which damage both the environment and human health in particular. Reduction of NO<sub>x</sub> emissions from fuel combustion at TPPs plays an important role in reducing the total level of nitrogen oxides NO<sub>x</sub> emitted into the atmosphere. One way to reduce the concentration of nitrogen oxides NO<sub>x</sub> is the stepwise combustion of the pulverized coal mixture, in particular the «Overfire Air» technology. The essence of this method is that the main volume of air is fed into the pulverized burners, and the rest of the air is further along the height of the torch through special nozzles. Structurally, the method of stepwise combustion of fuel can be carried out in boilers with a two-tier arrangement of burners along the height of the combustion chamber. In this case, practically no significant reconstruction of the boiler is required, which is associated with additional costs. In the present work, computational experiments on the use of modern overfire air technology (OFA) in the combustion chamber of the PK-39 boiler of the Aksu TPP were carried out and the fields of the main characteristics of heat and mass transfer, as well as the influence of the mass flow of the oxidant through the OFA injectors on the combustion process were obtained.

**Index Terms**— coal combustion, numerical simulation, overfire air technology.

## I. INTRODUCTION

AS OF TODAY Kazakhstan is one of the states possessing a huge stock of hydrocarbons, which render essential influence on formation and a condition of the world energy market [1-3].

**A. ASKAROVA**, is with Department of Science in Physics and Mathematics Al-Farabi Kazakh National University, (e-mail: [Aliya.Askarova@kaznu.kz](mailto:Aliya.Askarova@kaznu.kz)).

**S. BOLEGENOVA**, is with Dep. of Science in Physics and Mathematics Al-Farabi Kazakh National University, (e-mail: [Saltanat.Bolegenova@kaznu.kz](mailto:Saltanat.Bolegenova@kaznu.kz)).

**V. MAXIMOV**, is with Department of Science in Physics and Mathematics Al-Farabi Kazakh National University, (e-mail: [maximov.v@mail.ru](mailto:maximov.v@mail.ru)).

**S.BOLEGENOVA**, is with Dep. of Science in Physics and Mathematics Al-Farabi Kazakh National University, (e-mail: [Symbat.80@mail.ru](mailto:Symbat.80@mail.ru)).

**Z. GABITOVA**, is with Department of Science in Physics and Mathematics Al-Farabi Kazakh National University, (e-mail: [z.gabitova@kaznu.kz](mailto:z.gabitova@kaznu.kz)).

**A. YERGALIYEVA** is with Dep. of Science in Physics and Mathematics Al-Farabi Kazakh National University, (e-mail: [a.yergaliyeva@kaznu.kz](mailto:a.yergaliyeva@kaznu.kz)).

**A. NUGYMANOVA**, is with Dep. of Science in Physics and Mathematics Al-Farabi Kazakh National University, (e-mail [a.nugymanova@kaznu.kz](mailto:a.nugymanova@kaznu.kz)).

**M. BEKETAYEVA** is with Dep. of Science in Physics and Mathematics Al-Farabi Kazakh National University, (e-mail: [m.beketayeva@kaznu.kz](mailto:m.beketayeva@kaznu.kz)).

**SH. OSPANOVA**, is with Department of Science in Physics and Mathematics Al-Farabi Kazakh National University, (e-mail [sh.ospanova@kaznu.kz](mailto:sh.ospanova@kaznu.kz)).

Manuscript received May 14, 2018; accepted October 20, 2018.

DOI: [10.17694/bajece.475543](https://doi.org/10.17694/bajece.475543)

In the Republic of Kazakhstan, about 80% of the country's energy supply comes from the production of electricity by 69 power plants, the main source of which is Kazakh coal [4-6].

The coal mining in Republic is carried out basically by the open way, which makes this type of solid fuel the cheapest, but low-grade (high ash content in its composition) in our country a source of energy [3,7-8]. At the same time, the coal of Kazakhstan possesses a number of advantages – small sulphur content of coals and a high volatiles content on a dry ash-free basis.

For the sustainable development of heat and power industry of the country in the near future, it is necessary to optimize the combustion of traditional energy fuel (Kazakh coal), to develop and implement clean energy technologies; to protect the environment from harmful dust and gas emissions and ensure the efficiency of power plants. One of the methods for reduction of NO<sub>x</sub> concentration is the overfire air technology – OFA.

Technological methods for suppressing the formation of nitrogen oxides are based on a reduction in the peak temperature and oxygen content in the active combustion zone, as well as in the formation in the combustion chamber of zones with a reducing medium, where the products of incomplete combustion, reacting with the formed nitric oxide, lead to the reduction of NO<sub>x</sub> to molecular nitrogen N<sub>2</sub>.

Thus, in the zone of active combustion, an oxygen-depleted and fuel-enriched combustion zone is formed. Due to the lack of air in this area, the average temperature is lower than in traditional combustion, which allows to reduce the amount of fuel and thermal nitrogen oxides. Further, above the level of the main burners, additional air is supplied through the tertiary air nozzles necessary for afterburning the products of incomplete combustion and an oxidizing medium is formed [9-10].

The most difficult step in realization of the OFA technology is to define the optimal location height and diameter of nozzles through which air will be supplied, and to find the best ratio of air supplying through the main burner and OFA-injectors. These characteristics depend on design of the boilers and the method of supplying fuel-air mixture [10-11].

To effectively implement this technology on an industrial boiler, the height of the OFA injectors should be chosen so that in the active combustion zone a complete burn-out of the fuel and its afterburning to the final combustion products are ensured, since incomplete mixing of fuel and oxidant can

increase underburning [12].

## II. BASIC EQUATIONS OF HEAT AND MASS TRANSFER IN REACTIVE MEDIA

The computational experiment was carried out on the basis of the solution of the three-dimensional equations of convective heat and mass transfer taking into account the propagation of heat, thermal radiation, chemical reactions, and the multiphase nature of the medium. To describe the three-dimensional motion of reacting currents in the furnace chamber of the boiler PK-39, a system of differential equations [3,13-19] based on the control volume method [6, 18-20] is used:

– *The conservation law of mass or the continuity equation*

The ratio of the mass balance for control volume represents the continuity equation.

$$\frac{\partial \rho}{\partial t} = -\frac{\partial(\rho u_j)}{\partial x_j} \quad (1)$$

– *The conservation law of momentum or equation of motion*

Momentum balance is based on the second law of Newton-momentum change of the liquid in the control volume is equal to the sum of all external (surface and efficient volume) forces attached to the control volume.

$$\begin{aligned} \frac{\partial(\rho u_i)}{\partial t} = & -\frac{\partial(\rho u_i u_j)}{\partial x_j} + \frac{\partial}{\partial x_j} \left[ \mu \left( \frac{\partial u_i}{\partial x_j} \right) \right] - \frac{\partial p}{\partial x_i} + \rho f_i + \\ & + \frac{\partial}{\partial x_j} \left[ \mu \left( \frac{\partial u_j}{\partial x_i} - \frac{2}{3} \delta_{ij} \frac{\partial u_l}{\partial x_l} \right) \right]. \end{aligned} \quad (2)$$

– *The conservation law of energy*

The energy equation is based on the first law of thermodynamics.

$$\frac{\partial(\rho h)}{\partial t} = -\frac{\partial(\rho u_i h)}{\partial x_i} + \frac{\partial}{\partial x_i} \left( \frac{\mu}{Pr} \frac{\partial h}{\partial x_i} \right) + S_h \quad (3)$$

– *The conservation law of for the components of the substance*

In an isotropic medium consisting of  $\beta$  components, the components can move with different velocities  $u_{i,\beta}$ . For the mass balance of the  $\beta$ -component of the medium it can be written:

$$\frac{\partial(\rho c_\beta)}{\partial t} = -\frac{\partial(\rho u_i c_\beta)}{\partial x_i} + \frac{\partial}{\partial x_i} \left[ \rho D_{c_\beta} \frac{\partial c_\beta}{\partial x_i} \right] + S_\beta. \quad (4)$$

The combustion of coal dust in combustion chambers is turbulent, and in this connection, a standard  $k-\varepsilon$  model of turbulence was used to simulate turbulent viscosity and closure of the system [1,2,6,15]. The model includes

– *The equation of transport of turbulent kinetic energy  $k$ :*

$$\frac{\partial(\rho k)}{\partial t} = -\frac{\partial(\rho u_j k)}{\partial x_j} + \frac{\partial}{\partial x_j} \left[ \frac{\mu_{eff}}{\sigma_k} \frac{\partial k}{\partial x_j} \right] + P - \rho \cdot \varepsilon, \quad (5)$$

where  $P$  – turbulent kinetic energy production:

$$P = \left[ \mu_{turb} \left( \frac{\partial u_j}{\partial x_i} + \frac{\partial u_i}{\partial x_j} \right) - \frac{2}{3} \rho k \delta_{ij} \right] \frac{\partial u_j}{\partial x_i} \quad (6)$$

The equation of dissipation of turbulent kinetic energy  $\varepsilon$ :

$$\frac{\partial(\rho \varepsilon)}{\partial t} = -\frac{\partial(\rho u_j \varepsilon)}{\partial x_j} + \frac{\partial}{\partial x_j} \left[ \frac{\mu_{eff}}{\sigma_\varepsilon} \frac{\partial \varepsilon}{\partial x_j} \right] + C_{\varepsilon,1} \cdot \frac{\varepsilon}{k} \cdot P - C_{\varepsilon,2} \cdot \frac{\varepsilon^2}{k} \cdot \rho, \quad (7)$$

where  $\rho \varepsilon$  – transformation of the kinetic energy of the pulsating motion into internal energy (dissipation);

$\sigma_k, \sigma_\varepsilon$  – the corresponding turbulent Prandtl numbers.

Considering the processes of heat exchange in technical reacting flows in combustion chambers, heat exchange by means of radiation makes the greatest contribution to total heat transfer. In the flame zone, the contribution of radiant heat exchange is up to 90% of the total heat transfer and even more [21]. In this regard, the simulation of heat transfer through radiation in reacting flows in combustion chambers is one of the most important stages in the calculation of heat transfer processes in real combustion chambers.

At the calculations connected with radiant heat exchange, the characteristic values are the radiation energy  $E$  and the spectral intensity  $I_\nu$ . To describe the change in the magnitude of the spectral intensity in time, an infinitesimal volume is allocated in the investigated space, with an area  $dA$  and a length  $ds$ , in which emission, absorption and scattering of electromagnetic radiation quanta occur.

Thus, the change in the radiation intensity  $I_\nu$  along the infinitesimal volume can be written in the form of the energy balance equation (8):

$$\begin{aligned} \frac{1}{c} \cdot \frac{\partial I_\nu}{\partial t} + \frac{\partial I_\nu}{\partial s} = & - (K_{abs,\nu} + K_{sca,\nu}) \cdot I_\nu + K_{abs,\nu} \cdot I_\nu + \\ & + \frac{K_{sca,\nu}}{4\pi} \times \int_{4\pi} (P(\Omega_i \rightarrow \Omega) \cdot I_\nu(\Omega_i)) d\Omega_i \end{aligned} \quad (8)$$

In connection with the fact that the change in the radiation intensity in time is much less than the speed of light, the first term in the equation of the balance of radiant energy can be neglected. Due to the fact that the system is in thermodynamic equilibrium and the temperature of the radiant energy of the bodies radiated and absorbed is the same, then we can assume that the absorption and radiation coefficients are equal. In addition, in the paper all the bodies participating in heat transfer by radiation are represented as gray radiators.

Thus, the expression (8) can be written as [15,22]:

$$\begin{aligned} \frac{\partial I_\nu}{\partial s} = & - (K_{abs} + K_{sca}) I_\nu + K_{abs} \frac{\sigma}{\pi} T^4 + \\ & + \frac{K_{sca}}{4\pi} \times \int_{4\pi} (P(\Omega_i \rightarrow \Omega) \cdot I_\nu(\Omega_i)) d\Omega_i \end{aligned} \quad (9)$$

For calculation of heat exchange by radiation in furnace chamber the model of a stream was used, according to which Eq. (9) is integrated over solid angles, for which flows are assumed to be independent of direction.

## III. PHYSICAL AND GEOMETRICAL MODEL OF THE PK-39 BOILER

To solve the systems of differential equations describing the processes of heat and mass transfer in the combustion chamber of the boiler PK-39 of Aksu TPP, the control volume method [6, 18-20] was used.

The essence of the method is that the space of the combustion chamber is divided into control volumes and for each point of space surrounded by a certain volume, the

equations of conservation of physical quantity (mass, momentum, energy, etc.) are solved.

Before the numerical experiments using the PREPROZ program [22], files and startup programs were created for two investigated cases, including initial and boundary conditions, the characteristics of the fuel (elemental composition, heat of combustion, fractional composition of Ekibastuz coal), the geometry of the boiler and burner devices [6,13,23]. The main characteristics of the combustion chamber of the boiler PK-39 of Aksu TPP and burnt Ekibastuz coal are presented in table 1.

TABLE I  
CHARACTERISTICS OF THE COMBUSTION CHAMBER OF THE BOILER PK-39 OF AKSU TPP AND THE PULVERIZED COAL BURNED ON IT (EKIBASTUZ COAL) [3]

| The name of the characteristics, dimensionality        | Designation                 | Value    |
|--|-----------------------------|----------|
| Fuel consumption per boiler, kg/h                      | B                           | 87 500   |
| Fuel consumption per burner, kg/h                      | $B^B=B/Z$                   | 7291.1   |
| Fuel – Ekibastuz coal<br>Composition of coal,%         | W <sup>P</sup>              | 7.0      |
|  | A <sup>P</sup>              | 40.9     |
|  | S <sup>P</sup>              | 0.8      |
|  | C <sup>P</sup>              | 41.1     |
|  | H <sup>P</sup>              | 2.8      |
|  | O <sup>P</sup>              | 6.6      |
|  | N <sup>P</sup>              | 0.8      |
| Calorific value, MJ/kg                                 | Q <sub>H</sub> <sup>P</sup> | 15.87    |
| Volatile, %  | V <sup>F</sup>              | 30.0     |
| Coefficient of excess air at the exit from the furnace | $\alpha_T$                  | 1.25     |
| Coefficient of excess air in the burners               | $\alpha_r$                  | 1.15     |
| Temperature of the air mixture, °C (K)                 | T <sub>a</sub>              | 150(423) |
| Temperature of secondary air, °C (K)                   | T <sub>2</sub>              | 327(600) |
| Type of burners  | Vortex                      |          |
| Number of burners, pcs                                 | n <sub>B</sub>              | 12       |
| Height of the furnace, m                               | z(H)                        | 29.985   |
| Width of the furnace, m                                | Y                           | 10.76    |
| Depth of the furnace, m                                | X                           | 7.762    |

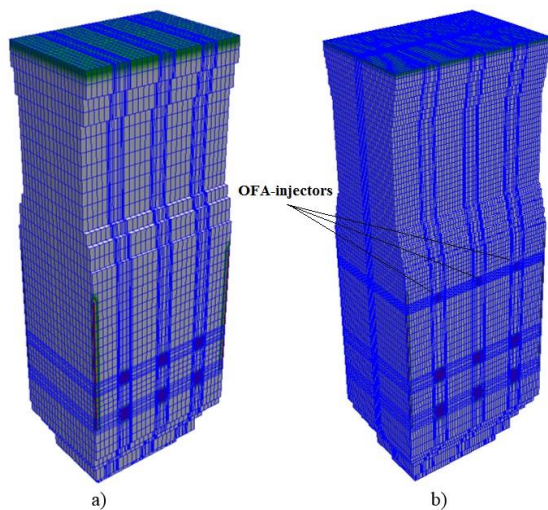


Fig.1. General view and a gridding of the PK-39 boiler

TABLE II

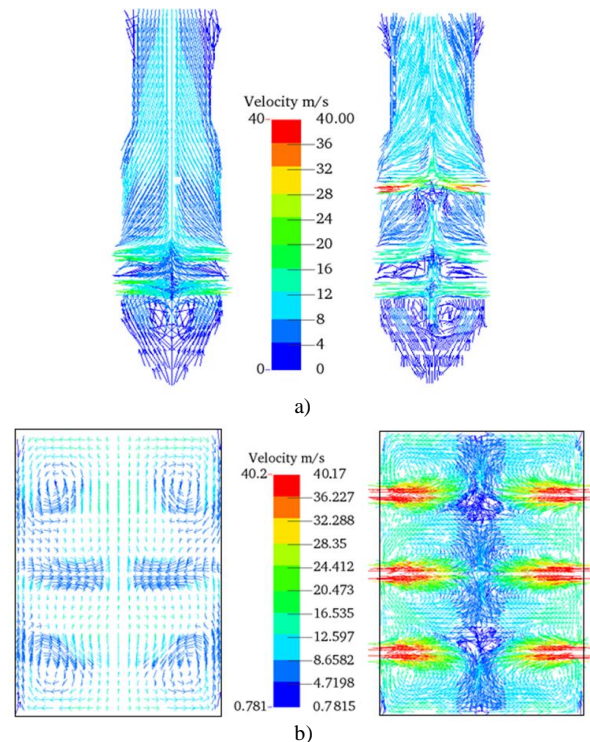
CONSTRUCTIONAL CHARACTERISTICS OF A BOILER PK-39 OF AKSU TPP AT THE ORGANIZATION OF STAGED COMBUSTION OF FUEL

| The characteristic                             | Value  |
|--|--------|
| Number of OFA-nozzles, pcs                     | 6      |
| The height of the tier of the lower burners, m | 7,315  |
| The height of the tier of the upper burners, m | 10,115 |
| The height of the tier of the OFA-nozzles, m   | 15,735 |
| Diameter of OFA-nozzles, m                     | 0,7    |

Fig. 1 provides a general view and a gridding of the boiler: for traditional pulverized coal combustion (Fig. 1a), at implement of secondary air nozzles – OFA (Fig. 1b). The major structural characteristics are presented in table 2. In the work, cases with a percentage of the supply air through the nozzles OFA equal to 0 (base case), 10 and 20% of the total amount of secondary and tertiary air supplied to the combustion chamber.

IV. RESULTS AND DISCUSSION

Results of researches obtained with the FLOREAN software package [25-30] are presented below in the paper. Fig. 2 shows the distribution of the full-velocity vector in different sections of the combustion chamber for the base case (OFA 0%) and with the use of the overfire air technology (OFA 20%). Analysis of the figures shows that with the use of OFA technology, the combustion process in the central part of the combustion chamber is more intense compared to the base case.



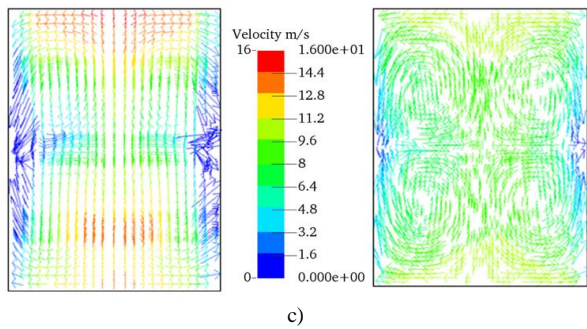


Fig.2. The distribution of the velocity vector in different sections of the combustion chamber a) the central longitudinal section ( $Y=5.38$  m); b) the cross-sectional area of the OFA-nozzles ( $Z=15.735$  m); c) cross-section at the outlet from the combustion chamber of the boiler PK-39 ( $Z=29,595$  m)

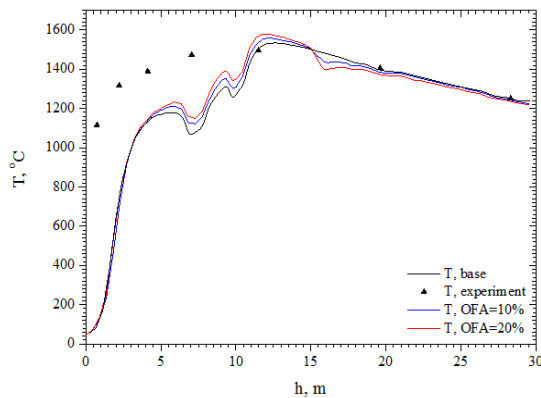


Fig.3. Temperature distribution over the height of the combustion chamber of the boiler PK-39 for different values of air supplied through the nozzles OFA and comparison with experiment [24]

Fig. 3 shows the distribution of average temperatures on height of furnace chamber for the investigated cases. The results of full-scale experiment conducted at Aksu TPP [24] are also plotted on the graph. Moving towards the exit of the furnace temperature field is equalized and differences in temperature values for different occasions decrease.

Also, it can be seen that the greatest differences between the results of computational and full-scale experiments are observed in the area of ignition of the pulverized coal mixture. Moving towards the exit from the furnace space, these differences are insignificant, which indicates good consistency and, as a consequence, the adequacy of the used models.

Fig. 4-5 show graphs of the distribution of combustion products – carbon  $CO_2$  and nitrogen  $NO$  oxides along the height of furnace chamber of PK-39 boiler of Aksu TPP. Analyzing the distribution of carbon monoxide (Fig. 4), it can be seen that the greatest differences in the values are noticeable in the area of the burner belt and OFA-injectors. To the exit from the combustion chamber with increasing mass flow of air through the OFA-nozzles, the concentration of carbon dioxide  $CO_2$  is reduced.

Fig. 5 represents the distribution of the concentration of nitrogen oxide  $NO$  along the height of furnace chamber of PK-39 boiler of Aksu TPP.

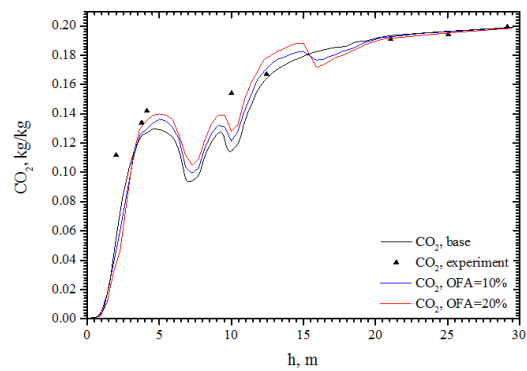


Fig.4. Distribution of  $CO_2$  concentration along the furnace chamber height for different values of air supplied through the nozzles OFA and comparison with experiment [24].

Analysis of Fig. 5 allows us to conclude that an increase in the mass flow of air supplied through OFA injectors leads to a decrease in  $NO$  concentration at the outlet from the furnace chamber of PK-39 boiler of Aksu TPP. This is confirmed by the known dependence of  $NO$  oxides formed on temperature [31] and analysis of the temperature distribution in the combustion chamber of the boiler PK-39, presented in Fig. 3.

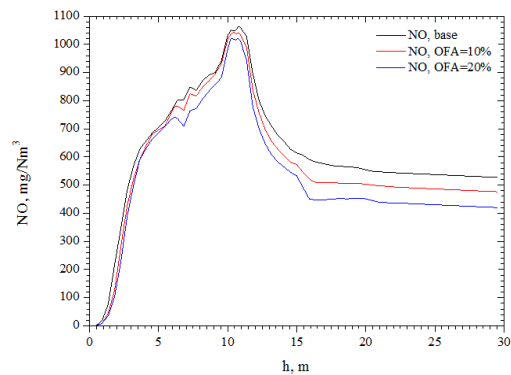


Fig.5. Distribution of  $NO_x$  concentration along the furnace chamber height for different values of air supplied through the nozzles OFA

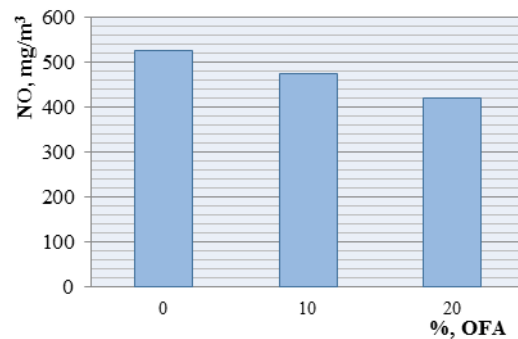


Fig.6. The effect of the percentage of mass air flow through the OFA injectors on the  $NO$  concentration at the outlet from the combustion chamber of the PK-39 boiler of the Aksu TPP

The increase in air supplied through the OFA injectors allows to reduce the concentration of nitric oxide at the outlet from the combustion chamber approximately on 20 %. The results of the studies are presented in the form of a diagram in Fig. 6.

## V. CONCLUSION

This paper presents the experiments on the implementation of the overfire air technology on the example of combustion chamber of PK-39 boiler of Aksu TPP. This technology is based on the separation of the oxidant supplied to the combustion chamber in such a way as to reduce the amount of fuel NO<sub>x</sub> in the burner location by reducing excess air, and reduce the amount of thermal NO<sub>x</sub> by reducing the temperature of the flame in the region of the location of the OFA-injectors.

Studies show that the implementation of OFA technology on the boiler PK-39 Aksu TPP leads to a change in the distribution of temperature T, the concentrations of carbon CO<sub>2</sub> and nitrogen NO oxides in the combustion chamber.

Thus, the studies in this paper demonstrate that overfire air technology is one of the most promising ways to reduce emissions of harmful substances (nitrogen oxide NO<sub>x</sub> and carbon dioxide CO<sub>2</sub>) in the atmosphere and can be used in the combustion of high-ash fuels in combustion chambers of coal-fired TPPs.

## ACKNOWLEDGMENT

This work was financially supported by the Ministry of Education and Science of the Republic of Kazakhstan – Grant №0115RK00599.

## NOMENCLATURE

$u_i$  – components of the velocity, m/s;  
 $t$  – time, s;  
 $\rho$  – density, kg/m<sup>3</sup>;  
 $\tau_{ij}$  – tensor of viscous tension;  
 $p$  – pressure, Pa;  
 $f_i$  – volume forces, N;  
 $h$  – enthalpy;  
 $q^{res}$  – energy flux density due to molecular heat transfer;  
 $S_h$  – a source of energy;  
 $c_n$  – mass concentration of the components of the substance;  
 $D_{c_n}$  – the diffusion coefficient of a component;  
 $S_{c_n}$  – the source term taking into account the contribution of the chemical reactions in the change in the concentration of components;  
 $k$  – turbulent kinetic energy per unit mass;  
 $\mu_{eff}$  – effective viscosity;  
 $\sigma_k, \sigma_\epsilon$  – turbulent Prandtl numbers – empirical constants in turbulence model;  
 $P$  – the production of turbulent kinetic energy, which is determined by the following equation;  
 $\epsilon$  – dissipation rate of turbulent kinetic energy per unit mass;  
 $\delta_{ij}$  – Kronecker delta;  
 $\mu_{turb}$  – turbulent viscosity;  
 $c_{\epsilon 1}, c_{\epsilon 2}, c_\mu$  – empirical constants;  
 $\nu$  – frequency of radiant energy emitted from the element area;  
 $ds$  – length of the infinitesimal element allocated in space;

$K_{abs}, K_{sca}$  – optical absorption and scattering coefficients;

$\Omega$  – the solid angle;

$A_i, B_i$  – the coefficients in the Taylor series expansion – functions of intensity of radiation;

$\sigma$  – Stefan-Boltzmann constant;

$b_{ij}$  – the matrix coefficient.

## REFERENCES

- [1] Askarova A., Bolegenova S., Bekmukhamet A., Maximov Yu.V., Beketayeva M., Ospanova Sh. Gabitova Z.K., “Investigation of turbulence characteristics of burning process of the solid fuel in BKZ 420 combustion chamber”, WSEAS Transactions on Heat and Mass Transfer, Vol.9, 2014, pp. 39-50.
- [2] Askarova A.S., Bekmukhamet A., Bolegenova S.A., Beketayeva M.T., Maximov Yu.V., Ospanova Sh.S., Gabitova Z.K., “Numerical modeling of turbulence characteristics of burning process of the solid fuel in BKZ-420-140-7c combustion chamber”, International Journal of Mechanics, Vol.8, 2014, pp. 112-122.
- [3] Askarova A.S., Bolegenova S.A., Maximov V.Y., Bekmukhamet A., Beketayeva M.T., Gabitova Z.K. et al. Computational method for investigation of solid fuel combustion in combustion chambers of a heat power plant, High temperature, Vol.53, No.5, 2015, pp.751-757.
- [4] Askarova A., Bolegenova S., Bekmukhamet A., Ospanova Sh., Gabitova Z., “Using 3D modeling technology for investigation of conventional combustion mode of BKZ-420-140-7c combustion chamber”, Journal of Engineering and Applied Sciences, Vol.9, No.1, 2014, pp. 24-28.
- [5] Askarova A.S., Bolegenova S.A., Bekmukhamet A., Maximov V.Yu., “Mathematical simulation of pulverized coal in combustion chamber”, Procedia Engineering, Vol.42, 2012, pp. 1259-1265.
- [6] Askarova A., Bekmukhamet A., Bolegenova S., Ospanova Sh., Bolegenova Symbat, Maximov V. Beketayeva M., Gabitova Z., Ergalieva A., “3D modeling of heat and mass transfer during combustion of solid fuel in BKZ-420-140-7c combustion chamber of Kazakhstan”, Journal of Applied Fluid Mechanics, Vol.9, No.2, 2016, pp. 699-709.
- [7] Askarova, A.S., Lavrichsheva, Ye.I., Leithner, R., Müller, H., Magda, A., “Combustion of low-rank coals in furnaces of Kazakhstan coal-firing power plants”. VDI Berichte, Vol.1988, 2007, pp. 497-502.
- [8] Askarova, A. S., Vockrodt S., Leithner. et al., “Firing technique measures for increased efficiency and minimization of toxic emissions in Kasakh coal firing” VDI, 19th German Conference on Flames, Germany, VDI Gesell Energietechn; Verein Deutsch Ingn., Combustion And Incineration, VDI Berichte, Vol.1492, 1999, P. 93.
- [9] Kuang M., Li Z., Liu C., Zhu Q., Zhang Y., Wang Y., “Evaluation of overfire air behavior for a down-fired 350 MWe utility boiler with multiple injection and multiple staging”, Applied Thermal Engineering, Vol.48, 2012, pp. 164-175.
- [10] Askarova A.S., Messerle V.E., Ustimenko A.B., Bolegenova S.A., Bolegenova S.A., Maximov V.Y., Ergalieva A., “Reduction of noxious substance emissions at the pulverized fuel combustion in the combustor of the BKZ-160 boiler of the Almaty heat electropower station using the “Overfire Air” technology”, Thermophysics and aeromechanics, Vol.23, No.1, 2016, pp. 125-134.
- [11] A.S. Askarova, E.I. Heierle, S.A. Bolegenova, V.Ju. Maximov, S.A. Bolegenova, R. Manatbayev, M.T. Beketaeva, A.B. Ergalieva, “CFD study of harmful substances production in coal-fired power plant of Kazakhstan”, Bulgarian Chemical Communications, Special Issue E, 2016, pp. 260-265.
- [12] Li M., Wang X., Sun S., Zhen X., Li Q., Zhang T., “Influence of Overfire air jet form on low NO<sub>x</sub> retrofit effect of an opposed firing boiler”, Journal of Chinese society of power engineering, Vol.4, 2015, pp. 263-269.
- [13] Askarova, A.S., Messerle, V.E., Ustimenko, A.B., Bolegenova, S.A., Maximov, V.Yu. Gabitova, Z.Kh., “Numerical simulation of pulverized coal combustion in a power boiler furnace”, High temperature, Vol.53, No.3, 2015, pp. 445-452.
- [14] Askarova, A.S., Bolegenova, S.A., Maximov, V.Y., Bekmukhamet, A., Beketayeva M., Gabitova Z., “Control of Harmful Emissions Concentration into the Atmosphere of Megacities of Kazakhstan

Republic”, IERI Procedia, International Conference on Future Information Engineering (FIE2014), Beijing, 2014, pp. 252-258.

- [15] A. Askarova, S. Bolegenova, S. Bolegenova, V. Maximov, R. Manatbayev, A. Yergaliyeva, Z. Gabitova, A. Maxutkhanova, Zh. Shortanbayeva, A. Boranbayeva, K. Berdikhan, “Application of 3D modelling for solving the problem of combustion coal-dust flame”, Bulgarian Chemical Communications, Special Issue E, 2016, pp. 236-241.
- [16] R. Leithner, A. Askarova, S. Bolegenova, S. Bolegenova, V. Maximov, Sh. Ospanova, A. Ergalieva, A. Nugymanova, M. Beketayeva, “Computational modeling of heat and mass transfer processes in combustion chamber at power plant of Kazakhstan”, *MATEC Web of Conferences*, 2016, 5p.
- [17] Askarova, A., Bolegenova, S., Bolegenova, S., Boranbayeva, A., Berdikhan, K., “Application of numerical methods for calculating the burning problems of coal-dust flame in real scale”, International Journal of Applied Engineering Research, Vol.11, No.8, 2016, pp. 5511-5515.
- [18] Askarova A., Bolegenova S. et al., “Influence of boundary conditions to heat and mass transfer processes”, International Journal of Mechanics, Vol.10, 2016, pp. 320-325.
- [19] Askarova A., Bolegenova S., Maximov V. et al., “On the effect of the temperature boundary conditions on the walls for the processes of heat and mass transfer”, International Journal of Mechanics, Vol.10, 2016, pp. 349-355.
- [20] Askarova, A. S., Bolegenova, S.A., Maximov, V.Y., Bekmukhamet, A., Ospanova, S.S., “Numerical research of aerodynamic characteristics of combustion chamber BKZ-75 mining thermal power station”, *Procedia Engineering*, Vol.42, 2012, pp.1250-1259.
- [21] Weber K., “Dreidimensionale Simulation der Gas-Feststoff-Strömung in kohlegefeuerten Dampferzeugern”, *Fortschritt-Berichte VDI-Verlag*, Vol.6, No.415, 1999, p. 198.
- [22] Askarova A.S., Bolegenova S.A., Bolegenova S., Bekmukhamet A., Maximov V.Yu., Beketayeva M.T., “Numerical experimenting of combustion in the real boiler of CHP”, International Journal of Mechanics, Vol.3, No.7, 2013, pp. 343-352.
- [23] Askarova, A.S., Messerle, V.E., Ustimenko, A.B., Bolegenova, S.A., Maksimov, V.Yu., “Numerical simulation of the coal combustion process initiated by a plasma source”, *Thermophysics and aeromechanics*, Vol.21, No.6, 2014, pp. 747-754.
- [24] Aliyarov B.K., Aliyarova M.B. *Szhiganie kazhastanskikh ugley na TES i na krupnykh kotelnih: opyt i problemy*, Almaty, 2012.
- [25] Leithner R., Müller H., “CFD studies for boilers”, Second M.I.T. Conference on Computational Fluid and Solid Mechanics, Cambridge, 2003, p. 172.
- [26] Leithner R., Müller H., Heitmüller R., “Dreidimensionale Simulation von Dampferzeuger-Brennkammern einschließlich der NOx-Schadstoffkinetik”, *VGB-Fachtagung: Dampfkessel und Dampfkesselbetrieb*, Essen, 1993. 152 p.
- [27] Müller H., “Numerische Berechnung dreidimensionaler turbulenter Strömungen in Dampferzeugern mit Wärmeübergang und chemischen Reaktionen am Beispiel des SNCR-Verfahrens und der Kohleverbrennung”, *Fortschritt-Berichte VDI-Verlag*, 1992, No.268, 158 p.
- [28] Askarova, A.S., Karpenko, E.I., Karpenko, Yu.E., Messerle, V.E., Ustimenko, A.B., “Mathematical modelling of the processes of solid fuel ignition and combustion at combustors of the power boilers”, 7th International Fall Seminar on Propellants, Explosives and Pyrotechnics. Xian, Vol.7, 2007, pp. 672-683.
- [29] A.S. Askarova, S.A. Bolegenova, Symbat Bolegenova, V.Yu. Maximov, R. Manatbayev, Zh.K. Shortanbayeva, A.M. Maksutkhanova, A.N. Aldiyarova, A.E. Boranbayeva, “Mathematical modeling of heat and mass transfer in the presence of physical-chemical processes”, Bulgarian Chemical Communications, Special Issue E, 2016, p. 272-277.
- [30] Askarova, A.S., Maximov, V., Beketayeva, M., Safarik, P., “Numerical Modeling of Pulverized Coal Combustion at Thermal Power Plant Boilers”, *Journal of thermal science*, Vol. 24, No.3, 2015, pp. 275-282.
- [31] Zeldovich J., “The oxidation of Nitrogen in combustions and explosions”, *Acta Physicochemica*, Vol.21, 1946, pp. 557-628.

## BIOGRAPHIES



**ALIYA ASKAROVA** (Doctor of Science in Physics and Mathematics, Professor) actively engaged in research work. In 1999, defended doctoral thesis on the topic “Convective heat and mass transfer in physically and chemically reacting media”. Currently is qualified in the field of thermal physics, engaged in mathematical and computer modeling of convective heat and mass transfer processes in physically and chemically reacting media, associated with combustion of gaseous and solid fuels and environmental issues of power system.



**SALTANAT BOLEGENOVA** (Doctor of Science in Physics and Mathematics, Professor) in 2003 defended her thesis on “Numerical study of chemically reacting turbulent gas jets in the presence of external influences”. In 2010 she defended her doctoral thesis on the topic “Modeling of turbulent heat and mass transfer in high-temperature and chemically reacting streams”. Scientific interests: heat and mass transfer, turbulence, modeling, fuel combustion.



**VALERIY MAXIMOV** (PhD) in 2013 completed his doctoral studies in the specialty “Technical Physics” and defended his thesis on the topic “Investigation of thermal processes and aerodynamic characteristics of coal-fired power plants”. Scientific interests: mathematical and computer simulation of the combustion of pulverized coal in the combustion chambers of thermal power plants.



**SYMBAT BOLEGENOVA** (PhD) in 2012 defended thesis “Modelling the physico-chemical processes occurring during combustion of pulverized coal”. Scientific interests: modeling of convective heat and mass transfer processes in reacting media.



**ZARINA GABITOVA** (PhD) in 2016 defended thesis “Simulation of heat and mass processes in combustion chamber of TPP”. Scientific interests: computer simulation of the combustion of pulverized coal in the combustion chambers, reduction of emissions of harmful substances in the atmosphere.



**AIGUL YERGALIYEVA** is a 3rd year PhD student at al-Farabi Kazakh National University. Scientific interests: heat and mass transfer, turbulent reacting flows, simulation, fuel combustion.



**AIZHAN NUGYMANOVA** is a 1st year PhD student at al-Farabi Kazakh National University. Scientific interests: heat and mass transfer processes in combustion chambers, reduction of emissions of harmful substances.



**MERUERT BEKETAYEVA** (PhD) in 2015 defended thesis “Three-dimensional modeling of the combustion of low-grade Kazakhstan coal in combustion chambers of thermal power plants”. Scientific interests: mathematical simulation of the combustion of pulverized coal at thermal power plants.



**SHYNAR OSPANOVA** (PhD). Scientific interests: study of free jets of gas and liquid at acoustic exposures; study of three-dimensional turbulent jets of gas and liquids; study of heat and mass transfer processes in physical and chemical reactive environments; combustion physics; statistical modeling of breakup, dispersion and evaporation of liquid drops in high turbulence.

# Estimation of Reduced Order Equivalent Circuit Model Parameters of Batteries from Noisy Current and Voltage Measurements

B. B. Alagoz, H. Alisoy

**Abstract**— Identification of reduced order equivalent circuit battery model from current and voltage measurements allows modeling, classification and monitoring of batteries, and these tasks are very essential for battery management systems. This study presents a theoretical study to investigate performance of computer-aided identification of the reduced order equivalent circuit battery model from noisy current and voltage measurement data. The battery model is expressed in the form of fractional order differential equation and time domain numerical solution of this model is numerically calculated according to Grünwald-Letnikov definition of fractional-order derivative. Paper demonstrates an application of this numerical solution so that it can fit noisy current and voltage measurement data, and thus parameters of the equivalent circuit battery model can be estimated. Particle swarm optimization (PSO) method is used to solve this model fitting problem. Performance of the parameter estimation method is investigated for various noise levels of the synthetically generated current and voltage profiles.

**Index Terms**— Battery model, fractional order system model, Grünwald-Letnikov definition, PSO.

## I. INTRODUCTION

**D**UE TO growing demand for mobility in daily life, battery utilization in real applications increase and hence battery monitoring and management methods are becoming an essential component of mobile systems. In fact, practical performance of many battery powered systems e.g. mobile devices, electrical vehicles depends on battery management performance [1,2]. Nowadays, monitoring battery health and optimal control of battery packs are major topics of battery research studies, and these studies has focused on modeling and real-time identification of battery model parameters, which is useful for evaluating battery status and health [3]. Therefore, online control and the management of batteries are performed based on model parameter estimations, which can provide the meaningful information related to conditions of batteries.

**B. B. ALAGOZ**, is with Department of Computer Engineering, Inonu University, Malatya, Turkey, (e-mail: [baykant.alagoz@inonu.edu.tr](mailto:baykant.alagoz@inonu.edu.tr)).

**H. ALISOY**, is with Department of Electronics and Communication Engineering, Namik Kemal University, Tekirdag, Turkey, (e-mail: [halisoy@nku.edu.tr](mailto:halisoy@nku.edu.tr)).

Manuscript received July 30, 2018; accepted October 28, 2018.  
DOI: [10.17694/bajece.449265](https://doi.org/10.17694/bajece.449265)

There are several models that were utilized for modeling batteries in different levels of complexity [3,4]. High complexity models can be useful for more proper representation of the behavior or properties of batteries in simulation environment, however increasing model complexity can heavily complicate real-time identification problem and model parameter estimation efforts. One of the widely utilized models for battery monitoring is the reduced order equivalent circuit model. This model can be used by battery monitoring algorithms and identified either in time domain by measuring current and voltage profiles or in the frequency domain by applying impedance spectroscopy measurements [2]. Figure 1(a) shows a reduced order equivalent circuit model based on the impedance spectrum data [2,5]. Figure 1(b) illustrates an s-domain transfer function representation of this model [6]. The fractional order capacitor element makes this model a fractional order system model [6] and time-domain analysis of this model requires application of fractional calculus. Since recent developments in fractional-order system analysis tools [7], the s-domain representation of this system can be preferable for battery parameter estimation and simulation purposes.

Grünwald-Letnikov (GL) definition of fractional order differentiation has been widely utilized for the numerical solution of fractional order differential equations, solution of fractional order system models in state space form and calculation of time response of fractional order transfer functions [7, 8, 9,10, 11,12]. Numerical calculation methods based on Grünwald-Letnikov definition are commonly used to develop fractional-order system analysis tools [7,10].

In previous studies, Grünwald-Letnikov based numerical solution of this battery model were utilized in many studies for estimating state of charge, parameter sensitivity analysis etc. [1,13,14,15]. Some of them were utilized metaheuristic optimization methods, such as hybrid multi-swarm particle swarm optimization and genetic algorithm, because model fitting problem is not so easy for fractional-order systems. In addition to model coefficients (component values), the estimation of fractional-orders of the differential equation models is required, and this significantly increases complexity of numerical solution of the problem compared to fixed order differential equation models, namely integer-order system models. Main reason of this complication comes from the long memory effect, that is, fractional order derivative depends on all past values of the fractionally derived function [7] and hence fractional-order derivative is not a local operator.

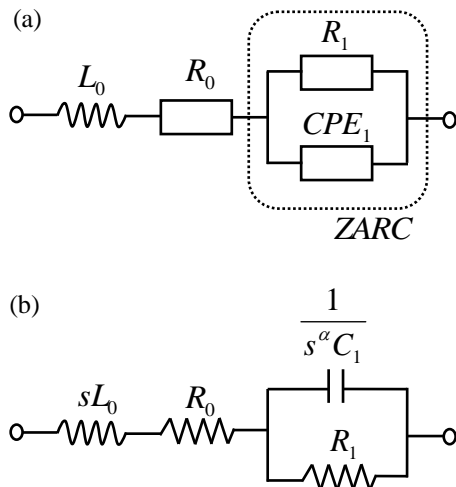


Fig. 1. (a) Reduced order equivalent circuit model [2], (b) Transfer function representation of this model in s-domain [6].

Performance of real-time model parameter estimation algorithms depends on a number of factors:

- (i) Limitation of computational resources such as the speed of processor, memory capacity can decrease practical performance. Computational complexity of the estimation method should be low enough so that it can be implemented on control cards by using embedded programming techniques.
- (ii) Negative impacts of measurement noise on the accuracy of parameter estimation can decrease practical performance. The estimation accuracy should be enough robust against measurement noises.
- (ii) For online analysis of model parameters, estimation method should be independent of waveform of the measured data because, in real applications, measured current and voltage can be in any waveforms. Real-time operating model identification algorithms should deal with waveform uncertainty of the measured data.

The current study discusses performance of a time-domain model identification approach that may be utilized for real-time estimation of parameters of the reduced order equivalent circuit model. This method performs fitting Grünwald-Letnikov based numerical solutions of the equivalent circuit model to noisy current and voltage data profiles that are measured from battery terminals. To achieve approximation of the model response to this measured data, an average of squared difference of numerical voltage and measured voltage values is used as the objective function that should be minimized to achieve identification. Here, PSO algorithm is employed to solve this optimization problem. To improve estimation of model parameters, this objective function, namely mean square error (MSE), is modified by taking logarithm of MSE function. This modification to objective function can improve minimization performance of PSO at very low values of MSEs because of the logarithmic stretching of MSE values at very low levels. Here, the logarithm of MSE can make objective function more distinguishable at very low values.

## II. PRELIMINARIES AND PROBLEM STATEMENTS

Impedance spectroscopy is a main technique that has been applied for identification of sophisticated equivalent circuit models [2, 5,16]. This method is performed by matching real or complex parts of frequency domain models or magnitude and phase responses for the each measured frequency [2]. In this manner, the equivalent circuit model shown in Figure 1(a) is expressed in the complex impedance form,

$$Z(\omega) = R_o + j\omega L_o + \frac{R_1}{1 + A_1 R_1 (j\omega)^\alpha} \quad (1)$$

The last term of the equation (1) expresses a fractional order behavior, which was also known as constant phase element [2, 17]. This term is also referred to as ZARC or Cole-Cole circuit element [17,18]. Parameters  $R_o$  and  $L_o$  are output resistance and inductance of the model, respectively.

We aim to perform time domain identification of the model from a given current and voltage data set. By considering  $s = j\omega$  relation, the transfer function model of the reduced order equivalent circuit model was written in the form [6],

$$Z(s) = R_o + sL_o + \frac{R_1}{1 + C_1 R_1 s^\alpha} \quad (2)$$

The s-domain equivalent circuit representation was shown in Figure 1(b) and this representation implies that fractional order system analysis methods can be applied to obtain time domain solutions of this model. Considering current and voltage in impedance function, by considering the equation (2), a fractional order system model is written as

$$V(s) = Z(s)I(s), \quad (3)$$

$$V(s) = R_o I(s) + sL_o I(s) + \frac{R_1}{1 + C_1 R_1 s^\alpha} I(s). \quad (4)$$

To facilitate time domain solution of battery voltage, the equation (4) can be decomposed as the sum of three voltage elements as,

$$V(s) = V_1(s) + V_2(s) + V_3(s), \quad (5)$$

where the voltage terms are  $V_1(s) = R_o I(s)$  for the voltage across  $R_o$ ,  $V_2(s) = L_o s I(s)$  for the voltage across  $L_o$  and

$V_3(s) = \frac{R_1}{1 + C_1 R_1 s^\alpha} I(s)$  for constant phase element. By taking

inverse Laplace transform of these voltage components, time domain solution of the components can be written as follows,

$$v_1(t) = R_o i(t), \quad (6)$$

$$v_2(t) = L_o \frac{di(t)}{dt}, \quad (7)$$

where  $i(t)$  is the battery current. To obtain time domain model for  $V_3(s)$ , one can reorganize it as  $C_1 R_1 s^\alpha V_3(s) + V_3(s) = R_1 I(s)$ , and by taking inverse Laplace transform and using the properties of  $L\{D^\alpha F(s)\} = s^\alpha f(t)$ , it can be expressed in time domain as,

$$C_1 R_1 D^\alpha v_3(t) + v_3(t) = R_1 i(t), \quad (8)$$

Numerical solutions of this fractional-order differential equation can be obtained by using Grünwald-Letnikov

definition of fractional-order derivative operator, which is written by [7],

$${}_a D_t^\alpha f(t) = \lim_{h \rightarrow 0} \frac{1}{h^\alpha} \sum_{j=0}^{\lfloor (t-a)/h \rfloor} w_j^{(\alpha)} f(t-jh), \quad (9)$$

where  $a$  parameter is a lower bound for time derivative and it limits calculations from the time  $a$  to current time. Although it reduces need of memory elements to store the past values, it results in a truncation error in calculations. For more accurate calculation of fractional derivatives in system analysis,  $a$  can be zero. Parameter  $h$  is step size (sampling period) for computations. The operator  $\lfloor (t-a)/h \rfloor$  expresses the rounding the value of term  $(t-a)/h$  to a nearest smaller integer number. The weight parameter  $w_j^{(\alpha)}$  for  $j=0,1,2,\dots$  is written recursively as [7],

$$w_0^{(\alpha)} = 1, \quad w_j^{(\alpha)} = \left(1 - \frac{\alpha+1}{j}\right) w_{j-1}^{(\alpha)}. \quad (10)$$

For a finite and non-zero time sampling  $h$  and considering values of  $f(t-jh)$  from zero to current time by taking  $a=0$ , one expresses an approximate formulation of Grünwald-Letnikov differentiation as,

$$D_t^\alpha f(t) \cong \frac{1}{h^\alpha} \sum_{j=0}^{\lfloor t/h \rfloor} w_j^{(\alpha)} f(t-jh). \quad (11)$$

The equation (11) is used in equation (8), the numerical solution of this differential equation can be found by solving,

$$C_1 R_1 \frac{1}{h^\alpha} \sum_{j=0}^{\lfloor t/h \rfloor} w_j^{(\alpha)} v_3(t-jh) + v_3(t) \cong R_1 i(t). \quad (12)$$

This equation can be rewritten as

$$C_1 R_1 \frac{1}{h^\alpha} w_0^{(\alpha)} v_3(t) + C_1 R_1 \frac{1}{h^\alpha} \sum_{j=1}^{\lfloor t/h \rfloor} w_j^{(\alpha)} v_3(t-jh) + v_3(t) \cong R_1 i(t). \quad (13)$$

By rearranging the equation (13), the solution  $v_3(t)$  can be written as,

$$v_3(t) \cong \frac{-C_1 R_1}{C_1 R_1 w_0^{(\alpha)} + h^\alpha} \sum_{j=1}^{\lfloor t/h \rfloor} w_j^{(\alpha)} v_3(t-jh) + \frac{R_1 h^\alpha}{C_1 R_1 w_0^{(\alpha)} + h^\alpha} i(t). \quad (14)$$

The weights  $w_j^{(\alpha)}$  is calculated recursively according to equation (10). By considering equation (5), a battery voltage solution with respect to a given current  $i(t)$  can found by

$$v(t) = v_1(t) + v_2(t) + v_3(t). \quad (15)$$

By considering equation (6), (7) and (14),  $v_1(t)$ ,  $v_2(t)$  and  $v_3(t)$  are calculated in discrete time domain for a current sampling  $i_m(n)$  with a sampling  $t = nh$ :

$$v_1(n) = R_o i(n) \quad (16)$$

$$v_2(n) = L_o \frac{i(n) - i(n-1)}{h} \quad (17)$$

$$v_3(n) = -\frac{C_1 R_1}{C_1 R_1 w_0^{(\alpha)} + h^\alpha} \sum_{j=1}^{\lfloor t/h \rfloor} w_j^{(\alpha)} v_3(n-j) + \frac{R_1 h^\alpha}{C_1 R_1 w_0^{(\alpha)} + h^\alpha} i(n) \quad (18)$$

where  $h$  is the sampling period and the battery voltage can be calculated by

$$v_a(n) = v_1(n) + v_2(n) + v_3(n) \quad (19)$$

An example Matlab code, which performs the numerical calculation of the reduced order equivalent circuit battery model is presented in Appendix section.

### III. IDENTIFICATION OF MODEL PARAMETERS

Let's denote the measured current and voltage from battery terminals by  $i_m(n)$  and  $v_m(n)$  signals, respectively. For fitting the  $i_m(n)$  and  $v_m(n)$  data ( $i=0,1,2,\dots,p$ ) to time domain solution of the equivalent circuit battery model, which is calculated by equation (15), a mean square error to minimize is commonly written by [10,13-15]

$$E = \frac{1}{p} \sum_{n=1}^p (v_a(n) - v_m(n))^2, \quad (20)$$

where,  $p$  is the total number of the sampled data. The  $v_a(n)$  is calculated according to the equation (19). To increase accuracy in the estimation of model parameters, MSE, given by equation (20), can be modified by taking logarithm of MSE function. This makes very low error values more distinguishable as a result of stretching effect of logarithmic at very low values. The logarithmic error function can be written by,

$$E_l = 10 \log \left( \frac{1}{p} \sum_{n=1}^p (v_a(n) - v_m(n))^2 \right). \quad (21)$$

To estimate the reduced order equivalent model parameters of battery, which are  $C_1, R_1, R_0, L_0$  and  $\alpha$ , the optimization problem  $\min_{C_1, R_1, R_0, L_0, \alpha} E_l$  can be solved by metaheuristic optimization methods. In this study, PSO algorithm is used to solve this optimization problem (see Figure 12 in Appendix section).

### IV. SIMULATION STUDY

To estimate model parameters  $C_1, R_1, R_0, L_0$  and  $\alpha$  according to battery terminal measurements  $i_m(n)$  and  $v_m(n)$ , we implemented PSO algorithm to minimize  $E_l$  by using numerical formulation that is derived in the previous section.

To evaluate parameter estimation performance of the method for noisy data, we considered Li-ion battery parameters that were identified as  $C_1 = 72$  F,  $R_1 = 4.17$  m $\Omega$ ,  $R_0 = 0.71$  m $\Omega$ ,  $L_0 = 3.51 \cdot 10^{-7}$  H and  $\alpha = 0.72$  in [2]. To generate synthetic noise at various SNR levels, a random noise signal is added to the ground truth current data  $i(n)$  and voltage data  $v(n)$ . The ground truth terminal voltage  $v(n)$  is calculated for a terminal current waveform  $i(n)$  by using equation (19). The synthetic noisy test data were generated as,

$$i_m(n) = i(n) + \eta_i(n), \quad (22)$$

$$v_m(n) = v(n) + \eta_v(n), \quad (23)$$

where  $\eta_i$  is random noise signal for current measurements and  $\eta_v$  is random noise signal for voltage measurements. PSO algorithm was applied for the parameter search ranges of  $C_1 \in [0,200]$  F,  $R_1 \in (0,20)$  m $\Omega$ ,  $R_0 \in [0,10]$  m $\Omega$ ,  $L_0 \in [0,10^{-6}]$  H and  $\alpha \in [0,2]$ . Population size of PSO was set to 30 particles and the maximum iteration number was configured to 1200 iterations. Simulation and test environment were developed in Matlab program.

Firstly, noise signals  $\eta_i$  and  $\eta_v$  were set to zero for noise-free test and model parameter estimation for this noise-free case was performed to verify operation of the algorithm. PSO yielded estimations of  $C_1 \cong 72.00 \text{ F}$ ,  $R_1 \cong 4.17 \text{ m}\Omega$ ,  $R_0 \cong 0.71 \text{ m}\Omega$ ,  $L_0 \cong 3.51 \cdot 10^{-7} \text{ H}$  and  $\alpha \cong 0.72$ , which are the almost exact values of ground truth (original) data of Li-ion battery model. Logarithmic MSE was obtained  $E_l = -196.88$ , which corresponds to  $E = 2.1948 \cdot 10^{-18}$ , that is, the error is almost zero. Figure 2 shows accurately fitting of the model voltage  $v_a(n)$  and the voltage data  $v_m(n)$  for this zero-noise case. To better view plots,  $v_m(n)$  is drawn subsampled in the figure.

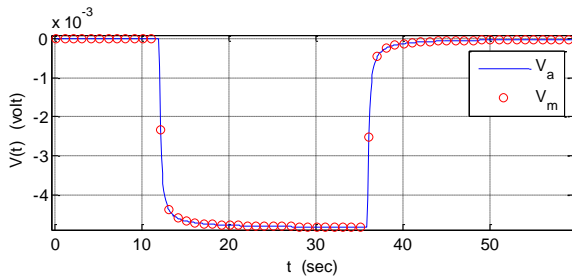


Fig. 2. Fitting of the model voltage  $v_a(n)$  and the voltage data  $v_m(n)$  for zero-noise case.  $v_m(n)$  data is shown subsampled in the figure.

For a low-level noisy measurement scenario, the current waveform was noised at  $SNR = 59.49 \text{ dB}$  and ground truth voltage was noised at  $SNR = 48.16 \text{ dB}$ . Figure 3 shows a satisfactory fitting of the model voltage  $v_a(n)$  and the voltage data  $v_m(n)$  for these noise data. After fitting by PSO algorithm, the model parameters were estimated  $C_1 \cong 72.04 \text{ F}$ ,  $R_1 \cong 4.16 \text{ m}\Omega$ ,  $R_0 \cong 0.72 \text{ m}\Omega$ ,  $L_0 \cong 5.12 \cdot 10^{-7} \text{ H}$  and  $\alpha \cong 0.716$ , which are the slightly different from ground truth values of parameters. Logarithmic MSE was obtained  $E_l = -91.01$ , which corresponds to  $E = 8.39 \cdot 10^{-10}$ . This level of MSE is acceptable for practical performance.

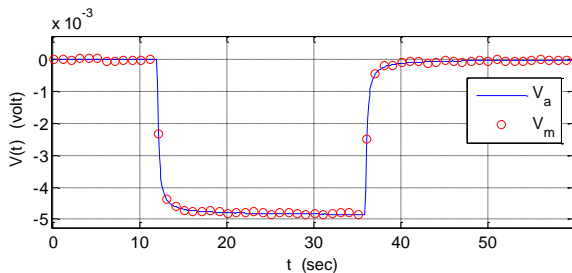


Fig. 3. Fitting of the model voltage  $v_a(n)$  and the voltage data  $v_m(n)$  for low-level noise current ( $SNR = 59.49 \text{ dB}$ ) and low-level noise voltage data ( $SNR = 48.16 \text{ dB}$ ).  $v_m(n)$  data is shown subsampled in the figure.

For a mid-level noisy measurement scenario, the current waveform was noised at  $SNR = 41.08 \text{ dB}$  level and the ground truth voltage was noised at  $SNR = 32.45 \text{ dB}$ . Figure 4

shows noisy current and noisy voltage data. Figure 5 demonstrates fitting performance of the  $v_a(n)$  and the  $v_m(n)$ . After performing PSO, the model parameters were estimated as  $C_1 \cong 74.31 \text{ F}$ ,  $R_1 \cong 4.24 \text{ m}\Omega$ ,  $R_0 \cong 0.64 \text{ m}\Omega$ ,  $L_0 \cong 1 \cdot 10^{-6} \text{ H}$  and  $\alpha \cong 0.714$ . They are more differentiated from ground truth values of parameters compared to previous low-noise measurement test. Logarithmic MSE was obtained  $E_l = -76.68$ , which corresponds to MSE of  $E = 2.30 \cdot 10^{-8}$ . This accuracy level can be acceptable for some battery parameter estimation applications.

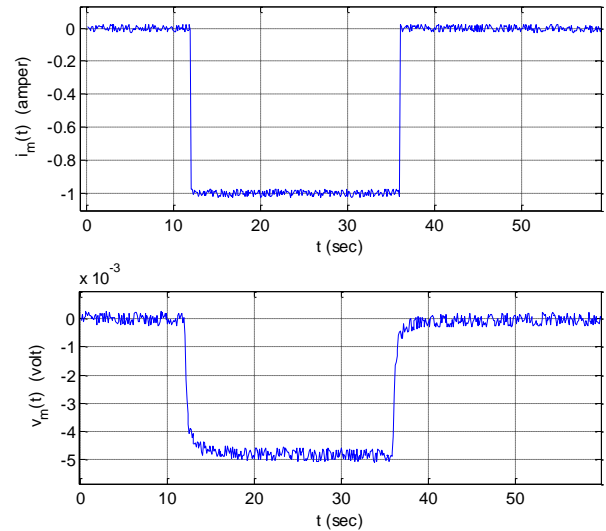


Fig. 4. Low-level noisy current data ( $SNR = 41.08 \text{ dB}$ ) and mid-level noisy voltage data ( $SNR = 32.45 \text{ dB}$ )

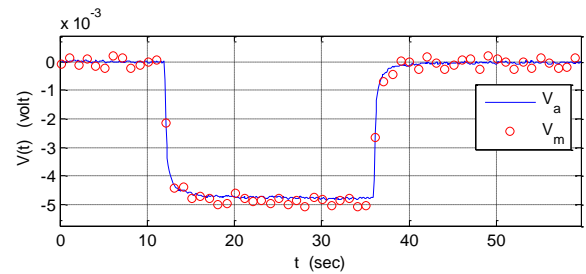


Figure 5. Fitting of the model voltage  $v_a(n)$  and the voltage data  $v_m(n)$  for mid-level noise current ( $SNR = 41.08 \text{ dB}$ ) and mid-low noise voltage data ( $SNR = 32.45 \text{ dB}$ ).  $v_m(n)$  data is shown subsampled in the figure.

For high-level noisy measurement scenario, the current waveform was noised at  $SNR = 36.22 \text{ dB}$  level and the ground truth voltage was noised at  $SNR = 28.46 \text{ dB}$  in Figure 6. Figure 7 shows the fitting of the model voltage  $v_a(n)$  to the  $v_m(n)$  under this noise levels. PSO algorithm found the model parameter as  $C_1 \cong 77.14 \text{ F}$ ,  $R_1 \cong 4.06 \text{ m}\Omega$ ,  $R_0 \cong 0.81 \text{ m}\Omega$ ,  $L_0 \cong 1 \cdot 10^{-6} \text{ H}$  and  $\alpha \cong 0.762$ . Logarithmic MSE was obtained  $E_l = -70.66$ , which corresponds to MSE of  $E = 8.92 \cdot 10^{-8}$ . This level of accuracy can be adequate for insensitive applications of battery parameter estimation.

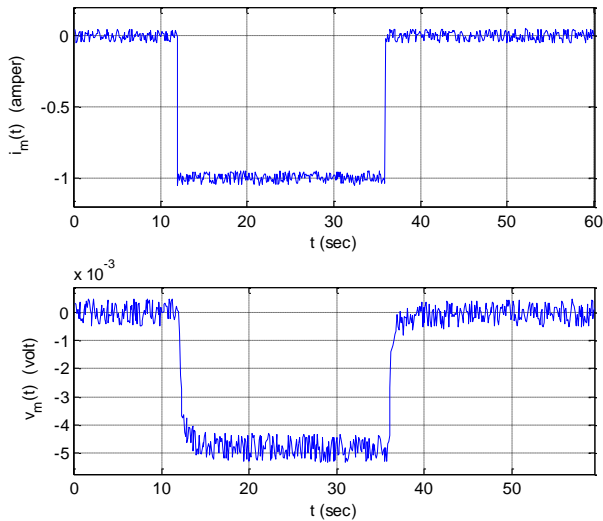


Fig. 6. High-level noisy current data ( $SNR = 36.22$  dB) and highly noisy voltage data ( $SNR = 28.46$  dB)

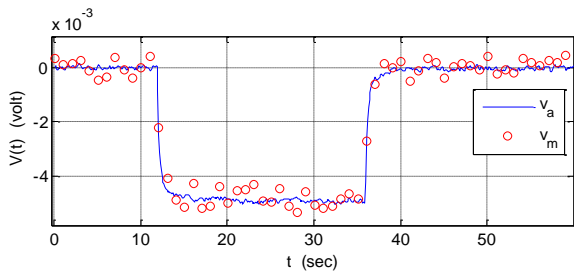


Fig. 7. Fitting of model the voltage  $v_a(n)$  and the voltage data  $v_m(n)$  for high-level noise current ( $SNR = 36.22$  dB) and high-level noise voltage data ( $SNR = 28.46$  dB).  $v_m(n)$  data is shown subsampled in the figure.

To test algorithm for a severe noisy measurement case, the current waveform was noised at  $SNR = 30.05$  dB level and ground truth voltage waveform was noised at  $SNR = 7.59$  dB as illustrated in Figure 8. Figure 9 shows the fitting of the model voltage  $v_a(n)$  and the voltage data  $v_m(n)$ . PSO algorithm estimated the model parameter as  $C_1 \cong 114.01$  F,  $R_1 \cong 4.31$  m $\Omega$ ,  $R_0 \cong 0.83$  m $\Omega$ ,  $L_0 \cong 110^{-6}$  H and  $\alpha \cong 0.869$ , which may not be enough accurate for sensitive battery management applications such as precise battery control. Inaccuracy of model parameters can cause misleading of controller tuning, and it decreases control system performance. Logarithmic MSE was obtained  $E_l = -50.79$ , which corresponds to a MSE of  $E = 8.3510^{-6}$ . However, fitting of model voltage  $v_a(n)$  and the voltage data  $v_m(n)$  may be acceptable for some insensitive battery applications.

Table 1 summarizes results of parameter estimations that were obtained in the analyses. The absolute relative errors for parameter estimations were calculated by  $e_r = |x_e - x_o|/x_o$ , where  $x_e$  stands for value of estimated parameter and  $x_o$  is its original (ground truth) value.

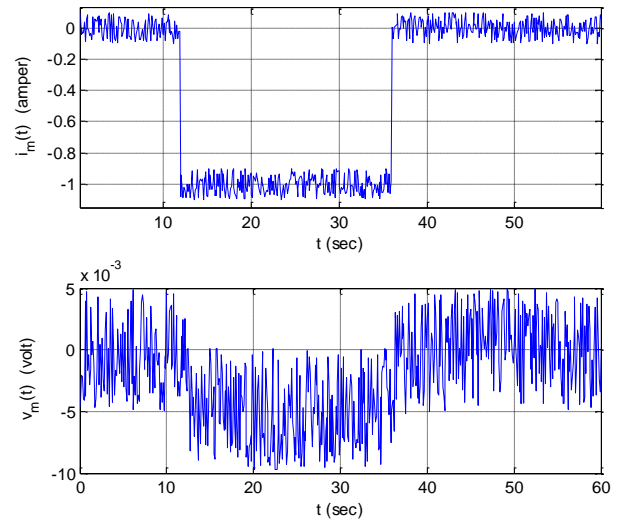


Fig. 8. Severely noised current data ( $SNR = 30.05$  dB) and voltage data ( $SNR = 7.59$  dB)

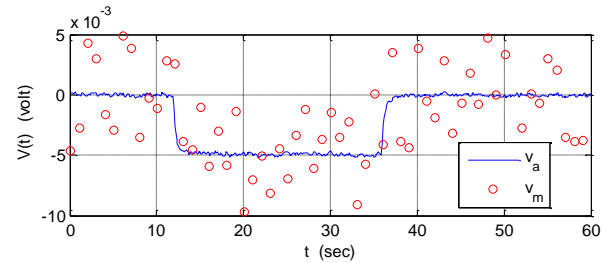


Fig. 9. Fitting of the model voltage  $v_a(n)$  and the voltage data  $v_m(n)$  for severely noised current ( $SNR = 30.05$  dB) and voltage data ( $SNR = 7.59$  dB).  $v_m(n)$  data is shown subsampled in the figure.

The performance data in Table 1 reveals that the estimation of resistance values,  $R_1$  and  $R_0$ , are more robust against noise interference than those of  $C_1$  and  $L_0$ . Main reason is that,  $R_1$  and  $R_0$  are static elements that are mainly effective in determining DC level of the measured signal. Smoothing effect of fitting operation can reduce negative impacts of irregular pattern of noise on the estimation of  $R_1$  and  $R_0$ , and this makes their estimations more robust against random noise signal. The dynamic components  $C_1$  and  $L_0$  mostly act on transient parts of the measured signal. Therefore, irregular motif of noise can easily interfere predictions of these parameters, and this may reduce accuracy of estimations of parameters  $C_1$  and  $L_0$ . In particular, since  $L_0$  parameter is directly associated with derivative of the measured current,  $L_0$  estimations are very sensitive to the noise of current measurements. Therefore, in case of noisy data, parameter search range of  $L_0$  should be confined to its realistic ranges in order to avoid misleading parameter estimation results. In our analyses, we restricted  $L_0 \in [0, 10^{-6}]$  in PSO. The  $10^{-6}$  values for  $L_0$  in Table 1 are mainly results of this restriction.

TABLE I  
A LIST OF PARAMETER ESTIMATIONS FOR VARIOUS NOISE CONDITIONS AND ABSOLUTE RELATIVE ERRORS IN PARAMETER ESTIMATION

| Parameters  | Original Values<br>( $x_o$ ) | Zero Noise Case<br>( $x_e, e_r$ ) | Low-level Noise Case<br>( $x_e, e_r$ ) | Mid-level Noise Case<br>( $x_e, e_r$ ) | High Level Noise Case<br>( $x_e, e_r$ ) | Severe Noise Case<br>( $x_e, e_r$ ) |
|-------------|------------------------------|-----------------------------------|--|--|---|-------------------------------------|
| $C_1$       | 72.00                        | 72.00, 0%                         | 72.04, 0.05%                           | 74.31, 3.2%                            | 77.14, 7.1%                             | 114.01, 58%                         |
| $R_1$       | 4.17                         | 4.17, 0%                          | 4.16, 0.2%                             | 4.24, 1.6%                             | 4.06, 2.6%                              | 4.31, 3.3%                          |
| $\alpha$    | 0.72                         | 0.72, 0%                          | 0.716, 0.5%                            | 0.714, 0.8%                            | 0.762, 5.8%                             | 0.869, 20.6%                        |
| $R_0$       | 0.71                         | 0.71, 0%                          | 0.72, 1.4%                             | 0.64, 9.8%                             | 0.81, 14%                               | 0.83, 16.9%                         |
| $L_0$       | $3.51 \cdot 10^{-7}$         | $3.51 \cdot 10^{-7}$ , 0%         | $5.12 \cdot 10^{-7}$ , 45.8%           | $10^{-6}$ , 184%                       | $10^{-6}$ , 184%                        | $10^{-6}$ , 184%                    |
| MSE ( $E$ ) | -                            | $2.19 \cdot 10^{-18}$             | $8.39 \cdot 10^{-10}$                  | $2.30 \cdot 10^{-8}$                   | $8.92 \cdot 10^{-8}$                    | $8.35 \cdot 10^{-6}$                |

Waveform of the current can affect accuracy of parameter estimations. While smooth current waveforms or steady parts of current waveforms can improve estimation of static elements, such as  $R_1$  and  $R_0$ , whereas the altering part of waveforms can improve the estimation of dynamic elements, which are  $C_1$  and  $L_0$  in the model. Figure 6 shows test results for a continuous sinusoidal current waveform that was obtained by  $i_m(t) = -2 + \sin(1.25t) + \sin(0.31t)$  with a low-level noise insertion at  $SNR = 48.98$  dB. The voltage response  $v_m(t)$  was obtained by the reduced order equivalent circuit model of Li-ion battery with a low-level noise insertion at  $SNR = 47.31$  dB. Figure 10 illustrates waveforms of the generated low-level noisy current and voltage data. Figure 11 shows fitting of output of the identified model to the measured voltage data. PSO algorithm found the model parameter as  $C_1 \cong 75.98$  F,  $R_1 \cong 41.05$  m $\Omega$ ,  $R_0 \cong 0.77$  m $\Omega$ ,  $L_0 \cong 1 \cdot 10^{-6}$  H and  $\alpha \cong 0.731$ . Logarithmic MSE was obtained  $E_l = -70.62$ , which corresponds to a MSE of  $E = 1.0710^{-7}$ . This simulation confirms that the method can be applied for any measurement waveforms, and therefore it can be used for real-time monitoring of batteries.

V. CONCLUSION

This study theoretically discussed performance of a scheme for online estimation of reduced order equivalent circuit model parameters of batteries from noisy and irregular waveform current and voltage measurement data. Battery model parameter estimation is needed for modeling, classification and monitoring of batteries in real applications. Temporal change of battery model parameters can be utilized for detection of battery status, diagnoses of aging effect, faults and defects. Besides, real-time identification of battery models can allow optimally control of battery charge and discharge processes. Therefore, properly estimation of battery model parameter is very essential for battery management systems and algorithms. Nowadays, increase of battery usage as a result of growing demands of electrical vehicles and mobile applications places battery modeling and parameter estimation efforts at the center of battery management system researches.

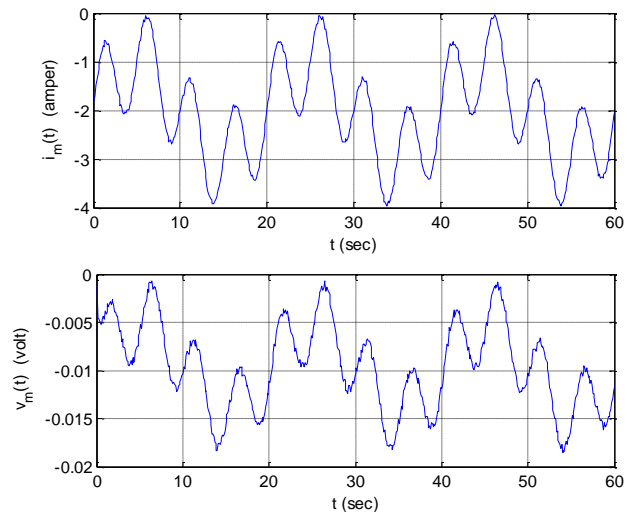


Fig. 10. Low-level noisy current data ( $SNR = 48.98$  dB) and low-level noisy voltage data ( $SNR = 47.31$  dB)

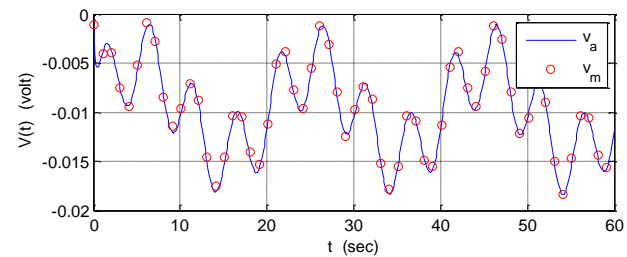


Fig. 11. Fitting of the model voltage  $v_a(n)$  and the voltage data  $v_m(n)$  for severely noise current ( $SNR = 48.98$  dB) and low noise voltage data ( $SNR = 47.31$  dB).  $v_m(n)$  data is shown subsampled in the figure.

The presented solution for battery parameter estimation can estimate the reduced order equivalent circuit model parameters by fitting Grünwald-Letnikov based numerical solutions of the battery model to current and voltage profiles of the batteries. This fitting problem was expressed in the form of minimization of a logarithmic MSE function of battery voltages and solved by employing PSO algorithm. The numerical studies, which were carried out for various levels of

random noise addition to input and output of Li-ion battery models, reveal that this method can work effectively in case of noisy measurements. Therefore, we conclude that the model parameter estimation of this method may be applied in real battery management applications. A future study should be conducted for experimental validation of performance of this method in experimental systems.

### Appendixes

An example Matlab code to perform for numerically calculation of voltage of the reduced order equivalent circuit battery model is given, below. This code calculates battery voltage  $v_a(n)$  for a given current waveform  $i_m(n)$  and the battery model parameters.

```
clear all;
% Sampling rate
h=0.01;
% Sampling time
t=0:h:100;
% Battery current measurements
I=-(1-exp(-t/5));
% Reduced order equivalent circuit
battery model parameters
alpha=0.9;
R1=4.17e-3;
C1=72;
Ro=0.71e-3;
Lo=3.51e-7;
% Calculation of v3(t)
b=1/C1;
a=1/(C1*R1);
w=1;wa(1)=1;
for j=2:length(t)
    w=(1-(alpha+1)/(j-1))*w;
    wa(j)=w;
end
top=0;
v3(1)=0
for i=2:length(t)
    top=0;
    for j=2:i
        top=top+wa(j)*v3(i-(j-1));
    end
    v3(i)=-
    1/(wa(1)+a*h^alpha)*top+b*h^alpha/(wa(1)+
    a*h^alpha)*(I(i));
end
% Calculation of v2(t)
DI=diff(I)/h;
v2=Lo*DI;
v2(length(t))=0;
% Calculation of v1(t)
v1=Ro*I;
% Calculation of battery voltage
va=(v1+v2+v3);
% Draws battery voltage v(t)
figure(1)
plot(t,va)
xlabel('t');ylabel('v_a')
```

This program performs equation (19) to obtain GL solution of battery voltage. This code can be used in optimization process as shown below.

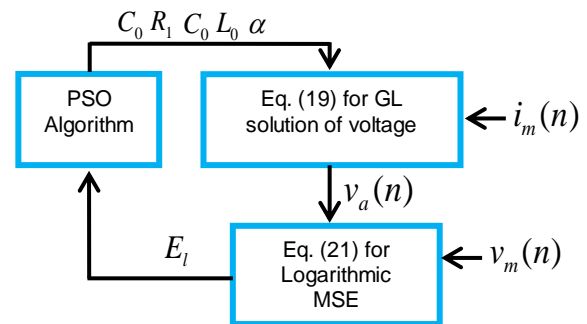


Fig. 12. A basic block diagram that shows application of PSO algorithm in this problem

### References

- [1] J.X. Chuntin, g C. Mi, B. Cao, J. Cao, "New method to estimate the state of charge of lithium-ion batteries based on the battery impedance model", *Journal of Power Sources*, Vol.233, 2013, pp.277-284.
- [2] W. Waag, S. Käbitz, D.U. Sauer, "Application-specific parameterization of reduced order equivalent circuit battery models for improved accuracy at dynamic load", *Measurement*, Vol.46, 2013, pp. 4085-4093.
- [3] C.B. Shin, *BATTERIES: modeling*, in: *Encyclopedia of Electrochemical Power Sources*, vol. I, Elsevier, 2009. pp.510-521.
- [4] X. Hu, S. Li, H. Peng, "A comparative study of equivalent circuit models for Li-ion batteries", *Journal of Power Sources*, Vol.198, 2012, pp.359-367.
- [5] S. Buller, "Impedance-Based Simulation Models for Energy Storage Devices in Advanced Automotive Power Systems", Institute for Power Electronics and Electrical Drives, RWTH Aachen University, Ph.D. Thesis, 2003.
- [6] T.J. Freeborn, B. Maundy, A.S. Elwakil, "Fractional-order models of supercapacitors, batteries and fuel cells: a survey", *Mater Renew Sustain Energy* Vol.4, No.2, 2015, pp.1-7
- [7] Y.Q. Chen, Ivo Petras, D. Xue, "Fractional order control-a tutorial", In: *American Control Conference*, 2009. ACC'09. IEEE, 2009. p. 1397-1411.
- [8] R. Scherer, S.L. Kalla, Y. Tang, J. Huang, "The Grünwald-Letnikov method for fractional differential equations", *Computers and Mathematics with Applications* Vol.62, 2011, pp.902-917.
- [9] C. Zhao, L. Luo, Y. Zhao, "Fractional Modeling Approach with Mittag-Leffler Functions for Linear Fractional-order System", 2012 Fifth International Conference on Intelligent Computation Technology and Automation, pp. 386- 389.
- [10] R.S. Awski, K.J. Latawiec, M. Lukaniszyn, W. Czuczvara, and R. Kopka, "Modeling and identification of fractional first-order systems with Laguerre-Grünwald-Letnikov fractional-order differences", 2016 21st International Conference on Methods and Models in Automation and Robotics (MMAR), 2016, pp.174-177.
- [11] P. Sopasakisy, S. Ntouskas, H. Sarimveis, "Robust Model Predictive Control for Discrete-time Fractional-order Systems", 2015 23rd Mediterranean Conference on Control and Automation (MED), Torremolinos, Spain, 2015, pp. 384-389.
- [12] E. Dorcák, J. Valsa, J. Terpák, E. Gonzalez, "Comparison of the methods for the calculation of fractional-order differential equations", In *Carpathian Control Conference (ICCC)*, 2011, pp. 80-84.
- [13] S.E. Li, B. Wang, H. Peng, and X. Hu, "An electrochemistry-based impedance model for lithium-ion batteries," *J. Power Sour.*, Vol. 258, 2014, pp.9-18.
- [14] B. Wang, Z. Liu, S.E. Li, S.J. Moura, H. Peng, "State-of-charge estimation for lithium-ion batteries based on a nonlinear fractional model", *IEEE Transactions on Control Systems Technology*, Vol.25, No.1, 2017, pp. 3-11.

- [15] D. Zhou, K. Zhang, A. Ravey, F. Gao, A. Miraoui, "Parameter sensitivity analysis for fractional-order modeling of lithium-ion batteries", *Energies*, Vol.9, No.3, 2016, pp.123.
- [16] A. Fotouhi, D.J.Auger,K. Propp,S. Longo,M. Wild,A review on electric vehicle battery modelling: From Lithium-ion toward Lithium–Sulphur, *Renewable and Sustainable Energy Reviews*,Vol.56,2016,pp.1008-1021.
- [17] E. Barsukov, J.R. Macdonald, *Impedance Spectroscopy: Theory, Experiment and Applications*, second ed., Wiley-Interscience, 2005.
- [18] M.E. Orazem, P. Shukla, M.A. Membrino, "Extension of the measurement model approach for deconvolution of underlying distributions for impedance measurements", *Electrochimica Acta*, Vol.47, 2002, pp.2027-2034.

## BIOGRAPHIES



**BARIS BAYKANT ALAGOZ** received bachelor degree in Istanbul Technical University, Department of Electronics and Communication Engineering in 1998, M.Sc. and Ph.D. degrees in Inonu University, Department of Electrical-Electronics Engineering in 2011 and 2015. His research interests include modeling and simulation of physical systems, control systems, systems and intelligence, smart grid. He is working at Computer Engineering Department in Inonu University.



**HAFIZ Z. ALİSOY**, was graduated from Moscow Technical University department of ElectroPhysics Engineering 1982. He had his PhD degree from USSR Science Academy Physics Institute of P.N. Lebedev and Doctor of Sciences degree (DSc) from International Ecology-Energy Academy. He became as Full Professor in 1995. He received award of Young Scientist. He works at Namık Kemal University, Department of Electronics and Telecommunication Engineering.

# Design and Simulation of Uniform Magnetic Field

A. Mukhamedgali and Z. B. Rakisheva

**Abstract**—This article describes the design, construction and calculation of the mathematical model of a homogeneous magnetic field, considering for this Helmholtz coil. Helmholtz coils consist of a pair of coils along one axis parallel to each other. By varying the distance, size, winding of these coils, it is enough to simulate a homogeneous magnetic field that simulates the real Earth's magnetic field in orbit. Circular and square coils, both with square cross section, are considered. Practical considerations such as wire selection, wire-wrapping efficiency, wire bending radius, choice of power supply, and inductance and time response are included. Numerical calculations of the magnetic flux density, the values of the magnetic field strength vectors in various directions are presented. The main goal of creating this simulator is to test the development of algorithms for orientation and control of the spacecraft, to improve the functioning of the components of the satellite in the Earth's orbit

**Index Terms**— Coil system, Helmholtz coils, Magnetic field, uniform field.

## I. INTRODUCTION

AT THE initial stages of development and design of the spacecraft (spacecraft), a hierarchical development of all functioning satellite subsystems is assumed. One of the most important service subsystems is the satellite attitude control system. To determine the orientation, various sensors, such as stellar, solar and magnetic sensors, can be used.

With the use of systems for determining the orientation based on the functioning of a magnetic sensor integrated into the onboard platform of a spacecraft, it is proposed to obtain these vectors of the Earth's magnetic field strength.

To test the operation of the designed control systems for spacecraft orientation, testing is conducted in laboratory conditions using various stands, simulators with which the conditions of outer space are simulated.

For this purpose, it is supposed in the laboratory conditions to create the imitation conditions of the geomagnetic field as much as it affects the onboard equipment and components of the satellite and the adequate functionality of the control algorithms for control and orientation of the spacecraft.

**A. MUKHAMEDGALI**, is with Dept. of Mechanics and Mathematics of Kazakh National University named after al-Farabi, Almaty, Republic of Kazakhstan, (e-mail: [adilmukhamedgali@gmail.com](mailto:adilmukhamedgali@gmail.com)).

**Z. B. RAKISHEVA**, is with Dept. of Mechanics and Mathematics of Kazakh National University named after al-Farabi, Almaty, Republic of Kazakhstan, (e-mail: [zaure.ra@gmail.com](mailto:zaure.ra@gmail.com)).

There is a need to test and verify the developed algorithms for controlling a satellite with a magnetic orientation system in simulated conditions before it is put into orbit in order to minimize the risk of fail-safety of space borne space vehicles. For this goal in this paper, we are traditional Helmholtz coils design. One device capable of generating a uniform magnetic field is the Helmholtz coil [1]. The Helmholtz coil is named after Hermann von Helmholtz (1821-1894), a German scientist and philosopher known for his contributions to electrodynamics, mathematics, and meteorology among many other sciences [1].

The system of solenoid coils or Helmholtz coils [2-4] is often used for generating homogeneous field and calibration magnetic fields sensors. General analysis of the magnetic field in Helmholtz coils and has been presented in [4-7]. However, it is noticed that the homogeneous region of magnetic field in As shown in Fig. 1, a Helmholtz coil consists of a pair of coils parallel to each other where each coil consists of number N wrappings. A magnetic field B results when charge is in motion, i.e. as current I passes through the coil pair.

## II. THEORETICAL DESCRIPTION

The Helmholtz coils illustrated in Fig.1 consist of two circular or square coils of the radius R or diameter D, arranged at a distance R or D from each other. The coils with current source are generating a homogeneous field [8]. According of the law of Bio-Savart-Laplace, the resulting of homogeneous field of two coils is equal to the vector sum of the fields generating by one coil.

The homogeneous field by one coil can be calculating according to (1):

$$B(z) = \frac{\mu_0 N I R^2}{2(R^2 + (z-h)^2)^{3/2}} \quad (1)$$

where:

$\mu_0$  - the magnetic permeability of vacuum, H/m;

$N$  - number of turns of each coil-;

$I$  - Current in the coils, A;

$z$  - the axis which generating of magnetic field, m;

$R$  - radius of coils, m;

$h$  - distance of the coil center from the beginning of the coil center coordinates, m.

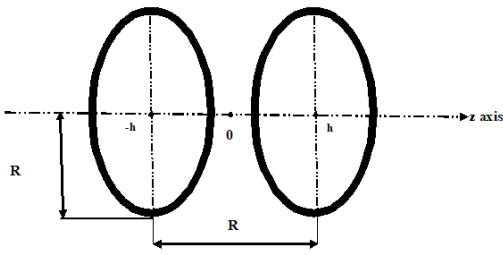


Fig.1. Geometric pattern of coils

Axial field of two coils can be calculated by formula:

$$B(z) = \frac{\mu_0 N I R^2}{2} \left\{ \left[ R^2 + (z + h)^2 \right]^{-\frac{3}{2}} + \left[ R^2 + (z - h)^2 \right]^{-\frac{3}{2}} \right\} \quad (2)$$

For calculating of Helmholtz, coils take the following form:

$$h = \frac{R}{2},$$

$$B(z) = \frac{\mu_0 N I R^2}{2} \left\{ \left[ R^2 + \left( z + \frac{R}{2} \right)^2 \right]^{-\frac{3}{2}} + \left[ R^2 + \left( z - \frac{R}{2} \right)^2 \right]^{-\frac{3}{2}} \right\} \quad (3)$$

Consider the successive derivatives of  $B(z)$  for estimate the homogeneity of the field in center of the coil system. A higher order of the first non-zero derivative at this point provides better homogeneity of the field in its vicinity[2].

Equation (3) can be expanded in a Taylor series in the variable  $z$  near zero:

$$B(z) = B(0) + \frac{1}{2} B^{(2)}(0) z^2 + \frac{1}{24} B^{(4)}(0) z^4 + \frac{1}{720} B^{(6)}(0) z^6 + \dots \quad (4)$$

Since the coils according to the Fig.1 are located at a distance of the radius from each other, the second derivative in the central system becomes zero. Then the change in the field  $\Delta B$  when moving from the point  $z = 0$  is given by (5) and has a fourth order of smallness:

$$\Delta B(z) = \frac{1}{24} B^{(4)}(0) z^4 + \frac{1}{720} B^{(6)}(0) z^6 + \dots \quad (5)$$

To determine the magnetic field according to the geometric center ( $z=0$ ) of the coils is determined by the following expression:

$$B(0) = \frac{16}{5\sqrt{5}} \frac{1}{2} \frac{\mu_0 N I}{R} \quad (6)$$

### III. THE DESIGN AND SIMULATING OF HELMHOLTZ COILS

The all of the design and simulating of coils was done in COMSOL Multiphysics software showed in Fig. 2.

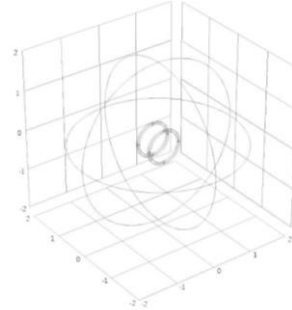


Fig.2. Geometry of Helmholtz coils in COMSOL

The simulating of the magnetic field produced by using module mf as only it allows you to use the section Multi-Turn Coil Domain for simulating this coil in 3D.

The grid size of coils was set 0.02m. The grid size of outer sphere was chosen Coarse

The two coils have a closed geometry with a circular cross-section perpendicular to the z-axis.

In addition, type of coil was choose of Circular type. The direction of the current in the coils corresponds to the geometric form of the coils, that is, along a circle in one direction in each of the coils in the direction of which our magnetic field is generated.

The Fig.3, 4 shows the generating finite element mesh.

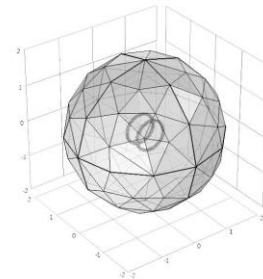


Fig.3. Generation the finite element mesh

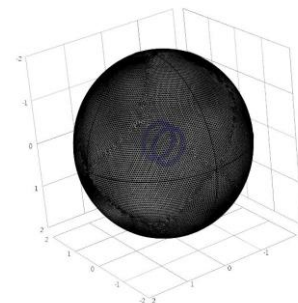


Fig.4. Generation the finite element mesh

After designing the Helmholtz coils in this program, we simulated our homogeneous field in the region of these coils.

The results showed the propagation and direction of the magnetic field vectors in the region of the generated field.

The simulation results of coils at a current power of 0.25 mA for the axial direction are showed in the Fig.5.

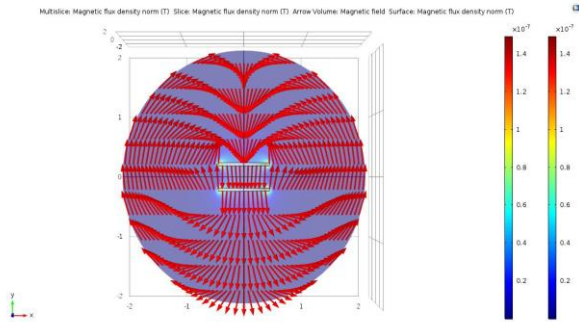


Fig.5. The distribution of the magnetic field in Helmholtz coils

As you can see in the Fig.6, the generated uniform field is concentrated in the central regions of the coils. The genetically determined field is measured in Tesla.

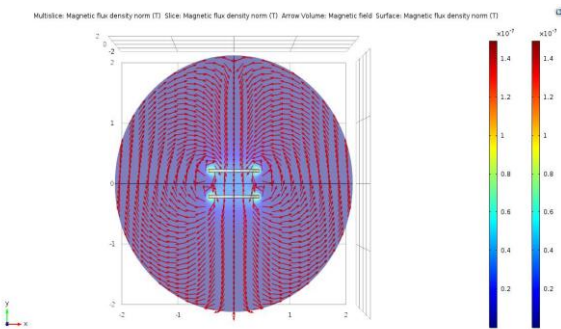


Fig.6. The distribution of the magnetic field in Helmholtz coils

The orientation of the vectors of the strengths of the generated uniform magnetic field is also illustrated in the Fig.7.

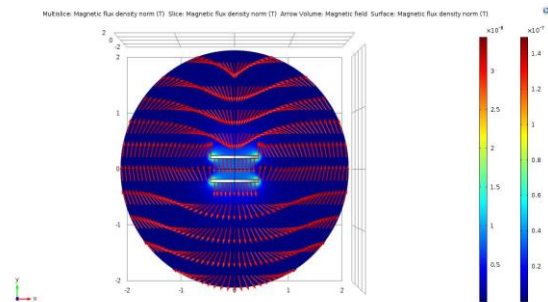


Fig.7. The distribution of the magnetic field in Helmholtz coils

Red and yellow-green colors are the places of maximum generation of a homogeneous field showed in Fig.8

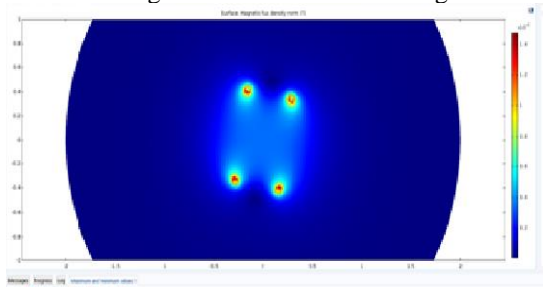


Fig.8. The areas of maximum generation of a magnetic homogeneous field

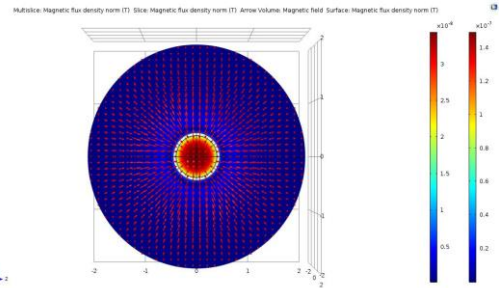


Fig.9. The distribution of the magnetic field in Helmholtz coils

IV. THE DESIGN OF SQUARE COILS

Square coils can be utilized instead of circular coils in the design as they provide a wider uniform field parallel to the coils as compared to circular coils.

The governing equation for the magnetic field  $B(z)$  can be calculated by formula:

$$B(z) = \frac{\mu_0 N I R^2}{2(d^2 + (z-d)^2)^{3/2}} \tag{7}$$

To simulate the magnetic field, a system of three pairs of square coils arranged usually perpendicular to one another (the Helmholtz cage) is used.

The sides of the squares of the coils are 2 m, 1,9 m, 1,8 m. When a current flows through the coils in the region inside the cell, a uniform magnetic field is created, the direction and magnitude of which depend on the strength and direction of the current in the coils.

Below this a description to design a 3 D model of cage we used SolidWorks software of the stand with the corresponding notation for the coils along the X-green, Y-red, Z-blue axes showed in Fig.10.

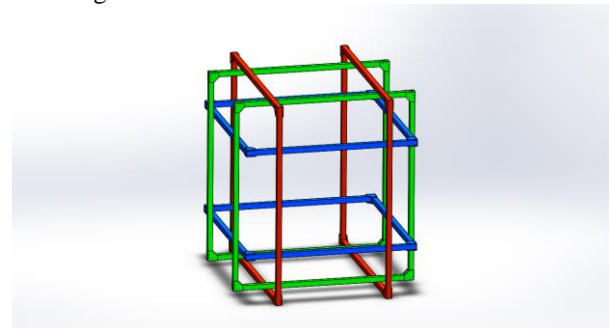


Fig.10. 3D model of Helmholtz cage

The all of the design and simulating of coils was done in COMSOL Multiphysics software.

For our goals, we designed each pair of coils separately showed in Fig.11.

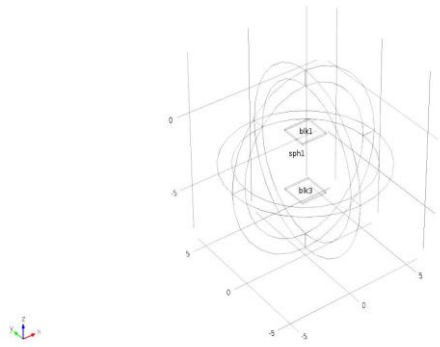


Fig.11. Geometry of square coil

The geometry of square coils showed in Fig.12.

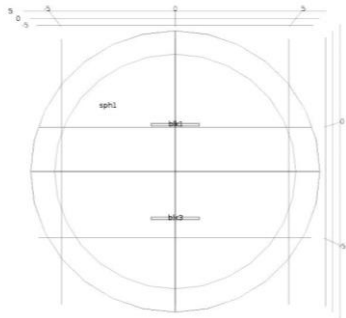


Fig.12. Geometry of square coils

In COMSOL Multiphysics, the AC/DC mf ('magnetic field') toolbox was used to simulate multi-turn coils with AWG12 wire (American Wire Gauge, Brown&Sharpe), which we also used to construct the coil later on. The coils have a closed geometry with a circular cross section and each wire is insulated.

Around the coils, we created a sphere of air with a diameter of 6 meters and an infinite sphere around the air sphere with 1-meter thickness (see Fig.12). The direction of current flow was specified by manually selecting a cross-sectional area of each coil, using the numeric coil type.

We used 1 A input current for the coils, which are connected in series.

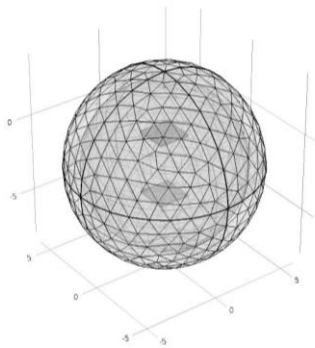


Fig.13. Output sphere with coils in finite mesh

The Fig.14 shows the external environment and coils without finite mesh

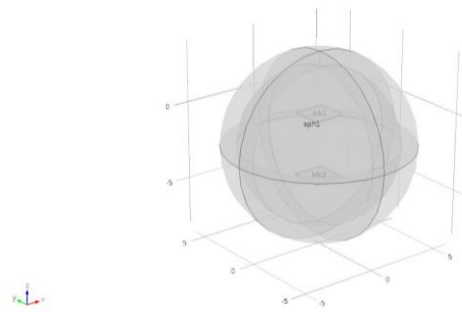


Fig.14. Output sphere with coils without finite mesh

After designing the Helmholtz coils in this program, we simulated our homogeneous field in the region of these coils. The results showed the propagation and direction of the magnetic field vectors in the region of the generated field.

The simulation results of coils at a current power of 0.5 A for the axial direction are showed in the Fig. 15.

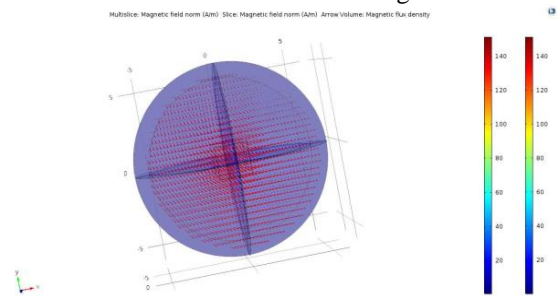


Fig.15. The distribution of the magnetic field in square coils

The orientation of the vectors of the strengths of the generated uniform magnetic field is also illustrated in the Fig.16

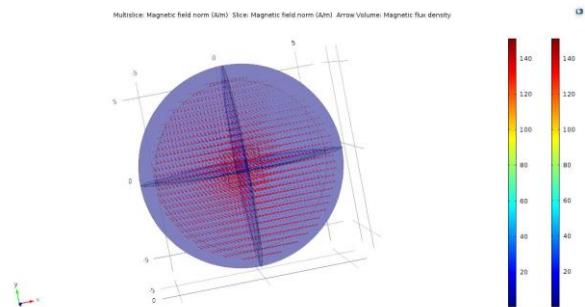


Fig.16. The distribution of the magnetic field in square coils

V. CONCLUSION

This article describes the basic theoretical and apathetic calculations of calculating Helmholtz coils to create a uniform magnetic field.

With models of circular coils, their geometric characteristics were modelled, 3D models of coils, models of the homogeneity of the magnetic field, and visualization of the direction of the stress vectors.

Based on these calculations given in this paper, it is entirely possible to create larger circular coils to create a stronger uniform magnetic field.

For designing Helmholtz coils of square type, theoretical and analytical models were analyzed, their geometric

characteristics, 3D models of coils and visualization of the homogeneity of the magnetic field in these coils were modelled.

In future works, it is planned to correct the results in the design of the Helmholtz coils of square type. Recalculations of geometric characteristics, created homogeneity of the magnetic field, visualization of the orientation of the tension vectors in these coils will be done to realize a real model of these types of coils in assembly form.

It is also planned to use methods of amplification of a homogeneous magnetic field, taking into account the complexity of implementing their design as for a circular or square type, or in the arrangement of these two types of coils.

It is also possible to analyze the Helmholtz coils between existing coils, in order to compare the generated uniform magnetic field.

In addition, carrying out a comparative analysis of their geometric characteristics and reliability for creating real models.

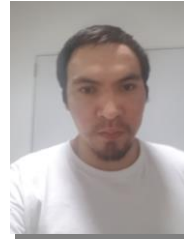
#### ACKNOWLEDGMENT

This work has been supported financially by the research project №AP05132939 «Control system design of the satellite formation motion for remote sensing of the Earth», for 2018-2020 of the al-Farabi Kazakh National University, which is gratefully acknowledged by the authors.

#### REFERENCES

- [1] Thesis Megan R. Brewer. Cubesat Attitude Determination and Helmholtz coil design. USA: Air force institute of technology, 19-20 (2012).
- [2] Thesis R.A. Schill, and H. Karin "Characterizing and calibrating a large Helmholtz coil at low ac magnetic field levels with peak magnitudes below the earth's magnetic field," Review of Scientific Instruments, 2001, vol. 72, no 6, pp. 2769–2776. [2] Po Gyu Park, et al., "AC magnetic flux density standards in the low frequency range," in Proc. Conf. Dig. CPEM, June 2008, pp. 456–457. [3] Po Gyu Park, et al., "AC/DC magnetic flux density standard systems at KRISS," in Proc. Conf. Dig. CPEM, June 2010, pp. 312–313.
- [3] Chapters J. C. Maxwell, "A Treatise on Electricity and Magnetism," Clarendon, Oxford, 1873, vol. I, Secs. 713, 714, and 715.
- [4] Chapters D. Lorrain and D. R. Corson, "Electromagnetism," Freeman, San Francisco, 1979, Chap. 8.
- [5] Chapters J. D. Kraus, "Electromagnetics," 2nd ed., McGraw–Hill, New York, 1973, Chap. 4.
- [6] Chapters P.M. Fishbane, S. Gasiorowicz, and S.T. Thornton, "Physics for Scientists and Engineers," 2nd ed., Prentice Hall, New York, 1996, Chap. 30.
- [7] Thesis Vitalia E. Baranova, Pavel F. Baranov. Cubesat The Helmholtz Coils Simulating and Improved in COMSOL Russian Federation: National Research Tomsk Polytechnic University, 1-2 (2014).

#### BIOGRAPHIES



**MUKHAMEDGALI ADIL** Republic of Kazakhstan, Almaty City, in 1991. He received the B.S. degree in mechanical engineering and M.S. degree in space technic and technologies from the Kazakh National University named after Al-Farabi, Almaty city, B.S. in 2012 and M.S. in 2014. Since 2014, he has been assistant professor, senior teacher Department of the Department on Mechanics of al-Farabi Kazakh National University. He is the author of 8 articles, and then 4 international conferences.

His research interests include magnetic field modeling, nature of the geomagnetic fields, motion control and optimization, dynamics of nano- and microsattellites, applications in space engineering and technologies.



**ZAURE RAKISHEVA** Balkhash, Karaganda City, in 1964. She received the degree of specialist in mechanics from the M.V. Lomonosov Moscow State University, USSR, in 1986 and the Ph.D. degree in mechanics from Kazakh State University (now al-Farabi KazNU), Almaty, Kazakhstan, in 1993.

From 1986 to 1996, she worked as engineer and researcher in the Scientific-Research Institutes of Academy of Sciences of Kazakhstan. Since 1996, she has been a Teacher, Associate Professor, Professor and Head of Department of the Department on Mechanics of al-Farabi Kazakh National University. She is the author of seven books, and more than 100 articles. Her research interests include dynamics of solid bodies, motion control and optimization, dynamics of nano- and microsattellites, applications in space engineering and technologies.

# Harmonic Analysis of Electros spindle System with Wavelet Packet Transform

I. Kiyak

**Abstract**— The electros spindle systems have been used in the maritime industry, they have recently become operative in automation systems. Along with the widespread use of harmonic generating machines and semi-conductor-based circuits in power and control systems, known reactive power compensation methods have been replaced by the use of filter-based compensation systems that consider harmonic distortion. This study used a voltage signal generated by an electros spindle generator with high harmonic distortion to obtain the amplitude time variation of the fundamental component by using Discrete Wavelet Packet Transform (DWPT). As a result of the analysis, it was observed that this method gives fast and accurate results that can be also used in real-time applications.

**Index Terms**— Electros spindle, discrete wavelet packet transform(DWPT), harmonic analyses, DC motor.

## I. INTRODUCTION

**E**LECTROSPINDLE POWER and motion production systems are composite machines used to produce rotational motion. The first use of these systems is known as the movement suppliers of analog gyroscopes on ships. Subsequently, they began to be used in computer hard disk drive circuits and CNC machines. Nowadays, they are also used in automation systems [1,2].

Today, electricity is produced and distributed only as alternating current energy. The alternating current the consumers draw from the grid consists of two components, the active current and the reactive current. The active power produced by the alternating current is made useful by the consumer, but the reactive power produced by the reactive current does not turn into useful power. Although reactive power cannot be turned into active power, it cannot be totally abandoned. The magnetic field required for normal operation of all operating devices, such as generators, transformers, coils and motors operating according to the electrodynamics principles, is introduced by the reactive current. The most important loads that require industrial compensation include low-voltage synchronous machines, transformers, coils, overhead lines, synchronous motors, rectifiers, induction furnaces, electric arc furnaces, welding machines, induction welding machines, lamp ballasts, rolling mills, electrical circuitry of rolling mills and asynchronous motors [3,4].

**I. KIYAK**, is with Department of Electrical and Electronics Engineering, Marmara University, 34722, Istanbul, Turkey, (e-mail: [imkiyak@marmara.edu.tr](mailto:imkiyak@marmara.edu.tr)).

Manuscript received July 17, 2018; accepted October 28, 2018.  
DOI: [10.17694/bajece.444567](https://doi.org/10.17694/bajece.444567)

Harmonic filters are basically divided into two categories; active filters and passive filters. Active filters are commercially produced and usually used for power factor correction in high-power applications. Passive filters are preferred in cost-effective applications without high energy [5].

The purpose of harmonic filters is to reduce or eliminate the effects of currents or voltages in one or more frequencies, i.e. the level of harmonics. It is aimed to eliminate the technical and economic inconveniences resulting from harmonics caused by filters. The tasks of harmonic filters are;

- To correct the voltage fluctuation of a load fed from a harmonic generating device,
- To prevent unwanted harmonic components introduced into the AC system,
- To eliminate radio frequency interference [6].

Harmonics that occur in power systems cause improper operation or no operation of equipment, overheating of transformers and motors, interference on communication lines, improper measurements, reduction of the service lives of electrical devices, increased power losses of receivers and systems [7,8]. Additionally, harmonics cause serious problems resulting from resonance in compensation units that are used in industrial plants for correcting the power factor [9,10].

Wavelet analysis is a very powerful signal processing method, especially in the analysis of non-stationary signals [5].

The increase in the operating temperatures of electrical machinery is the most effective parameter influential in the machine's lifespan. The loading period and switching of the machine, operation in hot environment, harmonics and unbalanced operation are the most important factors that increase the operating temperature of the machine[11,12].

This study used a voltage signal generated by an electros spindle generator with high harmonic distortion to obtain the amplitude time variation of the fundamental component by using Discrete Wavelet Packet Transform (DWPT). As a result of the analysis, it was observed that this method gives fast and accurate results that can be used in real-time applications.

## II. DATA ACQUISITION SYSTEM

The system for receiving data from DC shunt motor-synchronous generator-based electros spindle motor is schematically shown in Figure 1 [13].

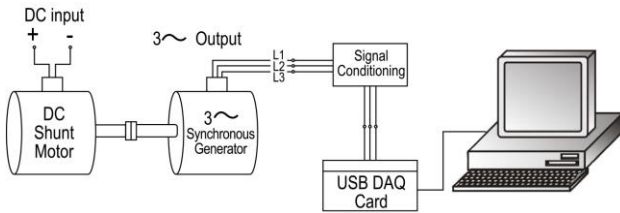


Fig. 1. Schematic Diagram of Data Acquisition System

The real-time data reception link picture of the system components and their connections is shown in Figure 2.



Fig. 2. Data acquisition system used in the study

USB data acquisition card has 14 bit, 48 kS/s analog digital converter. Rotation speed of DC shunt motor is 6000 rpm, their output voltage is 18 V and their power is 11 W. Pole number of synchronous generator is four and their frequency is 200 Hz.

Firstly, the voltages generated by the synchronous electrospindle generator were recorded with the data acquisition card at the sampling frequencies of 1600, 4000, 6400 and 12400 Hz. The voltage values of the phase are given in Figure 3-6.

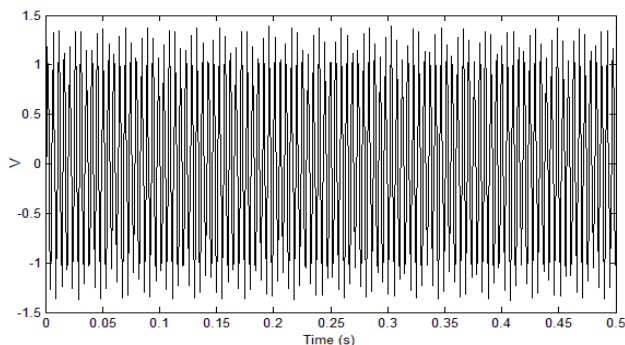


Fig. 3. A phase voltage of electrospindle generator with a sampling frequency of 1600 Hz

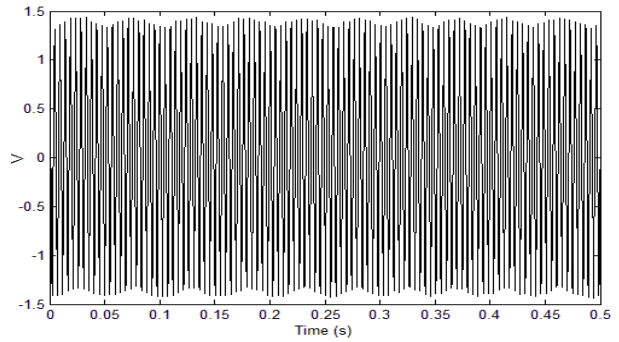


Fig. 4. A phase voltage of electrospindle generator with a sampling frequency of 4000 Hz

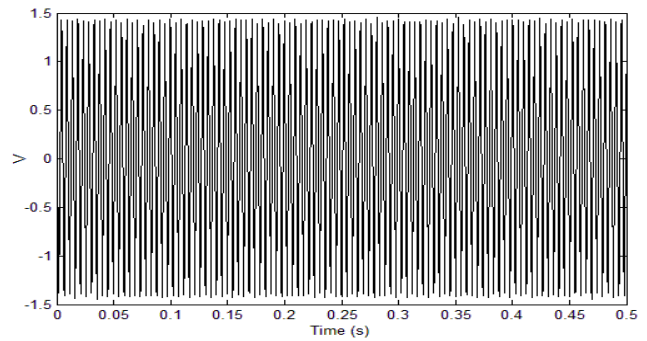


Fig. 5. A phase voltage of electrospindle generator with a sampling frequency of 6400 Hz

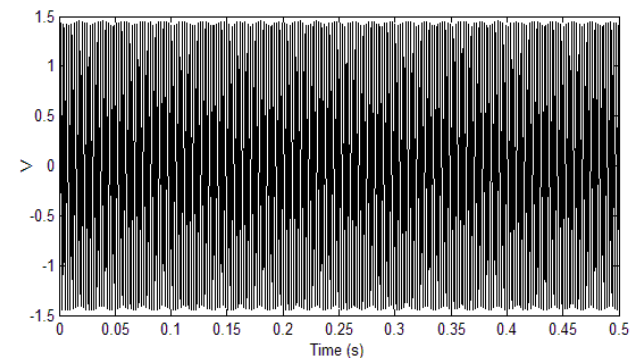


Fig. 6. A phase voltage of electrospindle generator with a sampling frequency of 12400 Hz

### III. DISCRETE WAVELET PACKET TRANSFORM (DWPT)

After finding the fundamental component of the generated voltages, it is necessary to obtain the amplitude time change of this component. One of the most effective methods to accomplish this is to use Discrete Wavelet Packet Transform (DWPT). With discrete wavelet packet transform, the voltage can be divided into components with fewer coefficients. This is accomplished with low-pass ( $g^{(n)}$ ) and high-pass ( $h^{(n)}$ ) filter banks and down-sampling (equations 3-4) [9-15].

$$x_1^1(n) = \sum_k X(k)h(2n-k) \quad (1)$$

$$x_2^1(n) = \sum_k X(k)g(2n-k) \quad (2)$$

Here,  $X(k)$  is discrete input signal,  $x_1^1(n)$  and  $x_2^1(n)$  are

the filter outputs, coefficients are half of  $X(k)$ ,  $x_1^1(n)$  and  $x_2^1(n)$  that are again passed through wavelet filters, and secondary level components are found, while the number of coefficients is again reduced by half [15-16].

$$x_3^2(n) = \sum_k x_1^1(k)h(2n-k) \quad (3)$$

$$x_4^2(n) = \sum_k x_1^1(k)g(2n-k) \quad (4)$$

$$x_5^2(n) = \sum_k x_2^1(k)h(2n-k) \quad (5)$$

$$x_6^2(n) = \sum_k x_2^1(k)g(2n-k) \quad (6)$$

The same procedure is applied to the second level components to find the third level components, and the number of coefficients is again reduced by half [9-15].

$$x_7^3(n) = \sum_k x_3^2(k)h(2n-k) \quad (7)$$

$$x_8^3(n) = \sum_k x_3^2(k)g(2n-k) \quad (8)$$

$$x_9^3(n) = \sum_k x_4^2(k)h(2n-k) \quad (9)$$

$$x_{10}^3(n) = \sum_k x_4^2(k)g(2n-k) \quad (10)$$

$$x_{11}^3(n) = \sum_k x_5^2(k)g(2n-k) \quad (11)$$

$$x_{12}^3(n) = \sum_k x_5^2(k)h(2n-k) \quad (12)$$

$$x_{13}^3(n) = \sum_k x_6^2(k)g(2n-k) \quad (13)$$

$$x_{14}^3(n) = \sum_k x_6^2(k)h(2n-k) \quad (14)$$

Thus, in the third level decomposition, eight components are obtained [9-16].

#### IV. EXPERIMENTAL STUDY

In order to apply the same wavelet tree to the voltages given in Figures 3-6, the number of data must be the same. For this purpose, the numbers of data of all voltages are converted to 6400 samples [13]. db20 was used as the main wavelet, and the number of coefficients and frequency ranges of the obtained wavelet components are given in Table 1 [7,9,18].

TABLE I  
WAVELET PACKET DECOMPOSITIONS AND FREQUENCY RANGE

| Decomposition | Frequency Range (Hz) | Number of Wavelet Coefficients |
|---------------|----------------------|--------------------------------|
| $x_7^3(n)$    | 2800 ~ 3200          | 400                            |
| $x_8^3(n)$    | 2400 ~ 2800          | 400                            |
| $x_9^3(n)$    | 2000 ~ 2400          | 400                            |
| $x_{10}^3(n)$ | 1600 ~ 2000          | 400                            |
| $x_{11}^3(n)$ | 1200 ~ 1600          | 400                            |
| $x_{12}^3(n)$ | 800 ~ 1200           | 400                            |
| $x_{13}^3(n)$ | 400 ~ 800            | 400                            |
| $x_{14}^3(n)$ | 0 ~ 400              | 400                            |

As seen in Table 1, the frequency range of  $x_{14}^3(n)$  was 0-400 Hz, and it contained the fundamental component frequency. By removing the other seven components, the filtered voltages were obtained (Figure 7-11) [7,9,18].

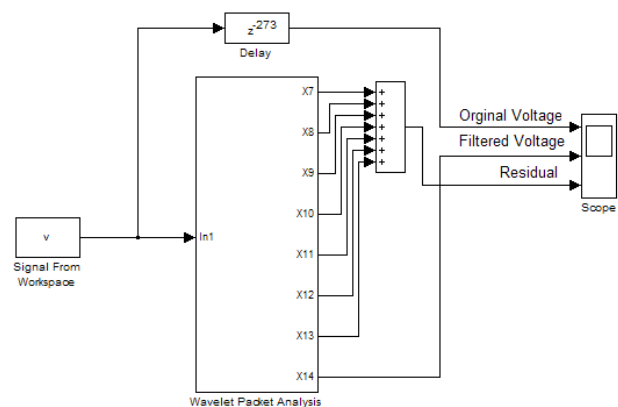


Fig. 7. Simulink Circuit

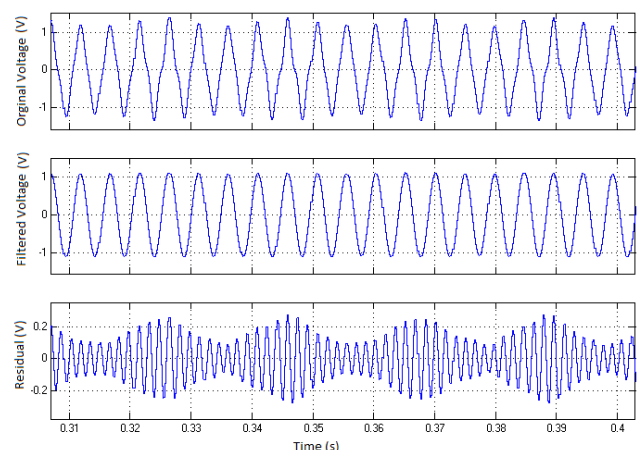


Fig. 8. Generator voltage filtered at 1600 Hz sampling frequency

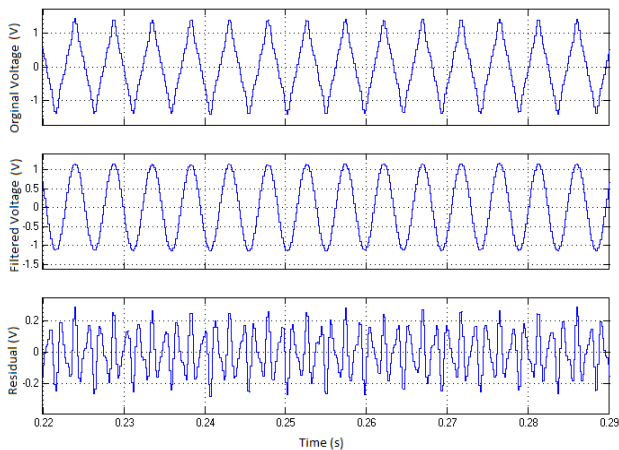


Fig. 9. Generator voltage filtered at 4000 Hz sampling frequency

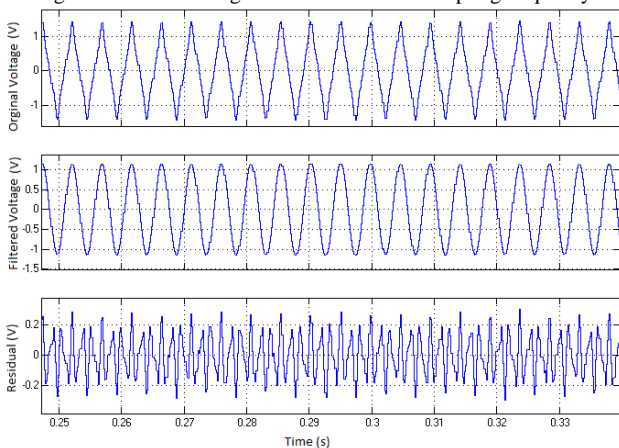


Fig. 10. Generator voltage filtered at 6400 Hz sampling frequency

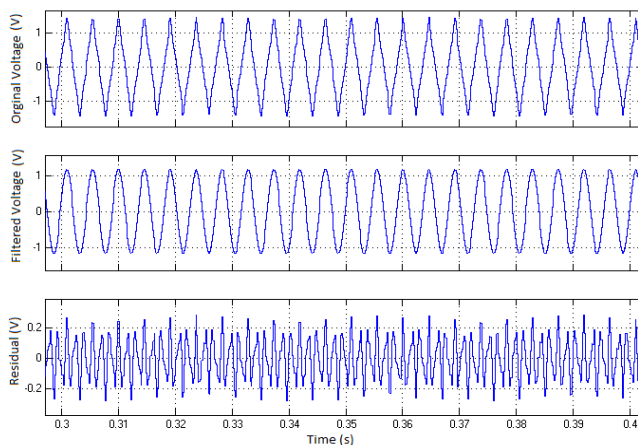


Fig. 11. Generator voltage filtered at 12400 Hz sampling frequency

When the previous study [13] is examined, it seen that residual of original voltage comprises from 300-800 Hz harmonic components in Fig.8, the second residual of original voltage comprises from 300-1000 Hz harmonic components in Fig 9, the third and last residual of original voltage comprise from 300-2700 Hz harmonic components in Fig 10,11. The filtered voltages always have fundamental frequency around 200 Hz and its shape is close pure sine waveform.

## V. CONCLUSION

This study aimed to obtain a more sinusoidal output voltage by removing the harmonics in the output voltage of an electrospindle generator. With DWPT, the generator

voltages are divided into components at different frequencies and the fundamental component and harmonic components are obtained.

The filtered voltages given in Figures 8-11 represent the fundamental component, while the residuals represent the sum of the voltages that cause harmonic distortion. The wave shape of the fundamental component was very close to sinusoidal. The Residual values were around 0.2 V. Different residual changes were observed at each sampling frequency. This was because, as the sampling frequency varies, the frequency range covered by the harmonics also varies.

The obtained filtered voltages will increase the operating performance of the gyroscope, but if the gyroscope's nominal operating values are taken into consideration, it may be necessary to increase the output voltage generated by the generator or increase the filtered voltage due to reduction in the amplitude of the filtered voltage.

## REFERENCES

- [1] Tamisier V., Font S., Lacour M., Carrere F., Dumur D., Attenuation of Vibrations due to Unbalance of an Active Magnetic Bearings Milling Electro-Spindle, *CIRP Annals- Manufacturing Technology* Vol. 50, Issue 1, 2001, p. 255-258.
- [2] Ziran, L., Wen J., Tao, He., Application of Adaptive Filtering Based on Harmonic Wavelet in the Dynamic Unbalance of Electro-Spindle, *Measuring Technology and Mechatronics Automation (ICMTMA), 2010 International Conference on*, DOI: 10.1109/ICMTMA.2010.348, 13-14 March 2010.
- [3] <http://www.mathworks.com/help/matlab/math/fast-fourier-transform-fft.html>. Access date 25.03.2014.
- [4] Kiyak, İ., Gökmen, G., Kentli, F. "Estimation End Effect of Single-Sided Linear Induction Motor by Using Discrete Wavelet Packet Transform and Artificial Neural Network" *International Review of Electrical Engineering*, Vol.6, n.5, 2011, p.2277-2285.
- [5] Robertson C. D., Camps O. I., Mayer J. S., Gish W. B. Wavelets and Electromagnetic Power System Transients. *IEEE Transaction on Power Delivery*, Vol.11, 1996, No. 2, p. 1050-1058.
- [6] The Mathworks, Inc. Signal processing toolbox. User's guide, R2013b, 2013, p. 27-413.
- [7] Gokmen G. Wavelet based reference current calculation method for active compensation systems. *Electronics and Electrical Engineering*, Vol. 108, No. 2, 2011, p. 61-66.
- [8] Onat, N., Kiyak, İ., Gökmen, G. "Experimental Wavelet Packet Transient-State Analysis of Electrical Machines Directly Fed by Photovoltaic Cells" *International Review of Electrical Engineering*, vol. 5, n.5, 2010, p. 2081-2087.
- [9] Janicek F., Mucha M., Ostrozlik M. A new protection relay based on a fault transient analysis using wavelet transform. *Journal of Electrical Engineering*, Vol. 58, No. 5, 2007, p. 271-278.
- [10] <http://www.mathworks.com/help/matlab/ref/fft.html>. Access date 25.03.2014.
- [11] Zhu H., Cai M., Wang Q., Chen Y., Controller of High-speed Electro-spindle with AC HMBs Based on Optimal Control Theory, power electronics and motion control conference (IPEMS'2009) *IEEE international*, V.978, Pp.3557-3563.
- [12] Baggini A., Hanzelka Z., Voltage and current harmonics, *Handbook of Power Quality*, John Wiley & Sons Press, England, 2008, p. 241-249.
- [13] Gökmen G., Analog jiroskop sistemlerinde kullanılan elektromekanik döner milli generatörün frekans analizi, *DÜMF Mühendislik Dergisi*, Vol.9, No. 2, 2018, p. 671-677.
- [14] Deng H., Ling H. Fast solution of electromagnetic integral equations using adaptive wavelet packet transform. *IEEE Transaction on Antennas and Propagation*, Vol. 47, No. 4, 1999, p. 674-682.
- [15] The Mathworks, Inc. wavelet toolbox. User's guide, R2014a, 2014, p. 138-224.
- [16] <http://www.mathworks.com/help/signal/ug/resampling.html>. Access date 25.03.2014.
- [17] Saleh S. A., Rahman M. A new transient model for three-phase power transformers using a wavelet filter bank. *IEEE Transaction on Power Delivery*, Vol. 20, Issue 2, 2005, p. 1409-416.

- [18] Akinci, T.C., Time- Frequency Analysis of the Current Measurement by Hall Effect Sensors for Electric Arc Welding Machine, *Mechanika*, 5(85), 2010, p. 66-71.

#### BIOGRAPHY



**ISMAIL KIYAK**, was born in 1977. He received B.S, M.S and PhD degrees from Marmara University, Istanbul, Turkey. He has been working as a Assoc. Prof. Dr. at Marmara University. His current interests are renewable energy sources, lighting technique, vocational education.

# Smart Techniques' Implementation for Small Entities and Central Power Grid in Almaty, Kazakhstan: Challenges and Possibilities

G. B. Nurpeissova, D. V. Panyukova, and A. T. Nurpeissov

**Abstract**— With growth of renewable energy sources' use the uncertainty in power grids is increasing tremendously. Optimal control and the equipment dispatching become challenging task for both central supplier and power consumer. Implementation of smart approach gives opportunity to provide such control with less human resources and power losses. In the article recently used techniques for control and dispatching in central grid of Almaty is described. Beside that new smart control methods and their possibilities within power system of Kazakhstan are reviewed. As a result, best solutions for the power system's control in both small entities and central grid are proposed.

**Index Terms**— Dispatching, optimal control, power grid, power system, renewable energy sources, smart grid.

## I. INTRODUCTION

CONTROL AND DISPATCHING of central power supply were always associated with variety of power demand. Its random nature was overcome by advanced forecasting of main grid parameters and by strict policy for industrial costumers' planned demand. But nowadays this approach is becoming less and less effective; because of wide spread usage of renewable energy sources (RES).

According to [1] RES' use worldwide has grown up to 20 555 TWh at 2012. And will not stop and reach incredible 55 000 – 85 000 TWh in 2050. In Kazakhstan trends are not as good yet. So, according to the forecast balances of the Ministry of Energy of the Republic of Kazakhstan [2] in next 6 years the internal power demand in the republic will increase by 2.4 billion kWh annually. Concurrently power output of existing stations will be orderly lowered for 1.5 billion kWh annually till 2023. It is planned to accomplish by both commissioning new stations and active use of renewable

**G. B. NURPEISSOVA**, is with Engineering School, Eurasian Technological University, Almaty, Kazakhstan.

**D. V. PANYUKOVA**, is with Department of Automation and Control, The Kazakh National Research Technical University after K.I.Satpaev, Almaty, Kazakhstan, (e-mail: [haleth@mail.ru](mailto:haleth@mail.ru)).

**A. T. NURPEISSOV**, is with Engineering School, Eurasian Technological University, Almaty, Kazakhstan.

Manuscript received May 14, 2018; accepted October 20, 2018.  
DOI: [10.17694/bajece.475538](https://doi.org/10.17694/bajece.475538)

energy sources. Thus renewable energy sources use will grow by 0.5 billion kWh annually till 2020 and 1 billion kWh annually till 2023.

RES are working directly on natural power gained from water, wind, sun, temperature. Most of those sources are partly predictable. Hence RES' use brings even more uncertainty in power grid either central or private. And power grid's dispatching and control become even more complex task.

Main goal for dispatching and control is to provide correct amount of power for customers with decreasing of power losses and power cost. It can be achieved both by reducing distance between supplier and customer and by minifying number of power plants and other equipment.

The techniques recently used in Kazakhstan's power grids are described in "Actual central grid" chapter of the article.

"New approaches" chapter is devoted to several approaches that are offered by international scientists and engineers.

At "Implementation perspectives" chapter possibilities and challenges of previously described methods in Kazakhstan are discussed.

In "Conclusion" general review of future perspectives of power grid control in the republic is provided.

## II. ACTUAL CENTRAL GRID

In Kazakhstan power grid's work regulates by market system and norms of governmental standard 32144-2013 "Electric energy. Electromagnetic compatibility of technical equipment. Power quality limits in the public power supply systems" [3]. It fully matches European standard EN 50160:2010 "Voltage characteristics of electricity supplied by public distribution networks" [4].

The standard [3] reveals values and norms of electric power quality at delivery point of 50 Hz of alternating current (AC) from general purpose power grid to customer of low, middle and high voltage. It includes frequency, values and forms of voltage and symmetry of voltages in three-phase systems. Also [3] regulates accidental changes in forms of voltage that leads to voltage deviation from rated. Such accidents occur from hardware damages of the grid or external effects (from nature or human factor). They include voltage interruption, voltage fall, voltage swell and impulse voltages.

Nonregulated decisions are made according to trade factors. Structure of wholesale market of electric power in the republic includes:

- Decentralized sale and purchase power market (bilateral purchase/sale agreements);
  - Centralized power market, where purchase and sale of power for short-term (spot-trading), middle-term (week, month) and long-term (quarter, year) is provided;
  - Real time balancing market, working for physical and financial regulation of hourly misbalances, appeared daily between real and agreed supply-consumption of electric power which is described in [5];
  - System and supplementary service market;
  - Electrical capacity market.
- System operator of Kazakhstan's central power grid is KEGOC JSC by order 61 of Ministry of Energy of Republic of Kazakhstan by 17.10.2014. And its' functions are:
- to provide system service for transmission of electrical energy by national power grid according to an agreement, ensure its' technical maintenance;
  - to provide system service for technical dispatching and centralized real time control of power grid's operating regimes according to agreements, including planning of power balances and daily graphic of supply-demand of electric power;
  - to ensure operational reliability of power grid in the republic;
  - to provide system service for regulation of electrical capacity;
  - to provide system service for balancing supply-demand of electric power;
  - to perform financial regulation of electric power misbalances strictly according to laws and regulations of Republic of Kazakhstan;
  - to determine amount, structure and distribution of power reserves between power supplying entities and also involvement of power reserves in central grid's work;
  - to provide real time functionality of the balancing market of electric power as well as the system and supplementary service market;
  - to cooperate with power grids of neighboring countries to control and stabilization of parallel work regimes and electric power regulation;
  - to provide technical and methodological guidance to create united information system, automation system of commercial accounting of electric power, associated hardware of relay protection and emergency controls for all entities of electric power's wholesale market;
  - to ensure equal terms for access to the central power grid;
  - to provide all necessary information excluding commercial or other legally protected secret for all entities of electric power's wholesale market;
  - to coordinate a release for maintenance of main equipment of power plants, transformer plant, electrical energy transmission line, relay protection and emergency controls, technological control systems and to ensure their availability for service;
  - to participate in operational regimes' design for hydraulic power plants due to their hydro economic balances and central grid regimes;
  - to provide computation of forecasting balances of electric power;
  - to provide functioning of electric capacity market;

- to provide certification of power capacity of supplying plants;
- to present quarterly information about coordinated schemes of power capacity supply.

Nowadays 118 both commercial and governmental electric power plants are utilized in the republic as stated in [6]. Biggest of them are:

- Ekibastuz GRES-1 LLP named after B.G. Nurzhanov;
- Ekibastuz GRES-2 Power Plant JSC;
- Power plant of EEC JSC, ERG, Eurasian Group;
- GRES of Kazakhmys Energy LLP;
- Zhambyl GRES JSC named after T.I. Baturov;
- Bukhtarma Hydro Power Complex of Kazzinc LLP;
- AES Ust-Kamenogorsk HPP LLP;
- AES Shulbinsk HPP LLP.

For 01.01.2017 their total installed capacity was 22055.5 MW. Whereas available capacity was 18789.1 MW. Mostly the plants can be divided in three groups:

- Large thermal plants of national importance, which work is defined in [7];
- Large hydraulic power plants of national importance;
- Combined heat power plants of industrial importance.

As can be seen most of the plants are either using conventional type of energy or using more predictable RES type as energy of falling water or fast running water. So, central power market in the country is not yet affected by uncertainty of RES.

If consider private sector, use of small RES plants can impact only on local power systems not influencing central power grid as is researched in [8]. Because unlike European system there are no possibility for supply of power leftover back to central grid. But it is promised to legally provide such opportunity in the nearest future [9].

For now, to provide power supply entity has to:

- have licenses as required by the laws of Kazakhstan;
- have access to the national or regional electric network;
- supply at least 1 MW of electricity on daily base to the wholesale market and have commercial metering systems, telecommunications harmonized with the System Operator.

Due to large territory and small population of the country not all of the inhabited areas have access to central power grid as mentioned in [10]. That is the main market for RES' use as it is more efficient in a long run than diesel generators as proved in [11]. The reason why diesel generators are more employed for now is that it requires less capital investments.

For any power grid the control process can be reduced to minimization of power cost  $M$  with at least one constraint:

$$E - T = C \quad (1)$$

Here:  $E$  - total power generated by all plant of the grid, kWh;

$T$  - total power loses for transportation of electric energy from a supplier to a customer, kWh;

$C$  - total power demand from the customers, kWh.

With a growth of demand  $C$  more  $E$  is needed to cover it and at the same time more distant power plants are connected, which leads to  $T$  increase and more  $E$  is required.

In conventional power grids the main source of uncertainty was  $C$ . But with RES' plants appearance  $E$  is also becoming

stochastic value. Whereas Eq.1 describes even more complex interrelationship.

### III. NEW APPROACHES

Electric power control and dispatching with RES' influence is not a newly appeared task for worldwide engineers' community. Consequently, there several approach offered by scientific community within last ten years. Some of them are mentioned in this chapter.

#### A. Dynamic tariffs

First and logical approach is to regulate one of the probability factors – power consumption. The only possible way is to stimulate customers to use less energy at the peak times when it is harder to cover power demand by dynamic tariffs. If take mathematical model from Eq. (1) such methodology helps to change distribution of C throughout a day and make it more linear.

Dynamic tariffs are far implemented in developed countries [12]. Such power tariffs are thoroughly legally regulated and have many application variants for private power systems like in [13, 14].

But such control technique is effective only for system at a state level, while for small communities or autonomous power grids it's not applicable.

#### B. Energy storage

Other possibility is to use some kind of power buffer for uncertain supplying plant and unpredictable consumer. Such buffer can be provided by some kind of energy storage.

This energy storage or, in other words, accumulator will need essential amount of material and human resources for proper implementation and operation. There several methodologies to calculate the capacity needed as, for example, in [15-17].

In situation with autonomous power grid of any size as in [18, 19] it's almost only opportunity to have energy reserve and not to lose power leftover at some point.

This method mathematically can be represented in Eq. (1) as a new variable B and will transform to:

$$\begin{cases} \Delta B = E - T - C, & \text{if } E > C + T, \\ C = E - T + \Delta B, & \text{if } E < C + T. \end{cases} \quad (2)$$

Here:  $\Delta B$  - difference of energy stored in any kind of accumulator, kWh.

#### C. Electric powered vehicle or EPV

In parallel with growth of RES' use electric powered vehicles are becoming more and more spreading. They start to be main part of power consumption in private sector. At the same time, they don't have much difference from specific energy storage for a power grid as mentioned in [20]. Hence they also can be used as previously mentioned buffer. The only concern is to provide optimum schedule of EPV's use beyond the power system.

#### D. Decentralization

Previously described approaches are mostly focused on minifying number of power plants and other equipment by reducing peak demand. But other distance between supplier and customer was out of focus.

For decentralization it's vice versa. This solution can not affect consumers. It concentrates on finding for each customer nearest supplier as described in [21]. By that energy expenses to match norms from [3] decreases significantly.

With wide implementation of RES plants private power system will become complex agent for a power grid. Because it will switch the role from consumers to suppliers and backwards according to own plants' output and own demand. Therefore, power grid can be considered as a multi-agent system where interconnection between agents can be described with Holonic architecture as in [22].

The main principle of Holonic architecture is that every big system or super-holon can be divided into subsystems or holons that can regulate most of inner processes without interaction with other part of super-holon. Whereas the holon become the super-holon for its own subsystems. Such architecture can penetrate power grid till exact EPVs, power plants or end consumer.

For example, if power demand can be covered by won power plants of the holon it will use own computational capabilities to control and dispatching. But if inner power resources will not be enough it will interact with his super-holon as a consumer. Visa versa if there is leftover energy within the holon it become a supplier in higher level.

Such approach permits to minimize distance between consumer and supplier as well as decreasing the demand for computational and technical capabilities of central grid. Also it accelerates a response from an end consumer or supplier.

Whereas dispatching and control process is the same classical optimization task as can be seen in [23] to minimize power cost M with at least one constraint:

$$E_h - T_h = C_h \quad (3)$$

Here:  $E_h$  - total power generated by all plant of one holon, kWh;

$T_h$  - total power loses for transportation of electric energy from a supplier to a customer of a holon, kWh;

$C_h$  - total power demand from one holon's customers, kWh.

The difference is that when it is not enough power sources within one holon it requests for supply from super-holon (power grid of higher level).

### IV. IMPLEMENTATION PERSPECTIVES

#### A. Dynamic tariffs

Energy system of Kazakhstan is still fuel oriented. This is due to high accessibility and relatively low cost of natural gas and coal. Whereas RES are very presented in the republic with current low cost of energy from conventional sources this trend is hardly changeable as discussed in [24]. Implementation of large and middle RES' plants is a risky investment at such high-risk business environment and

unformed urge as researched in [25]. That factors have an impact on country-wide absents of dynamic tariffs for electric power. And for foreseen future it is not an appropriate approach for the power grid.

### B. Energy storage

RES use in Kazakhstan is directly connected with energy storage technology as described in [26]. As mentioned previously there is no other possibility to deal with power leftovers. That power cannot be given back to central grid either because of regulations absents or absents of central grid itself.

To explain last statement, it's necessary to mention that most of the rural territory hasn't got any connection with central grid and work on totally autonomous power supply. Whereupon cannot work without some kind of energy storage.

### C. EPV

Big EPVs are not very presented in the republic both in urban and rural areas. But number of them is growing year by year. Anyhow EPV as an energy storage device can be used only with high involvement of end consumers in power grid operation. Otherwise it's hardly possible to provide scheduled charge of EPV as it is mandatory for such methodology.

### D. Decentralization

For any regulation changes there should be either economic or social interest for government. As described previously and also researched in [27] there is no economic reason for changing system for fuel oriented energy sector of the country. At the same time globally the power grid is already decentralized if taking autonomous rural territories into account. And Holonic architecture can provide massive economic impact for private power grids at isolated territories. And minimize expanses for energy storage equipment.

## V. CONCLUSION

Nowadays Kazakhstan energy sector is mostly fuel based with some amount of hydro energy use. But according to [28] most economic effect can be achieved by use of solar energy that is more than enough represented in geographical location of the country. Whereas hydro energy can be utilized even more and provide social effect. Also wind and biomass can impact on ecological situation of the republic.

And while the energy market doesn't have almost any practical motivation to force RES implementation in the immediate future the end users are concerned about possibility to use small plants in their daily live. Especially in rural territories distant from central grid as mentioned in [11].

Hence it appears that dynamic tariffs are not very applicable in case of Kazakhstan's central grid. But use of energy storage and in some future EPVs is indispensable. Furthermore, RES expansion is in straight connection with energy storage technologies. Formalization of decentralized autonomous part of republican energy sector is also forthcoming for rural and distant group of entities by its development in a nearest future.

## REFERENCES

- [1] Wina Crijs-Graus, "Renewable Energy: Past Trends and Future Growth in 2 Degrees Scenarios", *Energy Procedia*, No.100, 2016, pp. 14-21.
- [2] Order №460 from 26th of October 2016 of Ministry of Energy of Republic of Kazakhstan "About confirmation of forecasting balances of electric power for 2017-2023 years".
- [3] National State Standard 32144-2013 "Electric energy. Electromagnetic compatibility of technical equipment. Power quality limits in the public power supply systems".
- [4] European Standard EN 50160:2010 "Voltage characteristics of electricity supplied by public distribution networks".
- [5] Makpal Assembayeva, Jonas Egerer, Roman Mendelevitch, Nurkhat Zhakiyev, "A spatial electricity market model for the power system: The Kazakhstan case study", *Energy*, No. 149, 2018, pp. 762-778.
- [6] Kazakhstan Electric Power Industry Key Factors| KEGOC, <http://www.kegoc.kz/ru/elektroenergetika/elektroenergetika-kazahstana-klyuchevye-fakty>.
- [7] Nurkhat Zhakiyev, Yerbol Akhmetbekov, Javier Silvente, Georgios M. Kopanos, "Optimal energy dispatch and maintenance of an industrial coal-fired combined heat and power plant in Kazakhstan", *Energy Procedia*, No. 142, 2017, pp. 2485-2490.
- [8] M. Yilmaz, F. Kentli "Increasing of electrical energy with solar tracking system at the region which has Turkey's most solar energy potential". *Journal of Clean Energy Technologies*, 2015, 3(4), 287-290.
- [9] K. Kulikova, "How much can Kazakhstan citizens gain from electric power", *Karavan*, 19.01.2016, <https://www.caravan.kz/gazeta/kakiesummy-kazahstancy-zarabotayut-na-ehlektroehnergii-87862/>
- [10] G. B. Nurpeissova, T. B. Nurpeissova, D. V. Panyukova, "Estimation of wind energy resources at Kazakhstan territory for autonomous power supply of low power consumers", 14th International Multidisciplinary Scientific GeoConference SGEM 2014, SGEM 2014 Conference Proceedings, Albena, Bulgaria, Book 4, Vol. 1, 2014, pp. 213-220.
- [11] G. B. Nurpeissova, D. V. Panyukova, "Autonomous power supply systems based on wind power plants for agroformations", 14th International Multidisciplinary Scientific GeoConference SGEM 2014, SGEM 2014 Conference Proceedings, Albena, Bulgaria, Book 4, Vol. 1, 2014, pp. 49-56.
- [12] F. Kentli and M. Yilmaz, "Improving Tracking Efficiency of Two-Axis Sun Tracking Systems." *Energy Harvesting and Energy Efficiency*. Springer, Cham, 2017. 179-203.
- [13] Henrique Pombeiro, Maria João Machado, Carlos Silva, "Dynamic programming and genetic algorithms to control an HVAC system: Maximizing thermal comfort and minimizing cost with PV production and storage", *Sustainable Cities and Society*, No. 34, 2017, pp. 228-238.
- [14] Vivek Tomar, G. N. Tiwari, "Techno-economic evaluation of grid connected PV system for households with feed in tariff and time of day tariff regulation in New Delhi – A sustainable approach", *Renewable and Sustainable Energy Reviews*, No. 70, 2017, pp. 822-835.
- [15] Kenneth K. Zame, Christopher A. Brehm, Alex T. Nitica, Christopher L. Richard, Gordon D. Schweitzer III, "Smart grid and energy storage: Policy recommendations", *Renewable and Sustainable Energy Reviews*, No. 82/1, 2018, pp. 1646-1654.
- [16] Andrea Michiorri, Jesus Lugo, Nils Siebert, Robin Girard, George Kariniotakis, "Storage sizing for grid connected hybrid wind and storage power plants taking into account forecast errors autocorrelation", *Renewable Energy*, No. 117, 2018, pp. 380-392.
- [17] Yang Zhang, Pietro Elia Campana, Anders Lundblad, Jinyue Yan, "Comparative study of hydrogen storage and battery storage in grid connected photovoltaic system: Storage sizing and rule-based operation", *Applied Energy*, No. 201, 2017, pp. 397-411.
- [18] K.A. Kavadias, D. Apostolou, J.K. Kaldellis, "Modelling and optimisation of a hydrogen-based energy storage system in an autonomous electrical network", *Applied Energy*, No. 227, 2018, pp. 574-586.
- [19] G. Puglia, M. Moroni, R. Fagnani, G. Comodi, "A design approach of off-grid hybrid electric microgrids in isolated villages: a case study in Uganda", *Energy Procedia*, No. 105, 2017, pp. 3089-3094.
- [20] Kristyna Friedrischkova, David Vala, "Energy-independent concept of a house using an electric vehicle traction", *IFAC-PapersOnLine*, No. 49/25, 2016, pp. 535-540.
- [21] Sebastian Weckmann, Timm Kuhlmann, Alexander Sauer, "Decentral energy control in a flexible production to balance energy supply and demand", *Procedia CIRP*, No. 61, 2017, pp. 428-433.

- [22] Adriano Ferreira, Ângela Ferreira, Olivier Cardin, Paulo Leitão, "Extension of holonic paradigm to smart grids", IFAC-PapersOnLine, No. 48/3, 2015, pp. 1099-1104.
- [23] Javad Ansari, Amin Gholami, Ahad Kazemi, "Multi-agent systems for reactive power control in smart grids", International Journal of Electrical Power & Energy Systems, No. 83, 2016, pp. 411-425.
- [24] Marat Karatayev, Stephen Hall, Yelena Kalyuzhnova, Michèle L. Clarke, "Renewable energy technology uptake in Kazakhstan: Policy drivers and barriers in a transitional economy", Renewable and Sustainable Energy Reviews, No. 66, 2016, pp. 120-136.
- [25] James MacGregor, "Determining an optimal strategy for energy investment in Kazakhstan", Energy Policy, No. 107, 2017 pp. 210-224.
- [26] M. Assembayeva, N. Zhakiyev, Y. Akhmetbekov, "Impact of storage technologies on renewable energy integration in Kazakhstan", Materials Today: Proceedings, No. 4/3/A, 2017, pp. 4512-4523.
- [27] Marat Karatayev, Michèle L. Clarke, "A review of current energy systems and green energy potential in Kazakhstan", Renewable and Sustainable Energy Reviews, No. 55, 2016, pp. 491-504.
- [28] Salman Ahmad, Abid Nadeem, Gulzhanat Akhanova, Tom Houghton, Firdaus Muhammad-Sukki, "Multi-criteria evaluation of renewable and nuclear resources for electricity generation in Kazakhstan" Energy, No. 141, 2017, pp. 1880-1891.

## BIOGRAPHIES



**GULNARA B. NURPEISSOVA** Matay, Kazakhstan, in 1965. She received the specialist degree in automation and telemechanic engineering from the Leningrad Electrotechnical Institute after V.I. Ulyanov (Lenin), Saint-Petersburg, Russia, in 1988, the Ph.D. and the Doctor Habil. of Tech. Sci. degree in "Technologies and mechanization instruments for agriculture" specialty from KazSRIMEA, Almaty, Kazakhstan, in 2005 and in

2010 accordingly.

From 2012 to 2016, she was a Vice-President with the Kazakh Automobile and Road Academy named after L.B. Goncharov, Almaty, Kazakhstan. From 2016 to 2018, she was a Vice-President for Academic Affairs with the Eurasian Technological University, Almaty, Kazakhstan. Since 2016, she has been a Professor with Engineering School, Eurasian Technological University. She is the author of one book, more than 70 articles, and 4 patents. Her research interests include renewable energy, information technologies in general, in transport and in agrarian sector, smart grids.



**DINA V. PANYUKOVA** Saint-Petersburg, Russia, in 1987. She received the B.S. degrees in automation and control engineering from the Kazakh National Technical University after K.I.Satpaev, Almaty, Kazakhstan in 2009 and the M.S. degree in automation and control engineering from Saint Petersburg Electrotechnical University "LETI", Saint-Petersburg, Russia, in 2011. Started the Ph.D. degree program in automation and control engineering in the Kazakh National Research

Technical University after K.I.Satpaev, in 2016.

From 2009 to 2016, she was firstly Lecturer and then Senior Lecturer with Kazakh Automobile and Road Academy named after L.B. Goncharov. From 2016 to 2017 she was a Lecturer with the Kazakh National Technical University after K.I.Satpaev. She is the author of more than 10 articles. Her research interests include intellectual systems, load forecasting, renewable energy, smart grids, information technologies.



**ADILKHAN T. NURPEISSOV** Almaty, Kazakhstan, in 1992. He received the B.S. degrees in electric power engineering from the Almaty University of Power Engineering and Telecommunication, Kazakhstan in 2015. Started the master's degree program in electric power engineering in Eurasian Technological University, Almaty, Kazakhstan in 2017.

Since 2015, he has been an Instrumentation and Control Systems Engineer with JSC ALES CHPP 1, Almaty, Kazakhstan. His research interests include renewable energy, electronics and other electrical equipment, mechanical engineering, traditional energy, relay protection and automation.

# Trends in Power System Protection Researches: A Review of Fundamental Relays

N. Onat

**Abstract**—Power system protection is one of the main element of modern energy management concept. The main task of these systems is to deactivate the faulty element or network part as soon as possible. The protection relays, called intelligent electronic devices, also have different functions than these basic functions. However, overcurrent, distance and differential protection are still used as the three basic components. In this study, current studies on these relays for coordination of the protection system have been analyzed. The research topic is limited to the main functions of the relays. Further study will examine the tasks that these relays have in providing data to the energy management system. It can also focus on the concept of wide area protection, event recording and modern communication protocols.

**Index Terms**—power system protection, electrical safety, substation automation, fault protection, relays.

## I. INTRODUCTION

TODAY, POWER systems are very complicated structures in which production, transmission, distribution and consumption units work together at the same time. Production systems are diversified in terms of raw materials they use and conversion methods. In addition, the operations of these production centers can be government, private sector or multi-partner structures. The diversity and management of the consumption point is much more. The entire system has to be operated in conjunction with an interconnected structure. Power protection systems include the production, transmission and distribution phases of electrical energy. They are constructions aimed at using energy as safe as possible from failures or incidents that put any part of the power system in jeopardy. Making power systems 100% safe or 100% reliable is very expensive. Therefore, it is imperative to conduct risk analysis to keep the probability of failure and the possibility of being affected by failures at acceptable levels. The protection relays are the most important component of all the parameters (reliability, selectivity, speed, simplicity and economy) that are considered as the five basic features of a good protection system. The primary goal of the protection system is to deactivate the defective network element as quickly as possible. However, this is a problem that is very complex and is non-definitive for interconnected networks which are fed by multi points. Predicting all scenarios can sometimes force the protection system to work for any non-optimal case.

N. ONAT, is with Department of Electrical and Electronics Engineering, Manisa Celal Bayar University, Manisa, Turkey, (e-mail: nevat.onat@cbu.edu.tr).

Manuscript received July 18, 2018; accepted October 28, 2018.  
DOI: [10.17694/bajece.445344](https://doi.org/10.17694/bajece.445344)

If a relay is required to work for a specified condition, it must be able to adapt its settings to changing system requirements. Therefore, an improvement to be made at every stage of the protection system should include a balance between the concepts of economy-performance, reliability-security, complexity-simplicity, speed-sensitivity (selectivity) [1].

Until the end of the 19th century, in power systems mostly operated as DC, the main protection element was fusible wire fuses. In parallel with the increasing use of alternating current in these years, measurement transformers (Current Transformer (CT) and Voltage Transformer (VT)) have been developed. Thus, it is possible to detect high currents and voltages with secondary relays [2]. The concept of a protection system starting with the overcurrent, differential and directional relays from the beginning of the 1900s has expanded since 1920, including distance protection. The overcurrent inverse time relay, which was patented by C. E. L Brown in 1902, is regarded as the first AC relay [3], [4].

Nowadays, the addition of electronic and software components and the use of very different algorithms and the so-called intelligent electronic devices, relays continue to develop on the basic concepts mentioned above. Digital relays are being developed that fulfill the functions of event recording, sharing and providing statistical data, which have very important functions, especially from wide area protection and predictive maintenance aspects in energy systems. These relays are also very important in the automation of the transmission and distribution system, which is the main element of the “smart grid” concept [5], [6]. These developments make the protection systems associated with information and communication technologies (ICTs). This increases the complexity inherent in the subject [7]. The subjects for improving the coordination of the protection system in scientific research on power systems are the most studied concepts, together with stability researches.

In this study, state of art analysis was carried out on the basis of the studies made in recent years, especially over current, distance and differential protection relays. Artificial intelligence techniques, which are used to diagnose and classify failures, are also emphasized.

## II. OVERCURRENT RELAYS

Over current relays (OCRs) are the most commonly used protection elements, especially in distribution systems. In radial networks fed from one side, time coordination can be achieved by using these relays alone. However, for multi-side feeds, they usually have to be used in series with a directional relay. Under these conditions, they are called as directional overcurrent relay (DOCR). Fig. 1 shows the

DOCR circuit diagram. With the use of OCRs which only operate with current information, there will be no difference between F1 and F2 faults in the system. The relays are tripped for both faults. However, the series connection of the directional relay and the OCR using current and voltage information will remain insensitive to fault F2 when the system is doing primary protection for the F1 fault. This approach provides very important advantages especially in providing relay coordination in multi-point feed grids. For

primary protection, the operating time obtained from the characteristic curves of the OCR is expressed by the following equation.

$$t_{op} = \frac{\lambda \cdot TMS}{(I_F / PS)^\eta - 1} \tag{1}$$

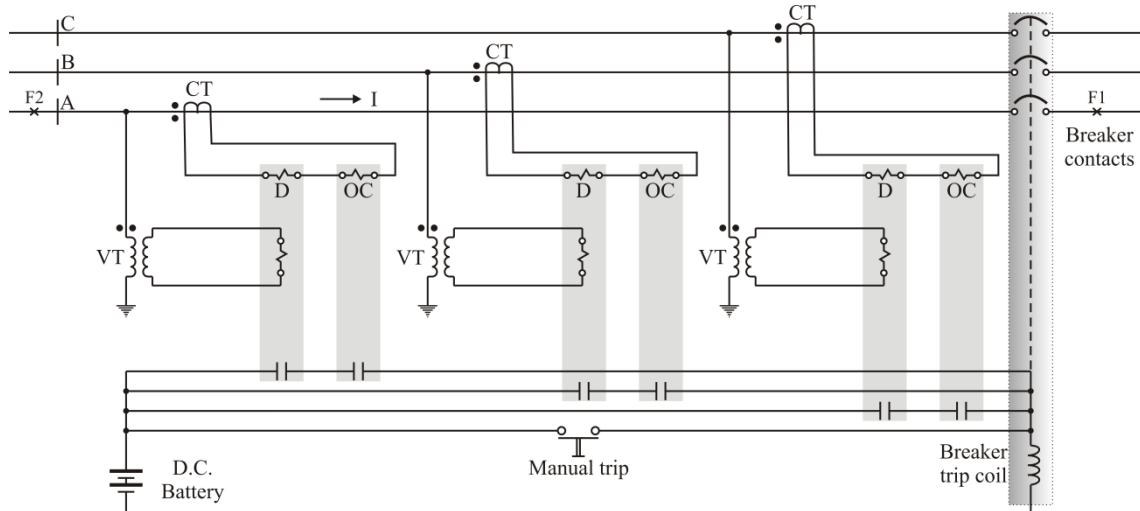


Figure 1. DOCR Circuit. OCRs use only current information. It is enough to use only CT for this. The voltage and current information must be used together to operate the directional relay. Thus, only one direction can be opened by detecting the direction of power flow.

In (1);  $PS$  and  $TMS$  represent current tap setting and time multiplier setting respectively.  $I_F$  indicates the value of the fault current flowing through the relay operating coil.  $\lambda$  and  $\eta$  are the constants which depend on the relay characteristics as shown in Table 1. Tripping time vs. current characteristics of OCRs are also given in Fig. 2.

TABLE I. CHARACTERISTIC CONSTANTS OF OCRs

| Relay characteristic | $\lambda$ | $\eta$ |
|----------------------|-----------|--------|
| Normally inverse     | 0.14      | 0.02   |
| Very inverse         | 13.5      | 1.0    |
| Extremely inverse    | 80        | 2.0    |

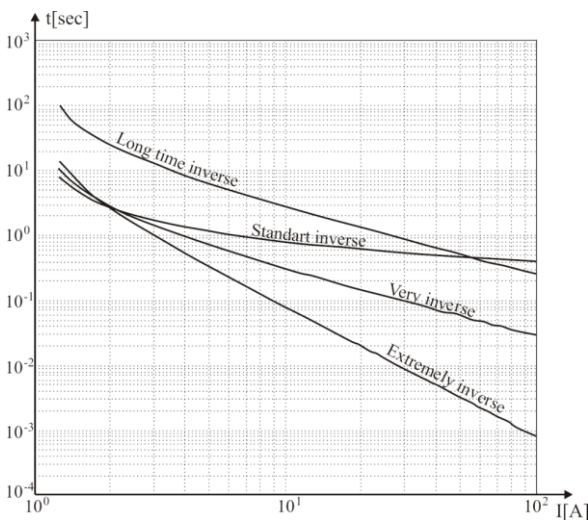


Figure 2. Tripping time vs. current characteristics of OCRs

relays. In a failure situation, the primary relay that should be engaged first must generally be back-up protected. This creates the necessity to define the protection coordination criterion. If a relay is defined for back-up protection ( $R_j$ ) of a primary relay ( $R_i$ ) on any  $k$  line, then the coordination constraint can be expressed in equation (2).

$$t_{ob,j} - t_{op,i} = MCT \quad \forall k \tag{2}$$

In (2),  $t_{ob,j}$ ,  $t_{op,i}$ ,  $MCT$ , are the back-up relay operating time, the primary relay operating time, and the minimum time coordination range that must be left for correct operation between these relays respectively. The operation speed of the relays should be kept at an optimum value depending on the structural factors. This restriction, which determines the speed of the relay, can be expressed as;

$$t_{i,min} \leq t_{op,i} \leq t_{i,max} \tag{3}$$

Therefore, the operation time of the relay must remain between the minimum ( $t_{i,min}$ ) and maximum ( $t_{i,max}$ ) run times structurally. Relay coordination is also constrained by the design of the relay and the time-quadrant settings. These settings are settled gradually in discrete mode in some models. In others it can be changed linearly at certain intervals. These constraints on the relay settings are also expressed by equation (4) [8], [9].

There are various restrictions in the coordination of the

$$\begin{aligned} TMS_{i,\min} &\leq TMS_i \leq TMS_{i,\max} \\ PS_{i,\min} &\leq PS_i \leq PS_{i,\max} \end{aligned} \quad (4)$$

There are many parameters that affect the operating times of OCRs since they interact directly with all transient events in the transmission and distribution systems. Bougouffa and Chaghi have argued the consequences of using thyristor-controlled series capacitors used in flexible alternating current transmission systems (FACTS) with reverse-time DOCRs. The behavior of series capacitors in the event of three phase short circuit failure and the effect of operating time on DOCR were investigated using linear programming techniques with MATLAB. The results are compared to systems without capacitors [10].

In the solution of the coordination problem, tap current setting and time multiplier setting values should be calculated. The tap setting is derived from the minimum fault current and maximum load current for each relay. One of the most important steps here is the definition of constraints, especially in grids fed by multi-points. Reducing the number of constraints will also provide ease of operation. Reference [11] proposed an algorithm that first solves the optimization problem by decreasing the number of constraints. First of all, the constraints are divided into categories and the number of which cannot be considered has been analyzed and a more simple structure has been tried to be achieved. In 8-bus and 11-bus systems, a 50% to 60% reduction in the number of constraints has been achieved.

#### A. OCR Coordination

OCR coordination is not a scientific discipline with definite consequences. In fact, it can be described as an art with some puzzles due to its complexity and irregularity. For this reason, it is difficult to argue that it is a method that gives a definite result on a global scale. Birla et al. have summarized the methods used in coordination of time-adjusted DOCRs in a successful review study [12]. Conventional coordination methods in large interconnected power grids can cause curve intersections and large operation times. Therefore, the use of optimization methods is generally recommended for better results [13], [14]. The following parameters are important in achieving optimal values in relay coordination;

- The optimization method used,
- Objective function,
- Type of power system (radial or interconnection),
- Nonlinear and linear relay characteristic proportional to time setting multiplier or time dial setting,
- Whether these settings are continuous or discrete mode [15].

Rahmati et al. have proposed over current protection system using local measurements without communication system. In this study, a simple solution is taken into account considering the parameters to which the Thevenin equivalent circuit of the network is connected. By using the relationship between the OCR pick-up current and the Thevenin impedance, optimization at tripping times is provided by local measurements [16].

Ezzeddine and Kaczmarek have done the optimization of

the time multiplier and pick-up current parameters of the relays with known optimization techniques by taking these two parameters as independent variables. First, optimal discrete values of the pick-up current are selected. In the second phase, adequate time characteristics of the relays were selected. In the third step, the optimal discrete values of the time multiplier are found [17]. There are two general restrictions on optimal relay coordination. 1-) Physically varying run-time constraints due to relay characteristics. 2-) Coordination constraint in determining the time interval between primary and backup relays. In literature, the effects of these restrictions are taken into account by various methods (barrier, punishment, etc.). So and Li have developed a model based on evolutionary programming for OCR coordination in ring distribution systems. The conventional optimization techniques fail because the coordination problem involves optimal points at every local point. The proposed model is much more successful than the classical mathematical optimization techniques.

This algorithm can be used in all overcurrent adjustments and provides the ability to control the correct coordination in all system constraints. Relay operations resulting from changes in the fault current distribution due to circuit breaker operation while the fault continues are also analyzed [18]. Papaspiliotopoulos and his et al. have recently addressed the coordination problem with a new approach using the equivalent quadratically constrained quadratic programming (EQCQP) model. The proposed method has greatly increased the efficiency of the optimization software in particular [19].

Linear programming (LP) and evolution algorithms (EA) are also used to solve the DOCR coordination problem [20], [21], [22], [23]. Pick-up current and trip time optimization studies using Mixed Integer Linear Programming (MILP) are also included in the literature [24]. Shih et al. compared different versions of differential evolution (DE) algorithms in the coordination of DOCRs used in large interconnected grids. Analysis criteria are 1-) in addition to maintaining selectivity, the value of suitability for minimizing the working time of primer and back-up relays, 2-) the number of violations of coordination constraints and 3-) the standard deviation of the process time. Developed DE gives the best results in terms of execution time, result quality, robustness and convergence ability compared to others analyzed in this study [13]. The DE algorithm was previously compared with the application results of the teaching learning-based optimization (TLBO) algorithm to provide optimal coordination of DOCR [25].

Reference [26] compared the performance of solving the coordination problem of DOCRs of five different metaheuristic algorithms. Time coordination values of DOCRs were analyzed by running Genetic Algorithm (GA), Particle Swarm Optimization (PSO), DE, harmony search algorithm (HS) and seeker optimization algorithm (SOA) 100 times under the same initial conditions. It has been determined that the DE algorithm always provides the lowest value by using the minimum opening time and coordination time interval, and also gives the best values when the relay characteristic curves are different. It is also determined that the values obtained by the DE are more predictable because of the low standard deviation.

Bedekar and Bhide used a continuous genetic algorithm (CGA) technique for optimal DOCR coordination in a ring feed distribution system. Constraints have been incorporated into the fitness function using the penalty method. The results has shown that the proposed model faster and requires less storage space than GA based on the classical binary number system because it eliminates the decoding process of chromosome codes [27]. A recent study on the use of GA in relay coordination was also carried out by Bottura et al. Here, however, the best time-quadrant value is obtained using a LP model. The value of the pick-up current is defined by GA. In the model called hybrid genetic algorithm (HGA), the short circuit current direction is considered. The obtained results are compared with known mathematical programs such as AlphaECP, BARON, BONMIN, DICOPT, KNITRO and SBB. In order to demonstrate the validity of the results, a real network system is considered. It has been shown that the proposed model shows 12-27% more optimal values than the conventional methods in determination of tripping time and pick-up current values, and the relay coordination is improved by these reductions [28]. Tahkur and Kumar have presented an optimization solution consisting of a bounded exponential transition and power mutation (BEX-PM) and a real-coded GA(RCGA) for the purpose of detecting optimal relay settings and at the same time minimizing the difference between backup and primer protection relays [29]. Protection optimization based on GA for a 7-ring ring system including transformer protection was performed by Chen et al. [30]. References [15] and [31] are also examples of GA-based selectivity studies.

In recent years, chaotic firefly algorithm (CFA) has also been the subject of studies on optimal relay coordination in the literature. In [32], MATLAB based CFA is presented for optimal time coordination of OCRs and the results are compared with classical firefly algorithm (FA). Meskin et.al. have focused on the identification of coordination starting points in OCR coordination in the case of multi-sided faults. In single-sided grids, the coordination is naturally started from the farthest relay to the source. However, the choice of coordination starting points is an important challenge for interconnection systems. The authors attempted to establish relay coordination by developing a procedure for finding breakpoints in these network. The proposed model especially contributes to the reduction of processor time in systems with many relays [33].

In order to solve the optimal coordination problem of DOCR, Mancor and colleagues have developed a PSO-time varying acceleration coefficient algorithm that takes the optimum pickup current as a discrete parameter and the TMS as a continuous parameter. The computation results with the proposed method are compared with the calculations made with MATLAB-GA, classical PSO and other techniques, and the algorithm has been shown to improve the solution of the problem [34]. Modified PSO algorithm is also presented to eliminate problems such as determining the starting point of the relay coordination, re-scanning the entire system in each iteration and based on the possibility of changing particle positions in each update in the classical PSO algorithm [35].

Bouchekarave et.al. used the modified electromagnetic field optimization (MEFO) method for shortening the operation time of DOCRs and for optimal coordination. The EFO approach is based on the behavior of electromagnet particles in different polarities. In EFO, each electromagnetic particle force is generated using a random number distributed uniformly between 0 and 1. By producing a new electromagnetic using three parameters obtained by multiplying by a factor depending on the magnitude of the force, a more balanced output is obtained in the production strategy. This study also deals with Constraints by means of a penalty method. The results show that the proposed system works efficiently in shortening the relay operation time for optimal coordination of DOCRs [36].

### B. OCR Modifications

Enriquez and Martinez has developed an adaptive function to increase the sensitivity determination of pick-up current of time delaying OCR. Reduction in load and increment in rated current causes that to observe as a fault current in some situations. This can cause mal operation of relay. In the proposed model, modification of the pickup current is made to be dynamic so as to respond to the operating conditions of the grid [37]. Directional relays have been used in protection of multi-point fed power systems since the 1950s. It is known that the conventional direction relays operate with voltage and current information and are used in different connection modes in determining the fault location. Directional capability is especially important in overcurrent and distance protection.

The conventional DOCRs use the reference voltage as the amount of polarity to estimate the direction of the fault. In the case of close disturbances, this traditional method can lead to false openings. Nojavan et.al. tested OCRs by providing a directional relay algorithm that uses only current signals for fault diagnosis. Because it does not require a phasor estimation, it offers a faster and simpler solution than traditional methods [38]. It has also been studied in the literature that digital signal processing based algorithms using fuzzy logic controller (FLC) can improve the operation time and accuracy performance of overcurrent relays [39], [40], [41], [42]. Hybrid use of FLC and artificial neural network (ANN) algorithms can improve DOCR's time quadrant and operation time values. The current multiplier and operation time curve values are transferred to a graphical axis plotted with the fuzzy approximation and given as the input to an ANN trained with data obtained for any trip time. Thus, the non-linear operation time and the time-quadrature relation are analyzed by ANN and the tripping time is determined [43], [44].

### III. DISTANCE PROTECTION

In high voltage (HV) and ultra-high voltage (UHV) power systems, 85% of failures occur in transmission lines. Incorrect opening or undoing may cause unacceptable results in these systems [45]. Distance relays (DRs) offer optimal solutions for line protection, especially in grid systems. The distance protection is generally designed according to three zone protection principle and uses line impedance information. The first zone is the primary

protection zone, covering 80% of the first line observed by the relay. For the second zone, backup protection is done by setting the impedance of the primary line to 1.2 times. Remote backup protection (zone 3 protection) is quite challenging in terms of coordination. Practically, the impedance value is taken as the sum of 100% of the first line and 120% of the second line. In some cases it may become impossible to coordinate the third zone protection [46]. Figure 3 shows the general structure of the distance relay connection circuit.

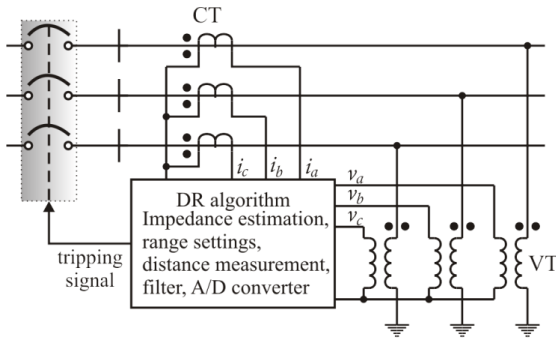


Figure 3. Distance relay circuit. VTs, CTs, impedance measurement system and directional sensitivity are standard. Various DR algorithms are used for distance determination, fault detection and classification. Filters reduce EMC effects on current and voltage signals. Analogue / digital converter systems have become the standard for digital relays in particular.

There are also some applications in the literature that aim to avoid mal operations with some modifications by way of the above conventional logic for remote backup protection [47]. Third zone settings in DRs apply as a firewall against the possibility of failure of the primer protection in remote substations [48]. However, mal operations in Zone 3 are among the most important causes of major energy interruptions in various countries. This inconsistency is caused by the overloads in zone 3 distorting the settings. It is difficult to draw the boundaries of the overload concept or to determine the overload only from the instantaneous current values. For this reason, Zone 3 protection can be replaced by computerized solutions based on pilot relays or artificial intelligence algorithms used today [49]. In the third zone coordination of DRs, various systems are designed to adaptively adjust the settings of relay by communicating with neighboring distribution stations [50]. DRs are called impedance relay or modified relay (mho relay) according to the range finding functions that make up the trip region (Fig. 4).

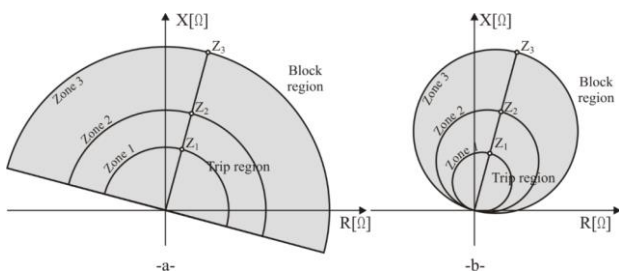


Figure 4. Zone protection with distance relay a-) Directional Impedance Relay, b-) Admittance (Mho) Relay.

The presence of FACTS controllers also causes mal operation of the DRs. Serial-parallel FACTS devices have greater impact on relay performance than other FACTS

devices. Furthermore, due to the high resistance values of these devices, the relay cannot reach this impedance value and cannot detect the fault correctly. In a recent study, a structure was presented to detect the imbalance by calculating the active power from voltage and current values of buses. In addition, a technique for the calculation of unified power flow controller (UPFC) data has also been proposed in this study. The resistance that occurs at the UPFC and the fault point increases the impedance measured by the DR. In this case, the relay does not switch on. In the proposed method, first, the fault point resistance is detected by calculating the active powers at both ends of the transmission line. In the second step, using the transmitted data, the voltage and current values given by the UPFC to the system are calculated. This value is subtracted from the impedance measured by the relay. The method is based on active power calculation. For this reason, the capacity and inductance values of the transmission line have no effect on the result [51]. Reference [52], has also taken into account that the presence of FACTS and static VAR compensators (SVCs) makes fault detection difficult in terms of DRs. It is based on the identification of the impedance measured at the operating point of the relay and the characteristic impedance of the relay for phase-ground and phase-phase faults in the case of SVC in a transmission line. Thus, it has been tried to make a stable distance protection at different compensation levels with SVC. Reference [53] proposed a transmission line protection model with pilot protection approach in which DOCR and DRs are combined. The OCR performs the back-up protection function for phase-ground failure. The DR carries out the protection of faults phase to phase. In order to determine the set values of the relays, a model using GA is presented considering the characteristics of maximum load, current and minimum fault current of the line.

Zubic et al. presented a new DR algorithm based on Maximum Overlap Discrete Wavelet Transform (MODWT). In this study, orthogonal filters based on the Fourier and Hilbert transform approach are used, especially for phasor estimation. As an alternative to traditional Wavelet Transform (WT) based phasor identification solutions, the proposed model was tested to verify the protection speed and reliability. It has been determined that it accelerates the operation time by around 10ms according to the conventional methods [54]. An adaptive transmission line protection system design based on synchronous phasor measurement units is also presented in reference [55]. Positive component voltage and current vectors at both ends are used to determine the line parameters and the fault point on the line. The proposed model has been demonstrated to be used in single-double circuit lines and to work steadily against power oscillations. A model reference [56] is also presented for testing the security and reliability of DRs.

For these calculations, it is necessary to statistically regulate the event records of the line that the relay is connected to. This demonstrates that the next generation distance protection systems must also include event recording functionality. Reference [57] also compares the classical harmonic filters (Cosine or Fourier) that filter the fault components embedded in the fundamental component of current in the DRs and Prony filter. Campos et.al. also

compared the time response and frequency response for four classical phasor estimation methods by improving the filtering of undesired frequency components of the signals. The performance of the proposed model was tested by digital DR application [58]. Signal distortions caused by the saturation effect of the measuring transformer, which provides the current information of the DRs, can be caused by incorrect operation. The Elman Recurrent Network (ERN) model in reference [59] is presented to remove the disturbing effects from the current signal and to reduce the deviation from the correct opening point. In case of earth faults caused by high impedance, values close to or above the impedance value set by the relay can occur. This may cause the DR not to trip. The drawbacks of operating with only impedance value in this type of malfunction are also subject to literature studies. Li and Lai have tried to define the ideal operating region for DRs by examining how active and reactive power flows in the line change in the event of such a fault [60]. The primary task of DRs is to protect transmission lines. However, harmonics in voltage and current signals and exponentially decaying DC components negatively affect relay performance. A method is proposed in reference [61] that focuses on estimating DR impedance by reducing the degree of disruptive effects described above with phasor estimation using ANN. This method continues to calculate the apparent impedance during the training of the ANN, given in the system online, using a multi-layer sensing architecture to estimate current and voltage signals. ANN is also subject to different studies aimed at reducing range errors in distance protection [62]. A model based on ANN training for identifying admittance relays' trip and block regions for first zone protection is presented in [63]. Load curtails or overload elements are used to prevent DRs from mal operations under heavy load conditions. These components try to keep relays in a block state when there is an overload in the system. ANN is used to distinguish overload conditions from fault conditions, especially those with low power factor overloads or small fault resistance [64].

When DRs are used on very long transmission lines, due to their high capacity values, measurement accuracy and measurement stability through complex and considerable harmonic components are adversely affected in conventional systems. As a result, the tripping speed may be somewhat reduced. To solve this problem, Wen et al. proposed a new DR algorithm for long transmission lines based on the differential equation algorithm using the pi-equivalent circuit of the transmission line. Current at the relay point and voltage at the fault point (high-frequency signals filtered with low-pass filter) still apply in systems with original distributed parameters. For this reason, the differential equation algorithm can be applied to transmission lines using pi-equivalent circuit [65].

In very long transmission lines, only one zone distance protection can be applied. Araujo and Pereira have developed a non-iterative first-zone DR for detecting a phase-to-ground fault in long parallel transmission lines. It has been taken into account that neglecting the propagation effects of shunt capacitance by processing the line solely in terms of serial impedance may cause a significant fault in impedance estimation at long distance lines. In the proposed

algorithm, the shunt capacity is produced from a distributed parameter which is fully taken into account for the mutual impedance and admittance values and is applicable to long parallel lines. The proposed model identified the fault location with an error of less than 1.8% for 85% of the total line length of 800 km [66].

Proper coordination between DRs and DOCRs in interconnected systems is important for system security. Reference [67] has addressed this problem and developed a problem formulation for the optimal coordination of DRs in the system where DOCRs are included as backup relays. Later, to overcome this complex problem, multiple embedded crossed PSO has been proposed. A successful study to determine the delay time of DRs in remote backup protection (zone 3 protection) was presented by Lukowicz et al. In the application based on the event tree risk analysis technique, a time dependent fault tree is created and the delay adjustment of DRs is selected for remote backup protection. By taking into account the natural delays of the relays and interrupts in the chain system, the events requiring the remote backup protection are logically connected to each other with time-dependent failures [68]. In systems where differential relays and pilot protection do primary protection, DOCRs serve as back-up protection. In this case, the behavior of DOCRs in large networks included distance relays also becomes important. Reference [69] provides a solution for ensuring coordination between the distance protection and DOCRS under these conditions. In another similar study, Marcolino et al. tried to provide optimal coordination using GA in a system where distance relay for phase-to-phase and DOCR for phase-to-ground failures [70].

#### IV. DIFFERENTIAL PROTECTION

Differential relays (DFRs) are used for rapid cleaning of internal faults in generators and transformers. Therefore, additional algorithms such as coordination and backup protection are not required. However, it is possible that these relays, especially due to the saturation effects of the CTs, can be tripped in the external faults or in the case of start-up process of transformers. Fig. 5 shows the general block diagram of the DFR and the internal and external fault opening zones.

Reference [71] used Fast Fourier Transform (FFT) to generate a constraint signal to prevent the relay from operating in the event of an external failure. A scheme for enhancing the safety of differential numerical relaying with second order harmonic generation is presented. Tripping signal of the differential relay is produced by comparing the vectors added to the secondary currents of the current transformers with the previously set value. The constraint signal is produced by comparing the second harmonic of the differential current with the algebraic sum of the second harmonics of the individual secondary flows.

An innovative scheme was developed in reference [72] that can observe and distinguish the behavior of power transformers under different operating conditions (such as rated load, inrush magnetizing current, over-excitation of the core, CT saturation due to internal and external failure). The PSO approach is used to train dual-layer feed-forward neural networks and to distinguish different operating

conditions. Two different ANN schemes were used as hybrids. The first one is the internal fault detector. The other is used to identify and define different operating conditions

such as normal, inrush current, over excitation, and CT saturation due to external malfunctions.

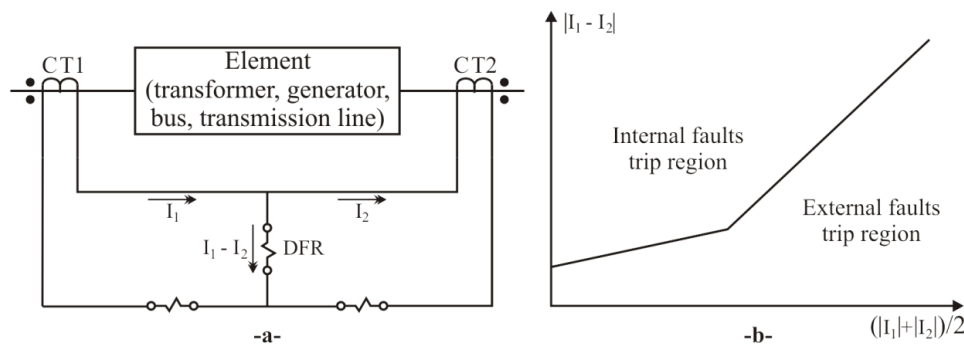


Figure 5 Traditional differential protection a-) circuit diagram (can be applied to transformers, generator, buses or transmission lines) b-) trip region characteristic.

Inrush magnetizing currents (startup currents) in transformers are an important influence that increases the risk of incorrect operation of DFRs. The distinction of these currents from actual fault currents can be achieved by comparing the two current behaviors in terms of phase angles [73], [74]. In addition, analysis of the primary and secondary currents, the transformer end voltage and the voltage values at the load ends is also necessary to make the distinction between internal and external faults more accurate. These comparisons can be achieved by the differential stability of the differential relay, its safe operation, the increased immunity to sudden magnetizing currents, and the more stable operation in external faults that contribute to saturation effects in current transformers [75]. Differential protection has also been used in power transmission lines in recent years. The [76] introduces a DFR method for transmission lines that is used spectral energy information provided by Fast Discrete S Transform (FDST). Unlike the classical S-Transform technique, frequency scaling, bandpass filtering and interpolation techniques have been used in different types to reduce the computational burden and eliminate redundant backup information. Due to the low computational complexity, the proposed algorithm is also suitable for real-time applications.

Reference [77] presented a model based on the energy conservation law for the differential protection of transmission lines. The active power values at both ends of the line (supply and load) are compared with a specific value previously determined. If the result is greater than this value, the result is an internal fault on the line. Power signals are used as input. A new limit has been set depending on the loss of the maximum power drawn from the transmission line. The proposed method is also suitable for long lines and underground cables. A similar differential protection algorithm using energy information is presented in a more recent study. Reactive currents due to increased capacity effect on long transmission lines prolong the operation period of DFRs. In order to overcome this drawback, the approach of measuring the momentary energy flows at both ends and comparing the energy consumptions of the line elements has been adopted. Since the line elements are fixed, it is necessary to have an energy balance at the input and output ends under normal conditions. When

this equilibrium is broken, it is decided that there is an internal fault on the line [78]. In wide area protection concept, differential protection of transmission lines is an important element. Differential approach with pilot protection logic at both ends of the transmission lines increases the reliability of the protection system [79], [80].

#### V. REAL-TIME FAULT DETECTION WITH ARTIFICIAL INTELLIGENCE TECHNIQUES

Artificial intelligence algorithms such as FLC, ANN, adaptive neuro-fuzzy inference systems (ANFIS) and wavelet transform (WT) can be used as stand-alone or hybrid especially for failure classification. The most important reasons of this are the development of high-speed communication technologies, and the elimination of the time gap between long distances with the global positioning system (GPS).

In WT analysis, the current and voltage signals are separated and compared to the components during the process of tripping of the breaker, which is formed by failure, fault process and start of fault. It is intended to identify extreme and abnormal changes by removing the electromagnetic noises from signals [81]. It is possible to analyze the current signals taken from both ends of long transmission lines with the same time and analyze it with WT technique. Thus, a differential protection operated with the pilot relay logic in which the fault conditions occur can be provided [82], [83].

ANN has been a subject for many years for fault detection and classification studies to assist the protection relays. Generally, training of the ANN with the values of the steady-state normal operation data and the values of the defective state behaviors can be regarded as the first stage [84]. The voltage and current in case of failure can be determined more quickly by taking the normalized peak values of the fundamental wave forms input data to the network [85]. Sidhu et al. presented a method of fault detection based on analyzing the radiation generated from arcing faults. In the proposed model, acoustic, infrared and radio waves are recorded with appropriate sensors via digital signal processor (DSP) based data acquisition (DAQ) system and classified by ANN [86]. WT and linear discriminant analysis (LDA) based fault detection and classification methods for symmetric and asymmetric faults

in dual circuit transmission lines are proposed in Reference [87]. The method was tested several operating conditions such as CT saturation, power flow changes, different failure types, fault impedances and fault startup angles. It has been determined that the proposed method can perform fault classification at 99% accuracy.

It is difficult to distinguish faults from normal switching operations when detecting faults over high impedance. This problem is the subject of study in the literature. Baquiet et.al. used a hybrid WT-ANN approach in classifying high impedance faults. The current waveforms generated under different transient conditions are processed by WT in the time and frequency domain and sent as input to the pre-trained ANN [88]. Travelling wave protection is used as a fault clearing method especially in very fast transient regimes. It is based on the determination of the time difference between the incident wave and the wave at the fault point [89].

A hybrid system reference [90] has been developed that uses data obtained from voltage and/or current signals separated to the components with the WT during faults. The fault point is determined by an algorithm that combines the travelling wave theory and impedance calculation on this data.

Abu-Elanien et.al. successfully detected internal failure on the HVDC line, which was fed from multiple sides by means of a two-ends travelling wave theory. For the synchronization of the relays at the two ends of the long transmission line, the GPS time data is used. The detection of the fault was made by DWT with high frequency transient regimes [91]. It is possible to eliminate the need for communication between ends in HVDC lines. For this, the algorithm based on the analysis of the high and low frequency components of the current at only one end with WT is presented in Reference [92]. In this case, the internal and external fault discrimination is provided by the shunt capacitors which are added to the system and filter the high frequency transient regime waves that occur in the external fault.

## VI. CONCLUSION

In this study, a study covering recent developments in overcurrent, distance and differential protection, considered as the most basic relays for the protection of power systems, has been presented. In power systems it is essential that a good protection system is operated at the highest standards, especially in terms of selectivity, speed, reliability and safety. However, the complexity of the systems and the necessity of working together on a large number of relays makes the exact solution impossible for these concepts. For this reason, researchers try to improve the parameters above mentioned by using artificial intelligence techniques to optimize certain parameters or to help relays by focusing on various points.

The main problem with OCRs is the shortening of the tripping time and the improvement of the selectivity. Researches are mostly focused on detecting the malfunction and improving the cleaning time. In addition, the optimization of the coordination time between primer and back up protection is discussed in detail.

Incorrect operation of remote backup protection in

distance relays poses significant problems. Remote backup protection becomes more difficult as the line length increases and the effect of elements such as SVC and FACTS on the line. For this reason, distance relays, especially zone 3 protection, can make unnecessary trips in overload situations. In addition, there are problems such as not being able to detect high impedance faults. This situation can cause very important energy interruptions. For this reason, the studies focus especially on the coordination of zone 3 protection and fault identification processes.

Differential protection is an effective method of internal fault detection applied mostly to transformers and generators. However, recent studies have focused on the use of differential protection in transmission lines, especially with the reliability and speed of communication and pilot protection between distribution centers. Optimization studies are also carried out to ensure that DFRs are insensitive to start up currents of generators or transformers, CT saturation, and sudden magnetizing currents. These investigations include the identification of internal faults in transmission lines by the differential protection approach.

In recent years, the use of artificial intelligence techniques has become widespread, especially in real-time troubleshooting. The failure models are presented with the models of current, voltage, power factor, symmetrical components, and analysis of the parameters using artificial intelligence techniques. Even in the future, the protection of the power system will be the main element of the smart grid concept. It is envisaged that efforts to improve the performance of the protection relays will be expected to increase in order to reduce the detrimental effects of factors such as varying producer/consumer structures, hypersensitivity to energy interruption. In future studies, it is aimed to refer to the functions of protection in modern energy management systems, communication technologies and failure (event) recording processes.

## REFERENCES

- [1] A. G. Phadke, H. Horowitz, "Adaptive relaying," *IEEE Comput. Appl.Pow. M.* 3:47-51, 1990.
- [2] W. Schossig, "Protection history the start of protection," *PAC History*, Autumn 68-74, 2007.
- [3] C. Christopoulos, A. Wright, "Electrical Power System Protection," p.104, Springer Science + Business Media, 1999.
- [4] A. Abdelmoumene, H. Bentarzi, "A review on protective relays' developments and trends," *J. of Energy in Southern Africa* 25(2): 91–95, 2014.
- [5] M. Begovic, D. Novosel, M. Milisavljevic, "Trends in power system protection and control," *Decis. Support Syst* 30:269–278, 2001.
- [6] A. Alvarez de Sotomayor, D. Della Giustina, G. Massa, A. Dedè, F. Ramos, A. Barbato, "IEC 61850-based adaptive protection system for the MV distribution smart grid," *Sustain.Energy, Grids and Networks* 15:26–33, 2018.
- [7] I. A. Tøndel J. Foros, S. S. Kilskar, P. Hokstad, M. G. Jaatun, "Interdependencies and reliability in the combined ICT and power system: An overview of current research," *Appl. Comput. and Inf.*, 14:17–27, 2018.
- [8] M. N. Alam, B. Das, V. Pant, "An interior point method based protection coordination scheme for directional overcurrent relays in meshed networks," *Electr. Pow. Energ. Syst.* 81:153–164, 2016.
- [9] H. C. Kılıçkiran, İ. Şengör, H. Akdemir, B. Kekezoğlu, O. Erdinç, N. G. Paterakis, "Power system protection with digital overcurrent relays: A review of nonstandard characteristics," *Electr. Pow. Syst. Res.* 164:89–102, 2018.
- [10] L. Bougouffa, A. Chaghi, Investigation of TCSC controller effect on IDMT directional overcurrent relay. *Proc. Soc. Be. Sci.* 195:2421–2429, 2015.

- [11] H. K. Karegara, H. A. Abyaneh, V. Ohis, M. Meshkin, "Pre-processing of the optimal coordination of overcurrent relays," *Electr. Pow. Syst. Res.* 75:134–141, 2005.
- [12] D. Birla, R. P. Maheshwari, H. O. Gupta, "Time-overcurrent relay coordination: A review," *Int. J. Emerg. Electr. Pow. Syst.* 2:1-13, 2005.
- [13] M. Y. Shih, A. C. Enríquez, T. Hsiao, L. M. T. Trevino, "Enhanced differential evolution algorithm for coordination of directional overcurrent relays," *Electr. Pow. Syst. Res.* 143:365–375, 2017.
- [14] H. K. Karegar, H. A. Abyaneh, V. Ohis, M. Meshkin, "Pre-processing of the optimal coordination of overcurrent relays," *Elect. Power Syst. Res.* 75:134–141, 2005.
- [15] F. Razavi, H. A. Abyaneh, M. Al-Dabbagh, R. Mohammadi, H. Torkaman, "A new comprehensive genetic algorithm method for optimal overcurrent relays coordination," *Electr. Pow. Syst. Res.* 78:713–720, 2008.
- [16] A. Rahmati, M. A. Dimassi, R. Adhami, D. Bumlauskas, "An overcurrent protection relay based on local measurements," *IEEE Trans. on Ind. Appl.*, 51(3):2081-2085, 2015.
- [17] M. Ezzeddine, R. Kaczmarek, "A novel method for optimal coordination of directional overcurrent relays considering their available discrete settings and several operation characteristics," *Electr. Pow. Syst. Res.* 81:1475–1481, 2011.
- [18] C. W. So, K. K. Li, "Overcurrent relay coordination by evolutionary programming," *Electr. Pow. Syst. Res.* 53:83–90, 2000.
- [19] V. A. Papaspiliotopoulos, G. N. Korres, N. G. Maratos, "A novel quadratically constrained quadratic programming method for optimal coordination of directional overcurrent relays," *IEEE T. Power Deliver.* 32:3-10, 2017.
- [20] A. J. Urdaneta, L. G. Perez, J. F. Gomez, B. Feijoo, M. Gonzalez "Presolve analysis and interior point solutions of linear programming coordination problem of directional overcurrent relays," *Electr. Pow. Energy Syst.* 23:819-825, 2001.
- [21] N. M. Stenane, K. A. Folly, "Application of evolutionary algorithm for optimal directional overcurrent relay coordination," *J. Comput. Commun.* 2:103-111, 2014.
- [22] J. A. Sueiro, E. Diaz-Dorado, E. Míguez, J. Cidrás, "Coordination of directional overcurrent relay using evolutionary algorithm and linear programming," *Electr. Pow. Energy Syst.* 42:299–305, 2012.
- [23] M. Singh, B. K. Panigrahi, A. R. Abhyankar, S. Das, "Optimal coordination of directional over-current relays using informative differential evolution algorithm," *J. Comput. Sci.* 5:269–276, 2014.
- [24] Y. Damchi, M. Dolatabadi, H. R. Mashhadi, J. Sadeh, " MILP approach for optimal coordination of directional overcurrent relays in interconnected power systems," *Electr. Pow. Syst. Res.* 158:267–274, 2018.
- [25] M. Singh, B. K. Panigrahi, A. R. Abhyankar, "Optimal coordination of directional over-current relays using Teaching Learning-Based Optimization (TLBO) algorithm," *Electr. Pow. Energy Syst.* 50:33–41, 2013.
- [26] M. N. Alam, B. Das, V. Pant, "A comparative study of metaheuristic optimization approaches for directional overcurrent relays coordination," *Electr. Pow. Syst. Res.* 128:39–52, 2015.
- [27] P. P. Bedekar, S. R. Bhide, "Optimum coordination of overcurrent relay timing using continuous genetic algorithm," *Expert Syst. Appl.* 38:11286–11292, 2011.
- [28] F. B. Bottura, W. M. S. Bernardes, M. Oleskovicz, E. N. Asada, "Setting directional overcurrent protection parameters using hybrid GA optimizer," *Electr. Pow. Syst. Res.* 143:400–408, 2017.
- [29] M. Thakur, A. Kumar, "Optimal coordination of directional overcurrent relays using a modified real coded genetical gorithm: A comparative study," *Electr. Pow. Energy Syst.* 82:484–495, 2016.
- [30] C. Chen, C. Lee, C. Chang, "Optimal overcurrent relay coordination in power distribution system using a new approach," *Electr. Pow. Energy Syst.* 45:217–222, 2013.
- [31] Singh M, B. K. Panigrahi, A. R. Abhyankar, "Optimal overcurrent relay coordination in distribution system," *International Conference on Energy, Automation, and Signal (ICEAS)*, 28-30 Dec. 2011, Bhubaneswar, Odisha, India, 2011.
- [32] S. S. Gokhale, V. S. Kale, "An application of a tent map initiated Chaotic Firefly algorithm for optimal overcurrent relay coordination," *Electr. Pow. Energy Syst.* 78:336–342, 2016.
- [33] M. Meskin, A. Domijan, I. Grinberg, "Optimal co-ordination of overcurrent relays in the interconnected power systems using break points," *Electr. Pow. Syst. Res.* 127:53–63, 2015.
- [34] N. Mancer, B. Mahdad, K. Srairi, M. Hamed, B. Hadji, "Optimal coordination of directional overcurrent relays using PSO-TVAC," *Energy Proc.* 74:1239-1247, 2015.
- [35] H. H. Zeineldin, E. F. El-Saadany, M. M. A. Salama, "Optimal coordination of overcurrent relays using a modified particle swarm optimization," *Electr. Pow. Syst. Res.* 76:988–995, 2006.
- [36] H. R. E. H. Bouchekara, M. Zellagui, M. A. Abido, "Optimal coordination of directional overcurrent relays using a modified electromagnetic field optimization algorithm," *Appl. Soft Comput.* 54:267–283, 2017.
- [37] A. C. Enriquez, E. V. Martinez, "Sensitivity improvement of time overcurrent relays," *Electr. Pow. Syst. Res.* 77:119–124, 2007.
- [38] M. Nojavan, H. Seyedi, M. Mehdinejad, "A novel scheme for current-only directional overcurrent relay," *Electr. Pow. Energy Syst.* 82:252–263, 2016.
- [39] Y. L. Goh, A. K. Ramasamy, F. H. Nagi, A. A. Z. Abidin, "DSP based overcurrent relay using fuzzy bang-bang controller," *Microelectron. Reliab.* 51:2366–2373, 2011.
- [40] Y. L. Goh, A. K. Ramasamy, F. H. Nagi, A. A. Z. Abidin, "DSP based fuzzy and conventional overcurrent relay controller comparisons," *Microelectron. Reliab.* 53:1029–1035, 2013.
- [41] S. B. A. Bukhari, R. Haider, M. S. U. Zaman, Y. S. Oh, G. J. Cho, C. H. Kim, "An interval type-2 fuzzy logic based strategy for microgrid protection," *Elect. Pow. and Energy Syst.*, 98:209–218, 2018.
- [42] M. Geethanjali, S. M. R. Slochanal, "A combined adaptive network and fuzzy inference system (ANFIS) approach for overcurrent relay system," *Neurocomputing*, 71:895–903, 2008.
- [43] H. K. Karegar, H. A. Abyaneh, M. Al-Dabbagh, "A flexible approach for overcurrent relay characteristics simulation," *Elect. Pow. Syst. Res.* 66:233-239, 2013.
- [44] M. H. Hussain, S. R. A. Rahima, I. Musirin, "Optimal overcurrent relay coordination: A review," *Proc. Eng.*, 53:332–336, 2013.
- [45] S. Zubic, P. Balcersek, C. Zeljkovic, "Speed and security improvements of distance protection based on Discrete Wavelet and Hilbert transform," *Electr. Pow. Syst. Res.* 148:27–34, 2017.
- [46] J. D. Glover, M. S. Sarma, T. J. Overbye, "Power system analysis and design," Fifth Edition, Cengage Learning Press, USA, 525-566, 2012.
- [47] M. Azari, M. Ojaghi, K. Mazlumi, "An enhanced adaptive algorithm to mitigate mis-coordination problem of the third zone of distance relays," *J. Appl. Res. Tech.* 13:87–96, 2015.
- [48] J. L. Blackburn, T. J. Domin, "Protective relaying: Principles and Applications," 3rd ed., CRC Press, FL, 2006.
- [49] S. H. Horowitz, A. G. Phadke, "Third zone revisited," *IEEE T. Power Deliver.* 21:23-29, 2006.
- [50] M. A. Haj-Ahmed, M. S. Illindala, "Intelligent coordinated adaptive distance relaying," *Electr. Pow. Syst. Res.* 110:163–171, 2014.
- [51] H. Mehrjerdi, A. Ghorbani, "Adaptive algorithm for transmission line protection in the presence of UPFC," *Electr. Pow. Energy Syst.* 91:10–19, 2017.
- [52] M. P. Thakre, V. S. Kale, "An adaptive approach for three zone operation of digital distance relay with Static VAR Compensator using PMU," *Electr. Pow. Energy Syst.* 77:327–336, 2016.
- [53] M. H. Marcolino, J. B. Leite, J. R. S. Mantovani, "Optimal coordination of overcurrent directional and distance relays in meshed networks using genetic algorithm," *IEEE Latin America T.* 13:2975-2982, 2015.
- [54] S. Zubic, P. Balcersek, C. Zeljkovic, "Speed and security improvements of distance protection based on Discrete Wavelet and Hilbert transform," *Electr. Pow. Syst. Res.* 148:27–34, 2017.
- [55] H. K. Zadeh, Z. Li, "Phasor measurement unit based transmission line protection scheme design," *Electr. Pow. Syst. Res.* 81:421–429, 2011.
- [56] S. J. Zubic, M. B. Djuric, C. V. Zeljkovic, "Probabilistic assessment of new time-domain distance relay algorithms," *Electr. Pow. Syst. Res.* 119:218–227, 2015.
- [57] L. A. T. Guajardo, "Prony filter vs conventional filters for distance protection relays: An evaluation," *Electr. Pow. Syst. Res.* 137:163–174, 2016.
- [58] A. K. X. S. Campos, W. L. A. Neves, D. Jr. Fernandes, "A new phasor estimation method for digital protective relays," *Electr. Pow. Syst. Res.* 142:227–236, 2017.
- [59] S. R. Mohanty, V. R. Pandi, B. K. Panigrahi, N. Kishor, P. K. Ray, "Performance evaluation of distance relay with CT saturation," *Appl. Soft Comput.* 11:4789–479, 2011.
- [60] K. K. Li, L. L. Lai, "Ideal operating region of digital distance relay under high resistance earth fault," *Electr. Pow. Syst. Res.* 43:215-219, 1997.
- [61] C. D. L. Da Silva, G. C. Junior, A. P. De Moraes, G. Marchesan, F. G. K. Guarda, "A continually online trained impedance estimation algorithm for transmission line distance protection tolerant to system frequency deviation," *Electr. Pow. Syst. Res.* 147:73–80, 2017.

- [62] S. M. Pasand, K. H. Zadeh, "An extended ANN-based high speed accurate distance protection algorithm," *Electr. Pow. Energ. Syst.* 28:387–395, 2006.
- [63] G. Chawla, M. S. Sachdev, G. Ramakrishna, "Design, implementation and testing of an artificial neural network based admittance relay," *IFAC Symposium on Power Plants and Power Systems Control, Kananaskis, Canada*, 2006.
- [64] K. H. Zadeh, Z. Li, "Adaptive load blinder for distance protection," *Electr. Pow. Energ. Syst.* 33:861–867, 2011.
- [65] M. Wen, D. Chen, X. Yin, "A novel fast distance relay for long transmission lines," *Electr. Pow. Energ. Syst.* 63:681–686, 2014.
- [66] M. R. Araujo, C. Pereira, "A practical first-zone distance relaying algorithm for long parallel transmission lines," *Electr. Pow. Syst. Res.* 146:17–24, 2017.
- [67] M. Farzinfar, M. Jazaeri, F. Razavi, "A new approach for optimal coordination of distance and directional over-current relays using multiple embedded crossover PSO," *Electr. Pow. Energ. Syst.* 61:620–628, 2014.
- [68] M. Lukowicz, J. Magott, P. Skrobaneck, "Selection of minimal tripping times for distance protection using fault trees with time dependencies," *Electr. Pow. Syst. Res.* 81:1556–1571, 2011.
- [69] C. A. Castillo, A. Conde, E. Fernandez, "Mitigation of DOCR miscoordination through distance relays and nonstandard overcurrent curves," *Electr. Pow. Syst. Res.* 163:242–251, 2018.
- [70] M. H. Marcolino, J. B. Leite, J. R. S. Mantovani, "Optimal coordination of overcurrent directional and distance relays in meshed networks using genetic algorithm," *IEEE Latin America Trans.*, 13(9):2975–2982, 2015.
- [71] M. Qais, U. Khaled, S. Alghuwainem, "Improved differential relay for bus bar protection scheme with saturated current transformers based on second order harmonics," *J. King Saud Un. Eng. Sci.*, 30(4):320–329, 2018.
- [72] M. S. Geethanjali, M. R. Slochanal, R. Bhavani, "PSO trained ANN-based differential protection scheme for power transformers," *Neurocomputing* 71:904–918, 2008.
- [73] A. Hosny, V. K. Sood, "Transformer differential protection with phase angle difference based inrush restraint," *Electr. Pow. Syst. Res.* 115:57–64, 2014.
- [74] B. Saravanan, A. Rathinam, "Inrush blocking scheme in transformer differential protection," *Energy Proc.*, 117:1165–1171, 2017.
- [75] U. N. Khan, T. S. Sidhu, "Protection of standard-delta phase shifting transformer using terminal currents and voltages," *Electr. Pow. Syst. Res.* 110:31–38, 2014.
- [76] K. R. Krishna, P. K. Dash, M. H. Naem, "Detection, classification, and location of faults in power transmission lines," *Electr. Pow. Energ. Syst.* 67:76–86, 2015.
- [77] M. M. Abdel Aziz, A. F. Zobaa, D. K. Ibrahim, M. M. Awad "Transmission lines differential protection based on the energy conservation law," *Electr. Pow. Syst. Res.* 78:1865–1872, 2008.
- [78] M. Wen, D. Chen, X. Yin, "An energy differential relay for long transmission lines," *Electr. Pow. Energ. Syst.* 55:497–502, 2014.
- [79] F. Namdari, S. Jamali, P. A. Crossley, "Power differential based wide area protection," *Electr. Pow. Syst. Res.* 77:1541–1551, 2007.
- [80] M. Monadi, M. A. Zamani, C. K. Ciobotaru, J. I. Candela, P. Rodriguez, "A communication-assisted protection scheme for direct-current distribution networks," *Energy* 109:578–591, 2016.
- [81] A. Ukil, R. Zivanovic, "Abrupt change detection in power system fault analysis using adaptive whitening filter and wavelet transform," *Electr. Pow. Syst. Res.* 76:815–823, 2006.
- [82] M. J. B. Reddy, D. V. Rajesh, D. K. Mohanta, "Robust transmission line fault classification using wavelet multi-resolution analysis," *Comput. Electr. Eng.* 39:1219–1247, 2013.
- [83] N. Zhang, M. Kezunovic, "A real time fault analysis tool for monitoring operation of transmission line protective relay," *Electr. Pow. Syst. Res.* 77:361–370, 2007.
- [84] W. W. L. Keerthipala, C. T. Wai, W. Huisheng, "Neural network based classifier for power system protection," *Electr. Pow. Syst. Res.* 42:109–114, 1997.
- [85] A. K. Pradhan, P. K. Dash, G. Panda, "A fast and accurate distance relaying scheme using an efficient radial basis function neural network," *Electr. Pow. Syst. Res.* 60:1–8, 2011.
- [86] T. S. Sidhu, G. Singh, M. S. Sachdev, "Arcing fault detection using artificial neural networks," *Neurocomputing* 23:225–241, 1998.
- [87] A. Yadav, A. Swetapadma, "A novel transmission line relaying scheme for fault detection and classification using wavelet transform and linear discriminant analysis," *Ain Shams Eng. J.* 6:199–209, 2015.
- [88] I. Baqui, I. Zamora, J. Mazón, G. Buigues, "High impedance fault detection methodology using wavelet transform and artificial neural networks," *Electr. Pow. Syst. Res.* 81:1325–1333, 2011.
- [89] J. Liang, S. Elangovan, J. B. X. Devotta, "Application of wavelet transform in travelling wave protection," *Electr. Pow. Energ. Syst.* 22:537–542, 2000.
- [90] M. Da Silva, M. Oleskovicz, D. V. Coury, "A hybrid fault locator for three-terminal lines based on wavelet transforms," *Electr. Pow. Syst. Res.* 78:1980–1988, 2008.
- [91] A. E. B. Abu-Elanien, A. A. Elserougi, A. S. Abdel-Khalik, A. M. Massoud, S. Ahmed, "A differential protection technique for multi-terminal HVDC," *Electr. Pow. Syst. Res.* 130:78–88, 2016.
- [92] A. E. B. Abu-Elanien, A. S. Abdel-Khalik, A. M. Massoud, S. Ahmed, "A non-communication based protection algorithm for multi-terminal HVDC grids," *Electr. Pow. Syst. Res.* 144:41–51, 2017.

## BIOGRAPHIES



**Nevzat ONAT** was born in Turgutlu/Manisa-Turkey, in 1973. He received the B.S. and M.S. degrees in electrical education from the University of Marmara, in 1999 and the Ph.D. degree in electrical education from Marmara University, in 2005. From 1997 to 2006, he was a Research Assistant with the Electrical Machines Laboratory in Marmara University. From 2006 to 2012, he was an Assistant Professor in Marmara University. Since 2016, he has been Professor with the Electrical and Electronics Engineering Department, Manisa Celal Bayar University. He is the author of a book, more than 30 articles, and more than 40 proceedings. His research interests include electrical machines, power system protections, renewable energy (photovoltaics).

# Ultra-High Accurate Attitude Determination and Control of Microsatellite Formation Flight

N. S. Doszhan, G.E. Ibrayev and R.R. Pilpani

**Abstract**—Nowadays, technology and space science are developing rapidly, providing new possibilities for multi-segment missions to become a frequent practice. This relates to small satellites, which could be used to organize a formation, in order to solve complex scientific and applied problems. A formation could serve as distributed instruments for atmospheric sampling, construct a large distributed antenna platform, or make a large distributed aperture for imaging and other applications what only a big satellite can achieve. Small satellite's formation flying is low cost space project compared to one big satellite. However, to develop satellite formation a lot of problems should be solved depending on its mission.

One of the important tasks in small satellite formation is an accurate determination and control of position and attitude. This paper provides a mathematical modelling of a small satellite's formation motion, which is essential to realize a synthetic aperture telescope. Furthermore, the paper describes the principle of formation configuration and its design.

**Keywords**— geostationary orbit, formation flight, formation flying control, microsatellite.

## I. INTRODUCTION

IN RECENT years, one of the most relevant tasks in the field of space monitoring especially for countries with large territories is observing of the Earth's surface in real time, which allows to monitor the rapid processes, such as, for example, the emergence and spread of steppe and forest fires. To achieve this goal, leading space agencies of the European Union, China and other countries are engaged in research and development of spacecrafts, which intended for remote sensing of the Earth from the geostationary orbit. Spacecrafts with a mass of several tons are not economically attractive, so recently an idea of launching a small spacecraft formation to a geostationary orbit appeared. For Kazakhstan which is

**N.S. DOSZHAN**, is with Department of Mechanics Kazakh National University named after al-Farabi, Almaty, Kazakhstan, (e-mail: [nursultan.sagynaiuly@gmail.com](mailto:nursultan.sagynaiuly@gmail.com)).

**G.E. IBRAYEV**, is with Department of Mechanics Kazakh National University named after al-Farabi, Almaty, Kazakhstan, (e-mail: [garyp.ybraev@gmail.com](mailto:garyp.ybraev@gmail.com)).

**R.R. PILPANI**, is with Department of Mechanics Kazakh National University named after al-Farabi, Almaty, Kazakhstan, (e-mail: [pilpani.roland@gmail.com](mailto:pilpani.roland@gmail.com)).

Manuscript received May 14, 2018; accepted October 20, 2018.  
DOI: [10.17694/bajece.475540](https://doi.org/10.17694/bajece.475540)

actively developing space activities in the field of remote sensing of the Earth and having a large territory, this idea is very promising. When developing a small satellite formation, the most intricate problem is a formation motion control. Therefore, currently development of control system of satellite formation motion on geostationary is scientifically new and actual task.

As is known, remote sensing satellites in low Earth orbit cannot monitor with high frequency. The revisit interval with a period of less than one hour requires more than 200 satellites. Satellites formation on geostationary orbit has 24-hour observability over a quarter of the Earth's surface, and data can be transmitted without time delay.

## II. THEORY

It is planned to use the telescopes as payload of the small satellite formation. Nowadays the available place for the payload of the satellite limits the current capability of space telescopes. The telescope must fit both in mass and in size. This greatly limits the capability of the telescope since the distance observable is related to the baseline of the telescope.

In traditional telescopes, the baseline is the diameter of the primary mirror. Some effort has been made to generate deployable or segmented telescopes, but they are still fundamentally limited. Alternate option is launching separated satellites and organizing them into formation [1]. For a formation flying telescope, the effective baseline of the telescope is the distance between the satellites. The light is collected from separated apertures, and then combined to form the image. The formation flight of the microsatellite is superior in cost, flexibility and robustness compared to a mission by one large satellite, and the future demand for synthetic aperture is remarkable [2].

There are four elements that are special to the formation flying problem: formation design, relative navigation, intersatellite communication, and formation control. These are described as follows.

### A. Formation design

Formation design observed as the collective guidance problem for the desired location of each satellite as a function of time. It is dictated by the science needs of the mission. The dynamics of relative motion as applied to formation design continue to be a major research area. The problem is not only the specification of where the satellite needs to be as a function of time but also how to do this in the most fuel-efficient manner. Concisely, formation design is the science of designing the desired relative motion of the vehicles to best meet science requirements without unreasonable fuel consumption.

### B. Relative Navigation

Relative navigation is the estimation of relative positions based on the measurements between adjacent satellites. Basically, the measurements are provided by sensors attached to the satellites. Accuracy class of the sensors depends on the purposes of mission.

### C. Communication

The inter-satellite communication system is the data bus of the formation. More so than in other data buses, robustness and continuity are essential. The primary areas of development are mass, power and cost reduction, and integration of communications and ranging functions. This area includes hardware (transceivers or transponders), algorithms and network architectures, and software. Substantial work is still needed in developing requirements for communication bandwidth and time synchronization and transfer for precision formation control performance. Since the formation control laws are implemented through this system, a lack of integrity in the system will be a showstopper.

### D. Formation Control

Formation control is responsible for rejecting disturbances, maintaining formation stability, and commanding the formation [3-4]. Specifically, this involves the application of forces and moments required to regulate and/or track desired formation geometry. Formation control includes the actuators, other components and algorithms, together with autonomy and higher-level command and control. The formation control function is heavily dependent on new technology. It is truly a system-level problem, depending critically on performance of the inter-satellite communications, the relative navigation, and the formation design. Formation control is the principal driver for concepts such as six degree of freedom satellite control and closed-loop orbit control.

## III. FORMATION FOR EARTH REMOTE SENSING IN REAL TIME

Applying proper methods to solve the problem of each of the formation flying elements, the model of microsatellite formation with ultra-high accurate attitude determination and control could be developed.

Idea is to develop the formation flying of 4 microsatellites for Earth Remote sensing. This formation of small satellites should have very precise attitude control and determination. The main goal is to make an observation of the Earth (or part of Earth) near real time using low cost small satellite formation with ultra-high accuracy attitude control.

It is planned to use small satellite formation to generate one large synthetic aperture for scanning the Earth near real time. Using small satellite formation to the Low Earth Orbit for scanning the Earth near real time is impossible, because of high rotational speed of formation around the Earth, therefore image will be blurred. It is planned to put the formation to the geosynchronous orbit (GEO) which is very good point to observe the Earth in near real time.

First point is formation design. To solve problems of the mission, we need to use 4 microsatellites. They will consist of three small aperture telescopes and one combiner satellite to which the light from the three telescopes is relayed to be

combined and detected. The distance between microsatellites will be 1 m (Fig.1).

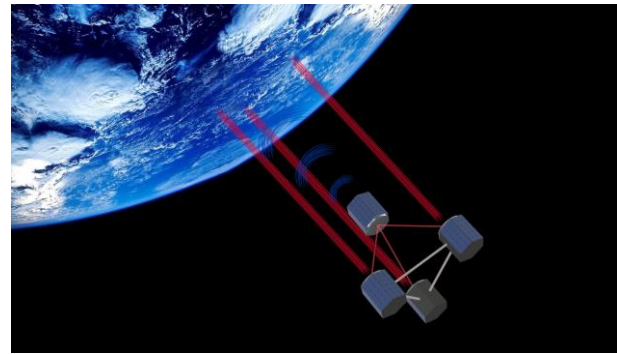


Fig.1. Satellite formation with aperture telescopes

It is planned to use the Fizeau type (Fig.2) synthetic aperture space telescope for each microsatellite to reach high resolution imaging [5].

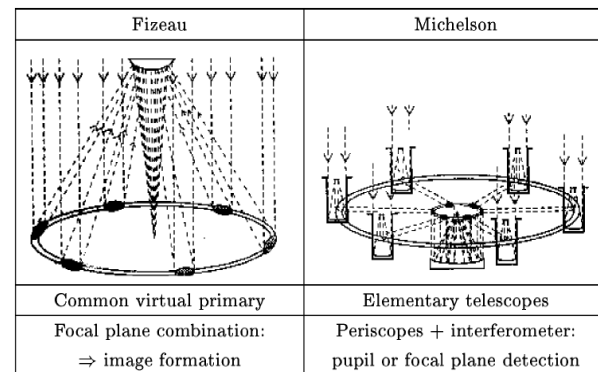


Fig.2. Imaging with multi-aperture optical telescopes and an application

A Fizeau synthetic aperture space telescope contains a set of mirrors forming a virtually common primary mirror, whose light is combined onto a common secondary mirror. The combination of the light beams coming from each piece of the primary mirror forms an image that is recorded in a common focal plane, in exactly the same way as for a monolithic telescope.

Secondly, to reach ultra-high accuracy of relative navigation between microsatellites it needs to be used very accurate sensor. Multiple sensor measurements can estimate the relative attitude and distance. In total, each microsatellite will involve 3-4 distance sensors [6-7].

Next stage is developing of formation control system (Fig.3). To change the attitude and position of satellites thrusters are necessary. Then again, within purposes of our mission the thrusters should be with high accuracy class [8]. As the accurate thruster we can use the  $\mu$ -PPT (micro pulsed-plasma thruster) with very small impulse bits ( $<25\mu$  -N-sec).

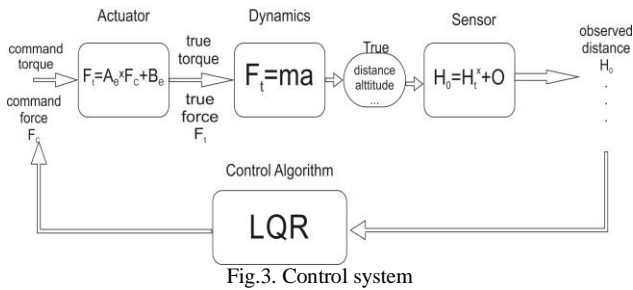


Fig.3. Control system

To success this mission there are some issues must be captured.

- For space science:
  - Measurement requires high resolution but not so much amount of light is coming to the telescopes. Longer exposure time will be one way to solve it.
  - Wave lengths which cannot be captured by ground telescope would be good target.

- For remote sensing:
  - Bush fire detection would be good starting target, as it gathers much public attention.
  - 100m/pixel, 16M pixels can cover 400 x 400km (FOV) within one exposure time (say, 5 sec)
  - FOV is scanned (by some way) over places of interest

The area of 7,741,220 square kilometres can be scanned every 5.5 minutes. Mission itself should interest government to obtain the initial investment. GEO remote sensing outside of meteorological satellite field is rather new area. The bush fire detection satellite is only required during summer seasons. In other time, it can be used for space observation, etc. (wave length consideration is of course required). Even if the satellite cannot be inserted into GEO, many technological/mission demonstrations and tests are still possible in other orbits.

IV. MATHEMATICAL MODELLING OF FORMATION MOTION IN GEO

The kinetic and potential energies for the formation from four satellite is the sum of each satellite’s energy:

$$E_k = E_{k_1} + E_{k_2} + E_{k_3} + E_{k_4};$$

$$E_p = E_{p_1} + E_{p_2} + E_{p_3} + E_{p_4}$$

(1)

where:

$E_k$  and  $E_p$  - Kinetic and potential energies of the satellite formation.

The kinetic energy of a solid body by the König theorem [9]:

$$\left. \begin{aligned} E_{k_1} &= \frac{1}{2} m_1 v_1^2 + \frac{1}{2} J_1 \omega_1^2; \\ E_{k_2} &= \frac{1}{2} m_2 v_2^2 + \frac{1}{2} J_2 \omega_2^2 \\ E_{k_3} &= \frac{1}{2} m_3 v_3^2 + \frac{1}{2} J_3 \omega_3^2; \\ E_{k_4} &= \frac{1}{2} m_4 v_4^2 + \frac{1}{2} J_4 \omega_4^2 \end{aligned} \right\}$$

(2)

where:

- $m$  - mass of the satellite;
- $v$  - velocity of the satellite;
- $J$  - moment of inertia;
- $\omega$  - angular velocity.

By the condition of the problem, the masses of three satellite with reflecting mirrors are equal.

Since all three satellites are at the same height, their speed is the same:

$$v_2 = v_3 = v_4 = v; m_2 = m_3 = m_4 = m$$

(3)

Then, the total kinetic energy of the system:

$$E_k = \frac{1}{2} m_1 v_1^2 + \frac{3}{2} m v^2 + \frac{1}{2} [J_1 \omega_1^2 + J_2 \omega_2^2 + J_3 \omega_3^2 + J_4 \omega_4^2]$$

(4)

To calculate the potential energy, it is necessary to show all the forces acting on the satellite formation. The system is acted upon by the gravity forces of the Earth and the forces of mutual attraction of satellites (Fig.4).

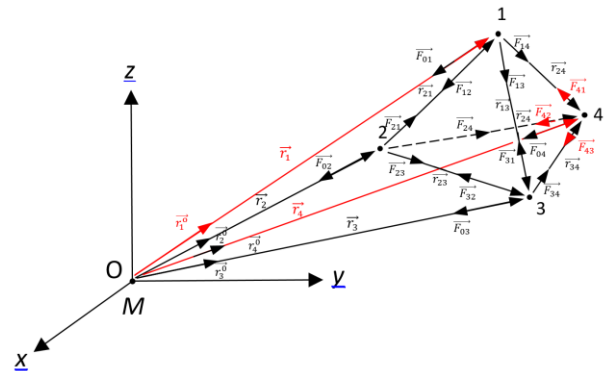


Fig.4. Gravity forces acting on the satellite formation  
Then the forces acting on the first satellite are equal:

$$\vec{F}_{01} = -G \frac{Mm}{r_1^3} \vec{r}_1^0, \quad \vec{F}_{12} = -G \frac{m_1 m}{r_{21}^3} \vec{r}_{21}^0, \quad \vec{F}_{13} = G \frac{m_1 m}{r_{13}^3} \vec{r}_{13}^0,$$

$$\vec{F}_{14} = G \frac{m_1 m}{r_{14}^3} \vec{r}_{14}^0;$$

(5)

where:

- $\vec{F}$  - forces acting on the satellite formation;
- $G$  - gravitational constant;
- $M$  - mass of the Earth;
- $m$  - masses of the satellites;
- $r$  - distances between the centers of the masses.

By the same way, it is possible to calculate the forces acting on the other satellites:

$$\vec{F}_{02} = -G \frac{Mm}{r_2^3} \vec{r}_2^0, \quad \vec{F}_{21} = G \frac{m m_1}{r_{21}^3} \vec{r}_{21}^0,$$

$$\vec{F}_{23} = G \frac{m^2}{r_{23}^3} \vec{r}_{23}^0, \quad \vec{F}_{24} = G \frac{m^2}{r_{24}^3} \vec{r}_{24}^0;$$

(6)

$$\vec{F}_{03} = -G \frac{Mm}{r_3^3} \vec{r}_3^0, \quad \vec{F}_{31} = -G \frac{mm_1}{r_{31}^3} \vec{r}_{31}^0, \quad \vec{F}_{32} = -G \frac{m^2}{r_{23}^3} \vec{r}_{23}^0$$

$$\vec{F}_{34} = G \frac{m^2}{r_{34}^3} \vec{r}_{34}^0$$

$$\vec{F}_{04} = -G \frac{Mm}{r_4^3} \vec{r}_4^0, \quad \vec{F}_{41} = -G \frac{mm_1}{r_{14}^3} \vec{r}_{14}^0$$

$$\vec{F}_{42} = -G \frac{m^2}{r_{24}^3} \vec{r}_{24}^0, \quad \vec{F}_{43} = -G \frac{m^2}{r_{34}^3} \vec{r}_{34}^0$$

For a central force field, the potential energy is expressed as:

$$E_p = -\int \vec{F} d\vec{r} + Const \tag{9}$$

If  $r = \infty$  and  $E_p = 0$  [10], then for the first satellite potential energy is:

$$E_{p_{01}} = \int G \frac{Mm_1}{r_1^3} r_1^0 dr_1^0 = G \frac{Mm_1}{r_1^3} r_1^2 = \frac{GMm_1}{|r_1|}, \quad E_{p_{12}} = \frac{Gm_1 m}{|r_{21}|}$$

$$E_{p_{13}} = -\frac{Gm_1 m}{|r_{13}|}, \quad E_{p_{14}} = -\frac{Gm_1 m}{|r_{14}|} \tag{10}$$

By the same way, it is possible to calculate the potential energy of other satellites:

$$E_{p_{02}} = \frac{GMm_1}{|r_2|}, \quad E_{p_{21}} = -\frac{Gmm_1}{|r_{21}|}$$

$$E_{p_{23}} = -\frac{Gm^2}{|r_{23}|}, \quad E_{p_{24}} = -\frac{Gm^2}{|r_{24}|} \tag{11}$$

$$E_{p_{03}} = \frac{GMm}{|r_3|}, \quad E_{p_{31}} = \frac{Gm_1 m}{|r_{31}|}$$

$$E_{p_{32}} = \frac{Gm^2}{|r_{23}|}, \quad E_{p_{34}} = -\frac{Gm^2}{|r_{34}|} \tag{12}$$

$$E_{p_{04}} = \frac{GMm}{|r_4|}, \quad E_{p_{41}} = \frac{Gm_1 m}{|r_{41}|}$$

$$E_{p_{42}} = \frac{Gm^2}{|r_{24}|}, \quad E_{p_{43}} = \frac{Gm^2}{|r_{34}|} \tag{13}$$

If assume that:

$$|r_{23}| = |r_{34}| = |r_{24}| = |r|, \quad |r_{13}| = |r_{14}| = |r_{12}| = |r'| \tag{14}$$

Then the potential energy of the system:

$$E_p = GM \left[ \frac{m_1}{|r_1|} + m \left( \frac{1}{|r_2|} + \frac{1}{|r_3|} + \frac{1}{|r_4|} \right) \right] \tag{15}$$

To calculate the rotational motion relative to the center of mass, it is necessary to use the Koenig coordinate system

relative to the center of inertia of the Earth. OXYZ is the coordinate system, where O is the center mass of the Earth. The x-axis is directed along the Greenwich, the z-axis is directed along the rotation axis of the Earth, and the y-axis completes the coordinate system to the right (Fig.5).

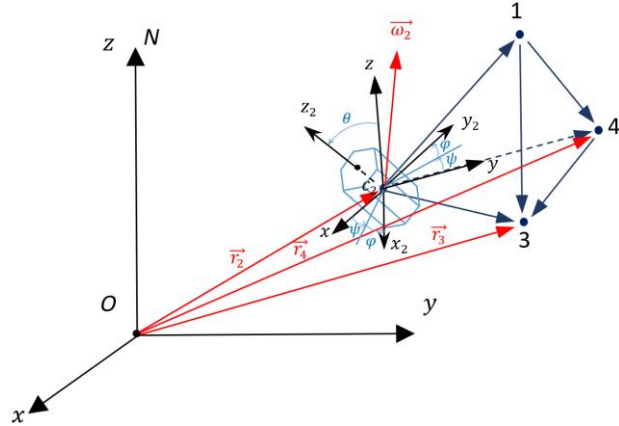


Fig.5. Koenig coordinate system relative to the center of inertia of the Earth.

$C_2X_2Y_2Z_2$  is Koenig coordinate system [11],  $C_2X_2Y_2Z_2$  is principal axes of the satellite. The projection of the angular velocity vector  $\vec{\omega}_2$  onto the movable axes:

$$\begin{cases} \omega_{2x_2} = \dot{\psi}_2 \sin \theta_2 \sin \varphi_2 + \dot{\theta}_2 \cos \varphi_2 \\ \omega_{2y_2} = \dot{\psi}_2 \sin \theta_2 \cos \varphi_2 - \dot{\theta}_2 \sin \varphi_2 \\ \omega_{2z_2} = \dot{\varphi}_2 + \dot{\psi}_2 \cos \theta_2 \end{cases} \tag{16}$$

where:  $\psi_2, \theta_2, \varphi_2$  - Euler angles for the second satellite. And the square of angular velocity module is:

$$\omega_2^2 = \dot{\psi}_2^2 + \dot{\theta}_2^2 + \dot{\varphi}_2^2 + 2\dot{\varphi}_2 \dot{\psi}_2 \cos \theta_2 \tag{17}$$

By the same way, it is possible to calculate the square of angular velocity module for other satellites:

$$\begin{cases} \omega_1^2 = \dot{\psi}_1^2 + \dot{\theta}_1^2 + \dot{\varphi}_1^2 + 2\dot{\varphi}_1 \dot{\psi}_1 \cos \theta_1 \\ \omega_3^2 = \dot{\psi}_3^2 + \dot{\theta}_3^2 + \dot{\varphi}_3^2 + 2\dot{\varphi}_3 \dot{\psi}_3 \cos \theta_3 \\ \omega_4^2 = \dot{\psi}_4^2 + \dot{\theta}_4^2 + \dot{\varphi}_4^2 + 2\dot{\varphi}_4 \dot{\psi}_4 \cos \theta_4 \end{cases} \tag{18}$$

Assuming that the generalized coordinates  $q_1 = x_1, q_2 = y_1, q_3 = z_1, q_4 = \psi_1, q_5 = \theta_1, q_6 = \varphi_1$  and substituting Equations (17) and (18) into Equation (4), then using the Lagrange equations of the second kind, the following equations of motion of the system are obtained:

$$\left\{ \begin{array}{l} \ddot{x}_1 = GM \frac{x_1}{r_1^3}, \quad \dot{\psi}_1 = \frac{\sin \varphi_1}{\sin \theta_1} p_1 + \frac{\cos \varphi_1}{\sin \theta_1} q_1 \\ \ddot{y}_1 = GM \frac{y_1}{r_1^3}, \quad \dot{\theta}_1 = p_1 \cos \varphi_1 - q_1 \sin \varphi_1 \\ \ddot{z}_1 = GM \frac{z_1}{r_1^3}, \\ \dot{\varphi}_1 = r_1 - p_1 \sin \varphi_1 \operatorname{ctg} \theta_1 - q_1 \cos \varphi_1 \operatorname{ctg} \theta_1 \\ J_x \dot{p}_1 + (J_z - J_y) q_1 r_1 = M_{x_1}, \\ J_y \dot{q}_1 + (J_x - J_z) p_1 r_1 = M_{y_1}, \\ J_z \dot{r}_1 + (J_y - J_x) p_1 q_1 = M_{z_1}. \end{array} \right. \quad (19)$$

## V. CONCLUSIONS

Formation Flying is quickly revolutionizing the way the space community conducts autonomous science missions around the earth and in space. For Earth remote sensing it is possible to use other orbit than LEO, also it is very important to decrease the time and cost to develop new space technologies. This paper demonstrates how optimally we can achieve the almost impossible mission using modern technologies and science. One important goal of this work is possibility of microsatellite formations development in university level, which can totally replace the large spacecrafts in near future.

For the future, it is planned to study the impact of the solar radiation pressure to small satellite formation in GEO. In addition, it is planned to develop methods of nm-class sensing between microsatellites and control methods of this formation using multilevel actuators. Furthermore, the study of cooperative work of low thrust engine and proximity sensor of each satellite in formation will be implemented using MatLab

## ACKNOWLEDGMENT

This work has been supported financially by the research project №AP05132939, for 2018-2020 of the al-Farabi Kazakh National University, which is gratefully acknowledged by the author.

## REFERENCES

- [1] Jesse Leitner. Formation Flying: The Future of Remote Sensing from Space. Proceedings of the International Symposium on Space Flight Dynamics, Munich, Oct., 2004, 11–15.
- [2] Saptashi Bandyopadhyay, Rebecca Foust, Giri P. Subramanian, Soon-Jo Chung, and Fred Y. Hadaegh. Review of Formation Flying and Constellation Missions Using Nanosatellites. Journal of Spacecrafts and Rockets, Vol. 53, No.3, 1-12 (2016).
- [3] D. C. Folta, L. K. Newman and T. Gardner. Foundations of Formation Flying for Mission to Planet Earth and New Millennium. AIAA, 1996, 656–666.

- [4] Gokhan Inalhan, Franz D. Busse and Jonathan P. How. Precise formation flying control of multiple spacecraft using carrier-phase differential GPS. Proc. of AAS/AIAA Space Flight Mechanics Conference, Clearwater, FL, Paper No. AAS 00-109, January 23-26, 2000.
- [5] Kun Liu, Yanfeng Qiao, Xiangyong Duan. Optical remote imaging using Fizeau synthetic aperture telescope. Proc. of Lasers & Electro Optics & The Pacific Rim Conference on Lasers and Electro-Optics, Shanghai China, August 31 – September 3, 2009.
- [6] <http://www.keyence.com/>
- [7] Journals William J Weber, Antonella Cavalleri, Rita Dolesi, Giorgio Fontana, Mauro Hueller, and Stefano Vitale. Position sensors for LISA drag-free control. Classical and Quantum Gravity, Vol.19, No.7, 1751-1752 (2002).
- [8] Proceedings (Transactions, Book of abstracts, Proceedings on CD, etc.) John K. Ziemer and Stephen M. Merkowit. Microthrust propulsion of the LISA mission. Proc. of 40th AIAA joint propulsion conference. Fort Lauderdale, Florida, July 12-14, 2004
- [9] Yablonskiy A.A., Nikiforova V.M., Kurs teoreticheskoy mehaniki. – SPb.: «Lan», 2001. – 504 p.
- [10] Markeev A.P., Teoreticheskaya mehanika, M.: «CheRo», 1999. – 96 p.
- [11] Beletskiy V.V., Dvizhenie sputnika otositelno tsentra mass v gravitatsionnom pole, M.: 1975, 17 p.

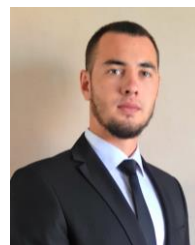
## BIOGRAPHIES



**NURSULTAN DOSZHAN** Republic of Kazakhstan, Aktobe city, in 1991. He received the B.S. degree in technical physics and M.S. degree in astronomy from the Kazakh National University named after Al-Farabi, Almaty city, B.S. in 2012 and M.S. in 2014. Since 2014, he has been researcher and senior teacher of the Department on Mechanics in al-Farabi Kazakh National University. He is the author of 10 articles, and the 4 international conferences. His research interests include small spacecraft design, spacecraft attitude determination and control, small spacecraft formation motion control



**IBRAYEV GULAMA-GARIP ALISHER** Republic of Kazakhstan, Uralsk city, in 1992. He received the B.S. degree in space technic and technologies and M.S. degree in space technic and technologies from the Kazakh National University named after Al-Farabi, Almaty city, B.S. in 2014 and M.S. in 2016. Since 2017, he has been PhD student, researcher and lecturer of the Department of Mechanics in al-Farabi Kazakh National University. He is the author of 1 book, 15 articles, and the 7 international conferences. His research interests include astrodynamics, solid mechanics, nonlinear oscillations and rotor dynamics



**PILPANI ROLAND** Almaty City, in 1997. He was enrolled in Kazakh National University named after al-Farabi in 2015, on the Faculty of Mechanics and Mathematics; specialty is “Space Engineering and Technologies”.

Since 2017, he has been a Laboratory Assistant. His research interests include designing and application of small spacecrafts, control system of spacecraft, satellite formation flying control systems.

# Implementation and Performance Analysis of a Switched Reluctance Motor Fed from Non-Energy Stored PV System

S. B. Efe, B. Kocaman and D. D. Aktaş

**Abstract**— In this paper, an actual system that consist of a switched reluctance motor (SRM) and photovoltaic (PV) generation was analyzed to determine operational behaviors in terms of both generating and motor units. System was designed without an energy storage unit. This type of design allows obtaining more convergence and actual results during operation in different conditions. According to this aim, a system that includes such structures was constructed physically. System was operated and observed for different weather and loading conditions. As the proposed system was aimed to use for agricultural electrical vehicle applications, results were discussed by using graphs that obtained from various points, especially in terms of these approaches.

**Index Terms**— Photovoltaic system, power system analysis, renewable energy sources, switched reluctance motor.

## I. INTRODUCTION

TECHNOLOGICAL DEVELOPMENTS increases the energy use in acceleration and the conventional energy sources cannot meet this demand. It became vital to integrate renewable energy sources to main grid for supplying quality and continuous energy to customers. One of the major loads in power systems are motor loads. As it is known that motor parameters are directly affect from supply parameters like voltage and current, in this study, a switched reluctance motor (SRM) that supplied by a photovoltaic (PV) system is analyzed during various operating conditions. It is aimed to obtain operational data to determine the motor efficiency while supplied by a renewable energy source. System was designed as not to include any storage unit like battery. This allows researchers to test the motor in limited supply capacity conditions and obtain more actual results. According to this aim, literature was reviewed for PV systems and motor applications. Studies on PV applications, which include design [1-3] and analysis [4-6] of such systems, can be observed

S. B. EFE, is with Department of Electrical and Electronics Engineering Bitlis Eren University, Bitlis, Turkey, (e-mail: [sbefe@beu.edu.tr](mailto:sbefe@beu.edu.tr)).

B. KOCAMAN, is with Department of Electrical and Electronics Engineering Bitlis Eren University, Bitlis, Turkey, (e-mail: [bkocaman@beu.edu.tr](mailto:bkocaman@beu.edu.tr)).

D. D. AKTAŞ, is MSc. student with Department of Electrical and Electronics Engineering Bitlis Eren University, Bitlis, Turkey, (e-mail: [dilandemir08@gmail.com](mailto:dilandemir08@gmail.com)).

Manuscript received August 30, 2018; accepted October 28, 2018.

DOI: [10.17694/bajece.455150](https://doi.org/10.17694/bajece.455150)

widely in literature. It is necessary to analyze the PV modules for energy output characteristics because of the mismatch losses and shading losses of such structures. PV system studies are divided into two in general as grid connected [7-8] and islanded or standalone [9-10] modes of operation. In addition, researchers are focused on the various types of motors as loads for PV systems. These papers are classified as induction motor [11-12] and DC motor [13-14] supplement. Besides the classical electric motors, in this research, SRM is chosen to use its advantages as given in following sections. The paper was designed as following; in section II mathematical models of system components, which are PV system and SRM, were given. Performance analysis was performed in section III and results were discussed in section IV.

## II. MATHEMATICAL BACKGROUND

Mathematical representation of the system elements have to be given for a better understanding of performance analysis results besides physical structures. Therefore, mathematical models and actual system components of PV system and SRM are given in subsections A and B respectively.

### A. Photovoltaic System

The PV effect is the creation of voltage or electric current in a material upon exposure to light. PV system works on the principle of photovoltaic effect, direct conversion of photonic energy to electrical energy using PV cells. The power generated from these PV cells depends directly on the level of solar irradiation [15].

Detailed analysis and study is necessary for an appropriate design of PV systems. Therefore, it should be started from cell level for better understanding. PV panels are formed by connecting photovoltaic cells series and parallel, which are created by semiconductor materials. General structure of a PV cell is given in Fig. 1. [16-18].

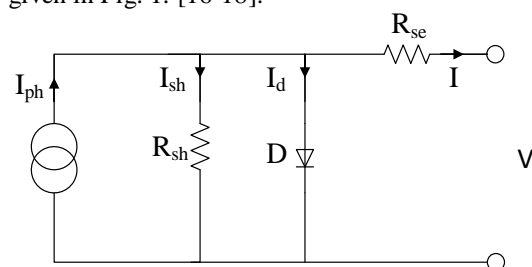


Fig. 1. PV cell circuit

According to the given equivalent circuit, mathematical model of a PV cell can be described as:

$$I = I_{ph} - I_d - I_{sh} \tag{1}$$

$$I = I_{ph} - I \left[ e^{\frac{q(V+IR_{se})}{kT}} - 1 \right] - \frac{V + IR_{se}}{R_{sh}} \tag{2}$$

In Equation (2), I shows the current, V represents the terminal voltage, q shows electron charge, k is the Boltzmann constant and T is the ambient temperature in terms of Kelvin. According to the design, Equation (2) can also be rewritten to obtain output voltage.

In this study, a PV system that is physically installed at Bitlis Eren University Rahva Campus is used as energy source for SRM. This structure is given in Fig. 2.



Fig. 2. PV panel and inverter

There were six PV panels, each has a power of 150 W, and a 24/220 V full sine inverter with a power of 3000 VA used for PV system.

**B. Switched Reluctance Motor**

SRM can be considered as an alternative to conventional electric machines. It is cheaper and simpler than the same powerful conventional machines because of the improvements in motor drive technology [19-20].

The equivalent circuit of SRM is shown in Fig.3. In this circuit, output emf can be modeled as a current controlled voltage source. Due to the saliency on rotor and stator side, SRM has non-sinusoidal current and flux across all windings.

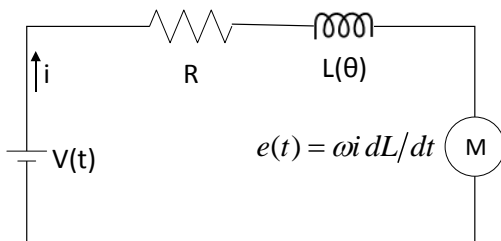


Fig. 3. SRM equivalent circuit

According to the Fig. 3, voltage equation for one phase can be given as,

$$v = Ri + \frac{d\psi}{dt} = Ri + \frac{d(Li)}{dt} = Ri + L \frac{di}{dt} + i \frac{dL}{dt} \tag{3}$$

$$= Ri + L \frac{di}{dt} + i \frac{dL}{d\theta} \frac{d\theta}{dt} \tag{4}$$

And finally

$$v = Ri + L \frac{di}{dt} + \omega_m i \frac{dL}{d\theta} \tag{5}$$

where v is terminal voltage, R is phase resistance, i is current,  $\psi$  is flux, L is phase inductance,  $\theta$  is rotor position and  $\omega_m$  is angular speed in rad/s.

Power value can be obtained as

$$P = Vi = Ri^2 + L_i \frac{di}{dt} + \omega i^2 \frac{dL}{d\theta} \tag{6}$$

As the torque equation is

$$T = \frac{P}{\omega_e} \tag{7}$$

Then the torque  $T_e$  that can be obtained from the motor

$$T_e = \frac{1}{2} i^2 \frac{dL(i, \theta)}{d\theta} \tag{8}$$

Similar as other motors, for SRM, torque is limited by maximum allowed current, and speed by the available terminal voltage, which is illustrated in Fig. 4.

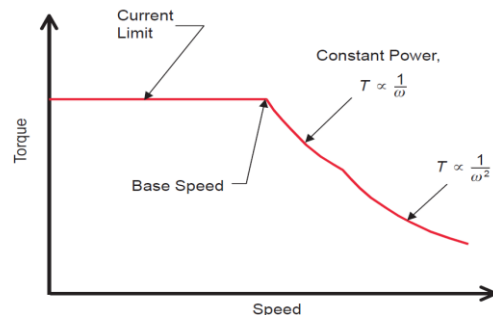


Fig. 4. SRM Torque – Speed Characteristics

Switched reluctance motor (SRM) has the advanced capability as it is the most suitable motor for variable speed applications like solar photovoltaic (SPV) array fed water pumping system. A PV pumping system using SRM is analyzed in [21-22] but it has some drawbacks due to use of battery [23]. The torque-speed operating point of an SRM is essentially programmable and determined almost entirely by the control. This is one of the features that makes the SRM an attractive solution for various applications [24].

An 8/6 SRM with an intelligent control unit was used in this study. SRM with intelligent control unit is shown in Fig. 5, where properties of the SRM that was used in system are summarized in Table 1.



Fig. 5. SRM and controller unit

TABLE I  
SRM PROPERTIES

| Parameter                  | Value          |
|----------------------------|----------------|
| Phase                      | 1 $\phi$       |
| Nominal Voltage            | 220 V          |
| Max. Power at Nom. Voltage | 1400 W         |
| Rotor Speed                | 50 to 5000 rpm |

III. EXPERIMENTAL PERFORMANCE ANALYSIS

Proposed system was tested for different operating conditions to obtain performance data. Fluke 435 power and energy analyzer was used for measurement. As the system has no storage unit, PV generation directly affect the SRM. Therefore, system was observed in two cases, first was for different loading conditions in case of full irradiance and second in case of partial shading. A powder-brake unit with torque controller, which is shown in Fig. 6, was used to adjust loading values.



Fig. 6. Load unit

A. Case 1- Nominal irradiance conditions

In this case, system was tested when the PV had nominal irradiance. SRM was adjusted to operate at 1000-rpm rotor speed, loaded with 15%, 30%, 45% and 60% respectively in such condition and results were summarized in Fig. 7.

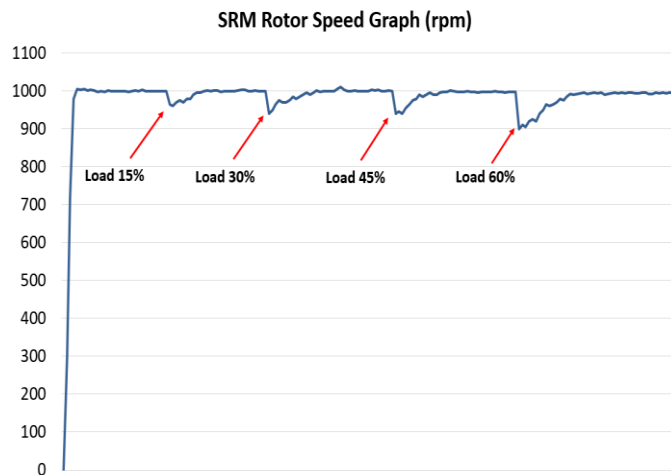


Fig. 7. Rotor speed during nominal irradiance

It is clear from Fig.7 that SRM could regulate the speed via intelligent control unit in nominal irradiance conditions. As there was a decrement in rotor speed, it was in tolerance limits that can be ignored. Therefore, it can be assumed that motor works efficiently under proposed conditions.

B. Case 2- Partial shading conditions

As it is common to occur irradiance decrement in case of possible shading at PV panels because of meteorological effects and dust, system was analyzed to obtain operational data for such conditions. In this case, irradiance was decreased 20% and 40% manually. Motor was loaded 15%, 30%, 45% and 60% for each level and results of 20% and 40% irradiance decrement were given in Fig. 8 and Fig. 9 respectively.

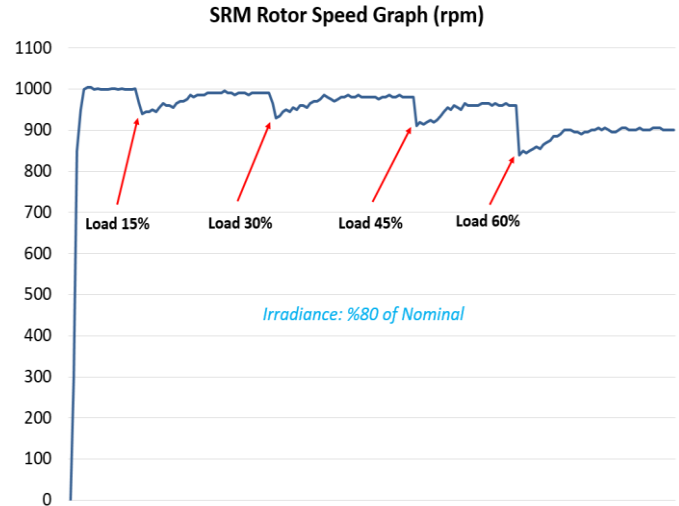


Fig. 8. Rotor speed during 80% of nominal irradiance

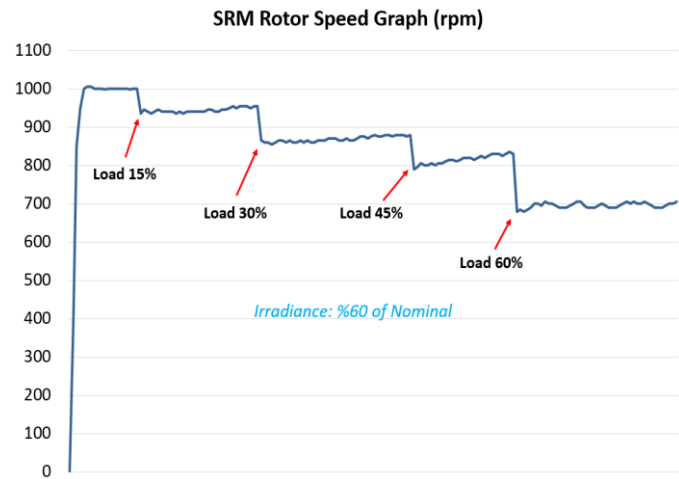


Fig. 9. Rotor speed during 60% of nominal irradiance

As irradiance is the major parameter of PV generation, it is clear from Fig. 8 and Fig. 9 that decrement in such parameter affect motor speed especially when loading value increased. Unlike the Case 1 results, as expected, motor speed cannot be recovered to nominal speed. However, it still continues to operate and shows stability in speed characteristic. Speed can be regulated by controlled load-shedding in case of generation level decrement by a closed loop algorithm.

IV. CONCLUSION

In this study, a SRM is analyzed under different operating conditions to obtain the behaviors in case of renewable energy source based supplement. These behaviors are vital for agricultural applications and especially to use SRM in PV

supplied electric cars. For such aim, system is analyzed for direct PV-fed mode of operation. Various loading and irradiance conditions are tested and results are discussed by using system graphs. It is clear that SRM is appropriate in using non-storage unit systems that have limited capacity of energy with an appropriate controlling unit. In case of decrement in generation values, motor speed can also be regulated by controlling loads. It should be noted that all meteorological effects are applied to experimental system and these affect results directly. Authors are in process of determine data for various conditions and applications.

#### ACKNOWLEDGMENT

This study is supported by Bitlis Eren University Scientific Research Projects Unit (BEBAP) with project number **BEBAP 2018.06**. Authors would like to thank BEBAP for valuable contribution.

#### REFERENCES

- [1] J. Matics and G. Krost, "Intelligent Design of PV Based Home Supply Using a Versatile Simulation Tool," 13th International Conference on Intelligent Systems Application to Power Systems, 2005, pp. 61–66.
- [2] B. Ramkumar H.M. Kittur, and P. M. Kannan, "A Solid 500 Sun Compound Concentrator PV Design," IEEE 4th World Conference on Photovoltaic Energy Conference, 2006, pp.694–697.
- [3] J. Xue, Z. Yin, B. Wu and J. Peng, "Design of PV Array Model Based On EMTDC/PSCAD," IEEE Asia-Pacific Power and Energy Engineering Conference, 2009, pp. 1–5.
- [4] H. So, B. G. Yu, H. M. Hwang, G. Yu, Y. Choi and I. Choy, "Performance Monitoring and Analysis of Middle Scale Grid-Connected PV System," IEEE the 7th International Conference on Power Electronics, 2007, pp. 451–454.
- [5] C.I. Wade, R. Torihara, Y. Fukamachi, T. Sakoda and N. Hayashi, "Numerical Analysis of I-V Characteristics and Diode Currents of a PV Module Reflected by Partial Shadow," IEEE Region 10 Conference (TENCON), 2016, pp. 2642–2645.
- [6] F.E. Tahiri, K. Chikh, M. Khafallah, A. Saad and D. Breuil, "Modeling and performance analysis of a solar PV power system under irradiation and load variations," 14th International Multi-Conference on Systems, Signals & Devices (SSD), 2017, pp. 234–238.
- [7] T. K. Roy, M. F. Pervej, M. I. Sarkar, and F. K. Tumpa, "Nonlinear Robust Controller Design for a Grid- Connected PV System Using DPC Approach," International Conference on Electrical, Computer and Communication Engineering (ECCE), 2017, pp. 11–16.
- [8] R. Abdul Rahman, S. Irwan Sulaiman, A. Maliki Omar, S. Shaari and Z. Md Zain, "Performance Analysis of a Grid- connected PV System at Malaysian Energy Centre, Malaysia," The 4th International Power Engineering and Optimization Conference (PEOCO2010), 2010, pp. 480– 483.
- [9] S. Choudhary, S. Saha, S. Jacob, S. Ikshith and M. Kher, "Reduction of Electricity Bill With Stand-Along Solar PV System," International Conference on Nascent Technologies in the Engineering Field (ICNTE-2017), 2017, pp. 1–5.
- [10] W.Saed, H.A. Gaber and A. Mami, "Sizing and Simulation of an Energy Sufficient Stand-alone PV Pumping System," International Conference on Promising Electronic Technologies, 2017, pp. 8–13.
- [11] K. Cherifi, Y. Miloud and M. Mostefai, "Performance of Five Level Inverter with Induction Motor Fed by PV Generator," 4th International Symposium on Environmental Friendly Energies and Applications (EFEA), 2016, pp. 1–5.
- [12] S.S. Dessouky, A. A. Elbaset, A. H. K. Alaboudy, H. A. Ibrahim and S. A. M. Abdelwahab, "Performance Improvement of A PV-Powered Induction-Motor-Driven Water Pumping System," Eighteenth International Middle East Power Systems Conference (MEPCON), 2016, pp. 1–7.
- [13] J.S. Kol, B.J. Jung, K.T. Park, C. H. Choi and D.H. Chung, "Maximum Power Point Tracking Control of PV System for DC Motors Drive with Neural Network," International Conference on Smart Manufacturing Application, 2008, pp. 514–519.
- [14] S. Krithiga, and N.A. Gounden, "A Microcontroller based Power Electronic Controller for PV assisted DC motor Control," 6th International Conference on Industrial and Information Systems, ICIIIS 2011, 2011, pp. 505–510.
- [15] M.R. Praful, A.M. Joshua, "Controller for Stand-Along PV Systems", IEEE International Conference on Power, Control, Signals and Instrumentation Engineering (ICPCSI), 2017, pp.1012–1017.
- [16] B. Kocaman, M. Akdağ, S.B. Efe, M. Akdeniz, "Implementation and Performance Analysis of a Hybrid PV-Wind Energy System", International Journal of Engineering and Advanced Technology, Vol.7 No.1, pp.100-104.
- [17] S.B. Efe, M. Cebeci, "Artificial Neural Network Based Power Flow Analysis for Micro Grids", Bitlis Eren University Journal of Science and Technology, 2015, Vol.5, No.1, pp.42-47.
- [18] S.B. Efe, M. Cebeci, H. Erdoğan, G. Öztürkmen, "A Novel Approach to Power Flow Analysis for Grid Connected Micro Grid", 13th ICEMES, 2015, pp.29-32.
- [19] S.B. Efe, B. Kocaman, D. Demir Aktaş, "Operational Analysis of a Switched Reluctance Motor Fed by PV System", IIER 2018, pp.56-59.
- [20] D. Demir, S.B. Efe, "Analysis of PV Supplied SRM for Different Operating Conditions", ICAT'18, 2018, pp. 269-272.
- [21] S. Belliwali, A.Chakravarti, A.B. Raju, "Mathematical modelling and simulation of directly coupled PV water pumping system employing Switched Reluctance Motor" IEEE PES Innovative Smart Grid Technologies, 2011, pp.386-390.
- [22] H.M.B. Metwally, W.R. Anis, "Performance Analysis of PV Pumping Systems Using Switched Reluctance Motor Drives", Energy Conversion and Management, 1997, Vol.38, No.1, pp. 1-11.
- [23] B. Singh, A.K. Mishra, R. Kumar, "Buck-boost converter fed SRM drive for solar PV array based water pumping", IEEE IAS Joint Industrial and Commercial Power Systems / Petroleum and Chemical Industry Conference, 2015, pp.153-160.
- [24] M.T. DiRenzo, "Switched Reluctance Motor Control – Basic Operation and Example Using the TMS320F240", 2000, Texas Instruments Application Report.

#### BIOGRAPHIES



**SERHAT BERAT EFE** was born in Diyarbakır, in 1979. He received the B.S. degree in Electrical and Electronics Engineering from Dicle University, (Turkey), in 2003, the M.S. degree in Electrical and Electronics Engineering from İnönü University, (Turkey), in 2007 and the Ph.D. degree Electrical and Electronics Engineering from Firat University, (Turkey), in 2014. Since 2014, he has been an Assistant Professor with the Electrical and Electronics Engineering department, Bitlis Eren University, (Turkey). His main research areas are power system analysis, power quality and renewable energy sources.



**BEHÇET KOCAMAN** was born in Bitlis, in 1972. He received the B.S. degree in Electrical Engineering from Yıldız Technical University, (Turkey), in 1993, the M.S. and PhD degrees in Electrical Engineering from Kocaeli University, (Turkey), in 1997 and 2015 respectively. Since 2015, he has been an Assistant Professor with the Electrical and Electronics Engineering department, Bitlis Eren University, (Turkey).



**DİLAN DEMİR AKTAŞ** was born in Bitlis, in 1991. She received the B.S. degree in Electrical and Electronics Engineering from Firat University (Turkey) in 2014. Since 2016, she has been a M.S. degree student with the Electrical and Electronics Engineering department, Bitlis Eren University (Turkey).

# Characterization and Measurement of Cable Losses Using Fractional-order Circuit Model

O. Aydin, B. Samanci and S. Ozoguz

**Abstract**—5G communication technology is used in very demanding applications, such as high-performance mobile devices, Internet of Things (IoT) applications, and wearable devices. Therefore, unlike the previous technologies, 5G technology requires massive bandwidth, mainly within three key frequency ranges, Sub-1 GHz, 1-6 GHz, and above 6 GHz. However, these challenges require more accurate and wide-band characterization of the circuits designed for 5G systems. To be specific, the losses, which can be neglected at lower frequencies, may substantially affect the performance of these circuits in the high frequency bands. This requires a comprehensive understanding and proper characterization of the loss mechanism within all frequency band of 5G. This paper investigates the viability of using the most common and easily accessible material FR-4 in circuits designed for 5G applications, and thus focuses on the proper modeling of the microstrip lines built around FR-4. For this purpose, we have used the fractional-order model of the lossy dielectric material, and ended up with a more accurate and simple model which fits well within a wide frequency range, from 1GHz to 16GHz.

**Index Terms**—Fractional-Order Calculus, 5G Communication Technology.

## I. INTRODUCTION

AS A RESULT of very demanding specifications of 5G systems, a comprehensive understanding and proper modeling of electrical circuits designed for this technology are required. On the other hand, due to the interdisciplinary nature of fractional calculus, there has been a growing research interest in using fractional-order calculus as a powerful tool in biochemical, medical and electrical engineering applications. In biomedical systems, it is shown that the accurate modelling of the biological cells and tissues require the utilization of fractional-order calculus [1-3].

**O. AYDIN**, is with the Department of Research and Development, Netas, 34912, Turkey (e-mail: aydin@netas.com.tr). Also with Department of Electrical and Electronics Engineering, Istanbul Technical University, Istanbul, Turkey

**S. OZOGUZ**, is with Department of Electrical and Electronics Engineering, Istanbul Technical University, 34469, Istanbul, Turkey (e-mail: ozoguz@itu.edu.tr).

**B. SAMANCI**, is with the Department of Research and Development, Netas, 34912, Turkey (e-mail: bsamanci@netas.com.tr).

Manuscript received September 24, 2018; accepted October 29, 2018.

DOI: [10.17694/bajece.473637](https://doi.org/10.17694/bajece.473637)

In another implementations, there are two types of the fractionalorder memristor: the capacitive and the inductive fractionalorder memristor [4]. Fractional order circuits for emulating the mechanical impedance model of the human respiratory system is discussed elsewhere [5].

The fractional-order model calculus is also applied to the modeling of electrical circuits. Among these, the fractionalorder model of transmission lines are presented in [6-7] based on the RLGC model approach. Basically, two main approaches have been presented for the RLGC based model of transmission line in the literature. In the first approach, the loss elements, which are due to the skin effect of the line and the dielectric absorption, are modeled by the serial resistance of the copper, R and the conductance G. However, this integer-order model produces inaccurate results and seem to characterize the transmission line loss for only high loss cases, where the main source of nonideality is due to the dispersion of the dielectric material [8].

On the other hand, fractional-order mathematical models developed for the reactive circuit elements, may provide more accurate representation of the electrical characteristics. The use of the fractional-calculus concept leads to the fractionalorder RLGC model of the transmission line, where the involved inductor and capacitor are used as the fractionalorder elements. In this model, fractional inductance is employed to model the skin effect, while the fractional order capacitance is used to model various nonidealities related to the dielectric [3, 5]. Following up in this direction, we use the fractional order model to characterize the FR-4 PCB loss to obtain more accurate model of this easily accessible element in the hope of using this element in wide bandwidth 5G applications.

In this paper, we have studied the proper modeling of the most common and widely available material FR-4, which offers reduced cost but suffers from higher loss. This may be useful in designing low-cost circuits for 5G technology built around high loss PCB materials. The fractional-order model provides higher accuracy and incorporates less number of model parameters. RLGC parameters of both models can be extracted from the measurement data. The evaluations of the models are performed based on a design of a microstrip transmission line with FR4 substrate with permittivity 4.4, substrate height of 1.0mm and loss tangent of 0.025 at microwave frequencies between 1 to 16 GHz. This paper is organized as follows: Section II describes the fundamental concepts related to the modeling of Transmission Lines. In Section III, the results and the comparison of the conventional

integer-order and fractional-order models are given. Finally, the conclusion is presented in Section IV.

II. TRANSMISSION LINE MODELS

II. 1 Conventional RLGC Model of the Transmission Line

Fig. 1(a) shows the Transmission Line model for integer order model. Per-unit model parameters can be given explicitly as follows:

$$\left. \begin{aligned} R &\approx R_o + R_s\sqrt{f}(1+i) \\ L &\approx L_o \\ C &\approx C_o \\ G &\approx G_o + G_d w \end{aligned} \right\} \quad (1)$$

where  $f$  is the frequency in Hz,  $R_o$  is the DC resistance of the line,  $R_s$  is the skin-effect resistance term,  $G_o$  is the DC shunt conductance and  $G_d$  is the conductance used to model dielectric-loss [9, 10].

According to the model, the propagation constant ( $\gamma$ ) and characteristic impedance ( $Z_o$ ) of the transmission line are defined as [10]

$$Z_o = \frac{R + j\omega L}{\gamma} = \sqrt{(R + j\omega L)/(G + j\omega C)} \quad (2)$$

$$\gamma = \alpha + j\beta = \sqrt{(R + j\omega L)(G + j\omega C)} \quad (3)$$

where  $\alpha$  is the wave attenuation constant (Np/m) and  $\beta$  is the phase constant (rad/m).

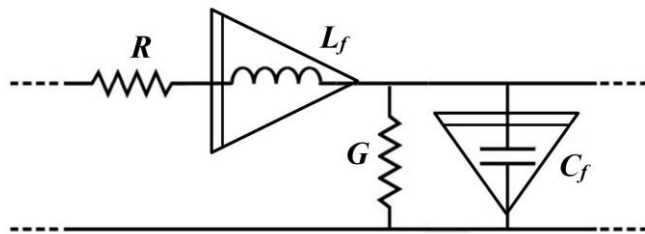
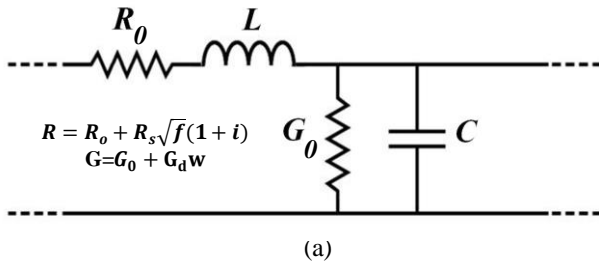


Fig. 1. (a) Classical RLGC unit cell equivalent model of transmission line. (b) Fractional-order equivalent model.

II. 2 Fractional-order Model of the Transmission Line

While the integer-order RLGC unit cell is the classical approach used to model transmission lines, researchers have been focused on using fractional-order models, in the last decade [6, 7, 11]. Fig. 1(b) shows the Transmission Line

RLGC model based on fractional-order elements. In this figure, the fractional-order capacitor is of the order  $\alpha_C$  with  $\alpha_C \in (0,1]$  and the fractional inductor is in the order  $\alpha_L$  and  $\alpha_L \in (0,1]$ . These elements are defined with the following relationships [2]:

$$i(t) = C_f \frac{d^{\alpha_C}}{dt^{\alpha_C}} v(t) \quad (4)$$

$$v(t) = L_f \frac{d^{\alpha_L}}{dt^{\alpha_L}} i(t) \quad (5)$$

For a general transmission line segment, the characteristic impedance  $Z_f$  and propagation constant  $\gamma$  are calculated as, respectively, as [11].

$$Z_f = \sqrt{\frac{Z_{L_f}}{Y_{C_f}}} = \sqrt{\frac{R_o + (j\omega)^{\alpha_L} L_f}{G_o + (j\omega)^{\alpha_C} C_f}} \quad (6)$$

$$\gamma_f = \sqrt{(R_o + (j\omega)^{\alpha_L} L_f)(G_o + (j\omega)^{\alpha_C} C_f)} \quad (7)$$

At high frequencies, the characteristic impedance,  $Z_f$  and propagation constant,  $\gamma_f$  can be evaluated using the following simplified expressions:

$$Z_f = \sqrt{L_f/C_f} \omega^{\frac{\alpha_L - \alpha_C}{2}} \left[ \cos \frac{(\alpha_L - \alpha_C)\pi}{2} + j \sin \frac{(\alpha_L - \alpha_C)\pi}{2} \right] \quad (8)$$

$$\gamma_f = \sqrt{L_f C_f} \omega^{\frac{\alpha_L + \alpha_C}{2}} \cdot \left[ \cos \frac{(\alpha_L + \alpha_C)\pi}{2} + j \sin \frac{(\alpha_L + \alpha_C)\pi}{2} \right] \quad (9)$$

II. 3 Extraction of Transmission Line Parameters Using S-Parameters

In order to extract the per-unit parameters of the RLGC model from the measurements, the measured S-parameters of the transmission line are first converted to the ABCD parameters. For this purpose, we use the inverse of the following relationship between two-port S-parameters and the ABCD matrix [10]

$$\begin{bmatrix} S_{11} & S_{12} \\ S_{21} & S_{22} \end{bmatrix} = \begin{bmatrix} \frac{A + B/Z_o - CZ_o - D}{A + B/Z_o + CZ_o + D} & \frac{2(AD - BC)}{A + B/Z_o + CZ_o + D} \\ \frac{2}{A + B/Z_o + CZ_o + D} & \frac{-A + B/Z_o - CZ_o + D}{A + B/Z_o + CZ_o + D} \end{bmatrix} \quad (10)$$

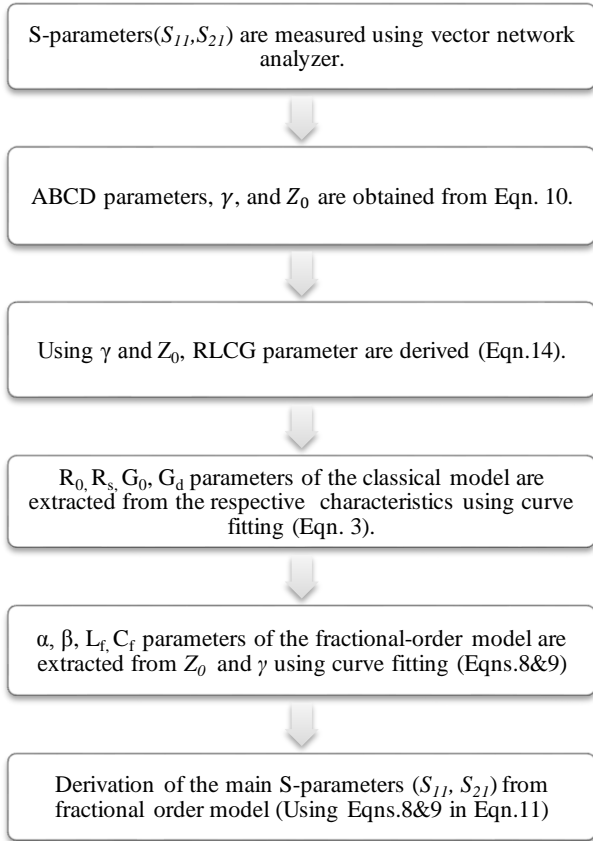
On the other hand, the ABCD matrix for a uniform transmission line with length  $l$  can be calculated in terms of the the characteristic impedance and the propagation constant as follows [12]:

$$ABCD = \begin{bmatrix} \cosh(\gamma l) & Z_o \cdot \sinh(\gamma l) \\ \sinh(\gamma l) / Z_o & \cosh(\gamma l) \end{bmatrix} \quad (11)$$

Given these basic relationships, we can now develop the procedure defined in Table I in order to retrieve the parameters of the transmission line model. Note that this

procedure can be applied both to classical integer-order and the fractional-order RLGC models.

TABLE I  
PROCEDURE FOR THE EXTRACTION OF THE FRACTIONAL-ORDER TRANSMISSION LINE PARAMETERS.



In the second step of the procedure in Table 1, we use a modified version of the method in [13] in order to extract the parameters  $Z_0$  and  $\gamma$  from the ABCD-parameters.

The complex propagation constant  $\gamma = \alpha + j\beta$  is mathematically defined by:

$$\gamma = \alpha + j\beta = \frac{\sinh^{-1} \sqrt{BC}}{l} \quad (12)$$

and  $Z_0$  is, in turn, computed from the complex propagation constant using the following equation:

$$Z_c = \frac{\gamma}{(G + j\omega C)} \quad (13)$$

where  $G = \omega C \tan \delta$ .

Finally, the RLGC parameters can be extracted from measurements using the following relationships:

$$R = \text{Re}\{\gamma/Z_c\}, \quad L = \text{Re}\{\gamma Z_c\}/\omega, \quad C = \text{Im}\{\gamma/Z_c\}/\omega, \quad (14)$$

$$G = \text{Re}\{\gamma/Z_c\}.$$

### III. EXTRACTION OF THE TRANSMISSION LINE PARAMETERS

In order to evaluate usefulness of the fractional order model, we have fabricated a microstrip line structure. The microstrip line geometries with FR-4 substrates are illustrated in Fig. 2.

For the microstrip line, the dimensions are set to  $l=25$  mm;  $w=2$  mm;  $h=1.0$  mm; and  $t=0.035$  mm. This transmission line is simulated in a high-frequency structure simulator (HFSS) and is optimized for the frequency range from 1 GHz to 16 GHz.

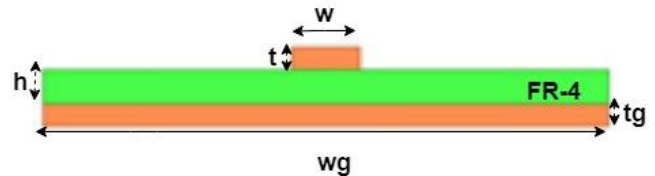


Fig. 2. Cross-section of the microstrip structure with FR-4 substrate.

Setup equipment employed are Keysight (m9374a) 20 GHz Vector Network Analyzer, Agilent 85052B/8719D 3.5mm calibration kit and RS Pro SMA connector.

TABLE II  
EXTRACTED PARAMETERS FOR INTEGER-ORDER AND FRACTIONAL-ORDER RLGC MODEL

| Integer RLGC Model    |             |                      |
|-----------------------|-------------|----------------------|
| Parameter             | Value       | Unit                 |
| $R_0$                 | 0.16        | $\Omega/m$           |
| $R_s$                 | 3.47        | $m\Omega/m \cdot Hz$ |
| $L_0$                 | 302.49      | $nH/m$               |
| $C_0$                 | 0.118       | $nF/m$               |
| $G$                   | 0.017       | $S/m$                |
| $G_d$                 | 2.37        | $Ps/m \cdot Hz$      |
| Fractional RLGC Model |             |                      |
| Parameter             | Value       | Unit                 |
| $R_0$                 | 1           | $\Omega/m$           |
| $L_f$                 | 355         | $(nVs^{-\alpha})A/m$ |
| $C_f$                 | 4.62        | $(nAs^{-\beta})V/m$  |
| $G$                   | 0.017       | $S/m$                |
| $\alpha, \alpha_c$    | 0.834, 0.79 | -                    |

The per-unit parameters of both integer and fractional order models are derived from the experimental measurements using the procedure described in Table I. The values of the parameters thus obtained are given in Table II. Since the model equations are highly nonlinear, the optimization problem has many local minima, thus the parameters given in Table II should be considered as near optimum values.

The evaluations of the model accuracies are performed based on the characteristic impedance,  $Z_0$  and the s-parameter,  $S_{21}$ . The experimental results, the simulated characteristics using the integer and fractional order models are all given in Figs. 3 & 4. Experimental results and the characteristics obtained from the model for the characteristic impedance,  $Z_0$  are given in Fig. 3(a), while the results related to the magnitude and phase functions of the  $S_{21}$  are given,

respectively, in Figs. 3(b) and (c). The integer-order and fractional-order model parameters are the optimum parameters given in Table II.

As can be seen from the results in Fig. 3(b), both integer and fractional-order models give similar results for the phase characteristic of  $S_{21}$ . However, the accuracies of the models differ significantly for the characteristic impedance,  $Z_0$  (see Fig. 3a) and the magnitude of the s-parameter,  $S_{21}$  in Fig. 3c. Therefore, in Figs. 4(a) and (b), we have also provided the variations of the error function for the characteristic impedance,  $Z_0$  and  $|S_{21}|$ , respectively.

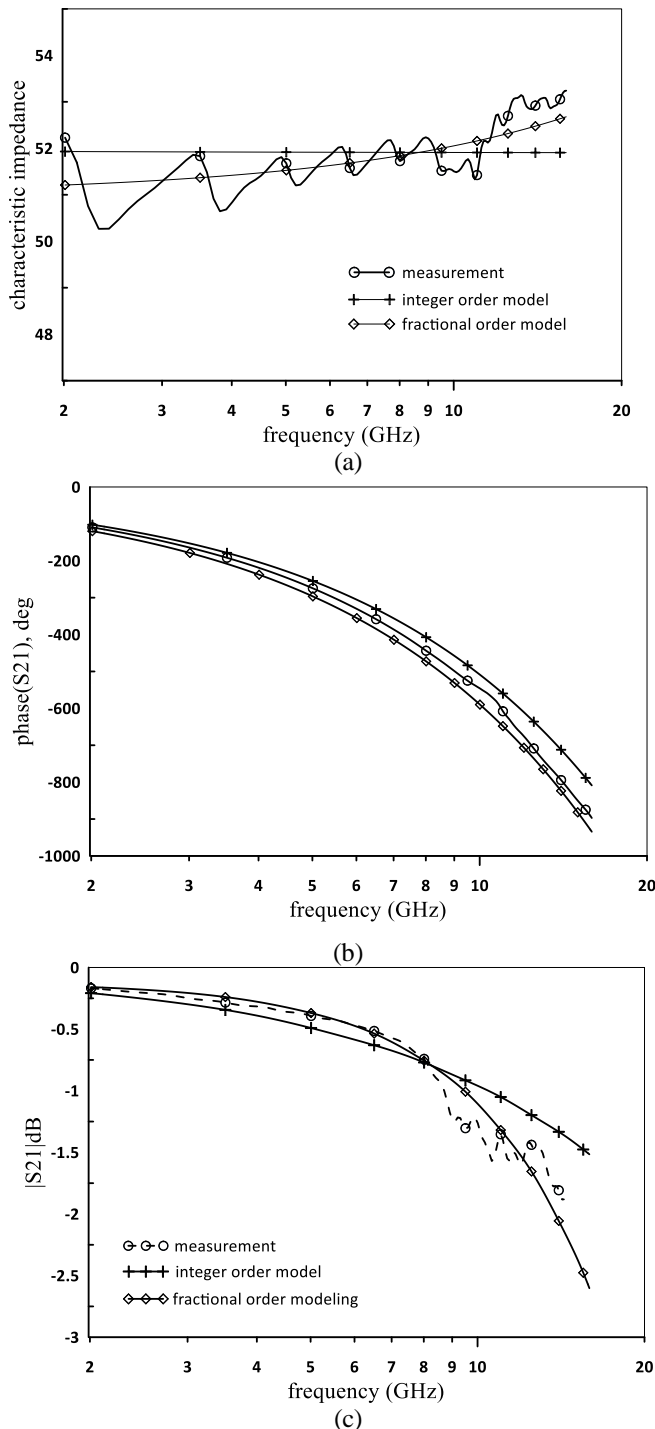


Fig. 3. Experimental results and RLGC model based

approximations of the (a) Magnitude of the characteristic impedance,  $Z_0$  (b) Phase of  $S_{21}$  in degrees, (c) Magnitude of  $S_{21}$  in dB.

From these characteristics, it is seen that fractional-order model approximates the experimental results more accurately in a wider-frequency range compared to the integer-order model. This advantage is more striking when the errors in the magnitude of the  $S_{21}$  are considered.

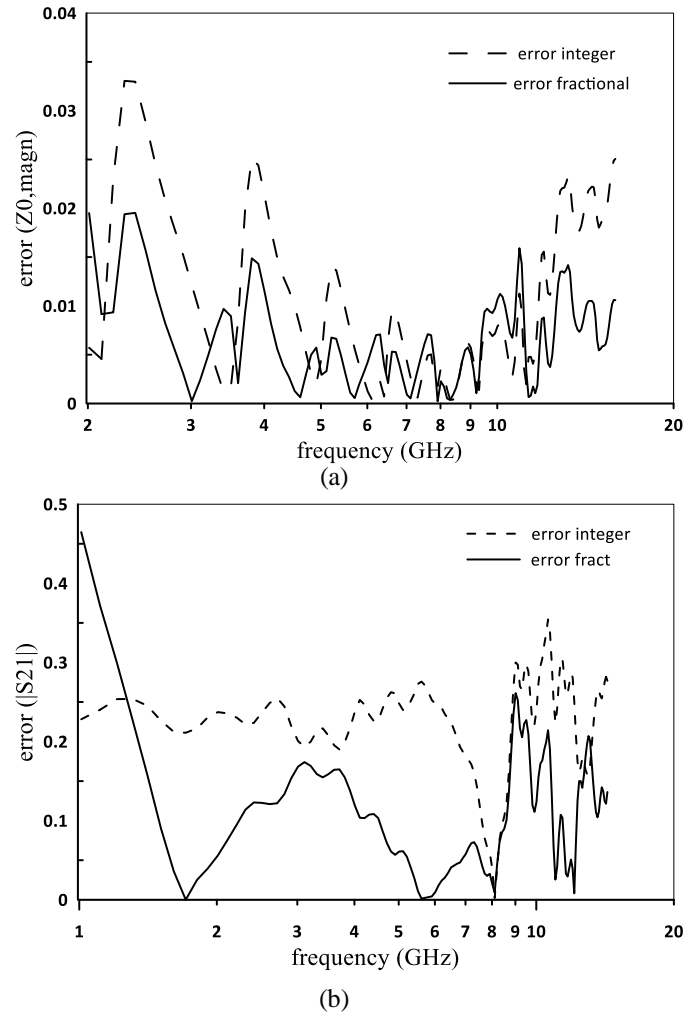


Fig. 4. Error variations of both integer-order and fractional-order RLGC models, (a) for the characteristic impedance,  $Z_0$  (b) for the magnitude of  $S_{21}$ .

#### IV. CONCLUSION

In this paper, the fractional-order model of the transmission line for the microstrip with FR-4 substrate is developed. This model is extracted via the measurements of the S-parameters. It is observed that fractional-order model allows more compact and accurate analytical model over wide-frequency band compared to the traditional integer order model. We have concluded that fractional-order characterization allows the derivation of an efficient model which incorporates the loss of the transmission line over a wide frequency range, thus is useful in applications requiring wide bandwidth. The results

may be useful for those who design circuits for 5G technology built around high loss but low cost PCB materials.

#### REFERENCES

- [1] A.S. Elwakil, "Fractional-Order Circuits and Systems: An Emerging Interdisciplinary Research Area", *IEEE Circuits and Systems Magazine*, 10, 4, 2010, pp: 40-50.
- [2] Ivo Petras, Yang Quan Chen "Fractional-Order Circuit Elements with Memory", *Proc. of the 13th International Carpathian Control Conference (ICCC)*, 2012, 28-31 May 2012, DOI: 10.1109/CarpathianCC.2012.6228706
- [3] Y.F. Pu, X. Yuan, and B. Yu "Analog Circuit Implementation of Fractional-Order Memristor: Arbitrary-Order Lattice Scaling Fracmemristor", *IEEE Transactions on Circuits and Systems I: Regular Papers*, 65, 9, 2018, pp: 2903-2916.
- [4] Y. Shang, H. Yu, and W. Fei, "Design and Analysis of CMOS based Terahertz Integrated Circuits by Causal Fractional-order RLGC Transmission Line Model", *IEEE JETCAS*, vol.3, no.3, pp: 355-366, September 2013.
- [5] C. Vastarouchas, C. Psychalinos, "Biomedical and Biological Applications of Fractional Order Circuits", *Proc. Of the Panhellenic Conference on Electronics and Telecommunications (PACET)* 2017, 17-18 Nov. 2017. DOI: 10.1109/PACET.2017.8259963.
- [6] Y. Shang, W. Fei, and H. Yu, "A fractional-order RLGC model for terahertz transmission line," *Proc. of the IEEE MTT-S International Microwave Symposium Digest (MTT)*, Jun. 2013, DOI: 10.1109/MWSYM.2013.6697392.
- [7] E. Fendzi-Donfack, J P Nguenang, L. Nana, "Fractional analysis for nonlinear electrical transmission line and nonlinear Schroedinger equations with incomplete sub-equation", *The European Physical Journal Plus*, 2018, 133: 32.
- [8] S. Cho, K. R. Kim, B.-G. Park, and I.M. Kang, "Non-quasi-static modeling of silicon nanowire metal-oxide-semiconductor field-effect transistor and its model verification up to 1 THz," *Jpn. J. Appl. Phys.*, vol.49, p. 110206, Nov. 2010.
- [9] M. J.Degerstrom, B.K. Gilbert, and E. S. Daniel, "Accurate resistance, inductance, capacitance, and conductance (RLGC) from uniform transmission line measurements" *IEEE Electrical Performance Electron. Packag.*, pp. 77-80, Oct. 2008.
- [10] D. M Pozar., *Microwave Engineering*. Hoboken, NJ :Wiley, 2012..
- [11] Y. Zhang and D. Xue, "Modeling and simulating transmission lines using fractional calculus", *Proc. of the Int. Conf. Wireless Commun., Network. Mobile Comput. (WiCOM)*, 21-25 Sep. 2007, pp. 3115-3118, DOI: 10.1109/WICOM.2007.773.
- [12] D. D. Pollock, *Physical Properties of Materials for Engineers*, 2nd ed. Boca Raton, FL: CRC Press, 1993, pp. 499-575.
- [13] J. Zhang, J. L. Drewniak, D. J. Pommerenke, M. Y. Koledintseva, R. E. DuBroff, W. Cheng, Z. Yang, Q. B. Chen, and A. Orlandi, "Causal RLGC(f) models for transmission lines from measured S-parameters," *IEEE Trans. Electromagn. Compatibil.*, vol. 52, no. 1, pp. 189-198, Feb. 2010.

#### BIOGRAPHIES



**OMER AYDIN** has received his B.Sc. and M.Sc. in Electronics Engineering from Istanbul Technical University in 1982, 1985, respectively. He has completed his PhD on 4G and 5G radio power frequency amplifiers in 2016 in Istanbul Technical University (ITU). He is now working as a leader of Defence Technologies R&D, Netas Telecom. He has more than 20 scientific papers on 5G communication systems. His research interests include 5G communication systems, theoretical and practical aspects of radio frequency power amplifier designs.



**BETUL SAMANCI** has received her B.Sc. and M.Sc. degrees in telecommunication engineering from Istanbul Technical University, in 2015 and 2018, respectively. She is currently pursuing a Ph.D. degree in Telecommunication Engineering. Since 2017, she is working at the department of research and development, in Netas Telecom. Her research interests are mainly electromagnetic theory and inverse problems.



**SERDAR OZOGUZ** has received his B.Sc. and M.Sc. in Electronics Engineering from Istanbul Technical University in 1991, 1993 and 2000 respectively. Since 2009, he is working as a full professor in Istanbul Technical University. He is currently a full professor in electronics, teaching graduate and undergraduate courses. He is also the co-author of 150 papers published in scientific reviews or conference proceedings.

His research interests include analog circuit design, chaotic circuits and chaos applications.

# Publication Ethics

The journal publishes original papers in the extensive field of Electrical-electronics and Computer engineering. To that end, it is essential that all who participate in producing the journal conduct themselves as authors, reviewers, editors, and publishers in accord with the highest level of professional ethics and standards. Plagiarism or self-plagiarism constitutes unethical scientific behavior and is never acceptable.

By submitting a manuscript to this journal, each author explicitly confirms that the manuscript meets the highest ethical standards for authors and coauthors

**The undersigned hereby assign(s) to *Balkan Journal of Electrical & Computer Engineering* (BAJECE) copyright ownership in the above Paper, effective if and when the Paper is accepted for publication by BAJECE and to the extent transferable under applicable national law. This assignment gives BAJECE the right to register copyright to the Paper in its name as claimant and to publish the Paper in any print or electronic medium.**

Authors, or their employers in the case of works made for hire, retain the following rights:

1. All proprietary rights other than copyright, including patent rights.
2. The right to make and distribute copies of the Paper for internal purposes.
3. The right to use the material for lecture or classroom purposes.
4. The right to prepare derivative publications based on the Paper, including books or book chapters, journal papers, and magazine articles, provided that publication of a derivative work occurs subsequent to the official date of publication by BAJECE.
5. The right to post an author-prepared version or an official version ( preferred version) of the published paper on an internal or external server controlled exclusively by the author/employer, provided that (a) such posting is noncommercial in nature and the paper is made available to users without charge; (b) a copyright notice and full citation appear with the paper, and (c) a link to BAJECE's official online version of the abstract is provided using the DOI (Document Object Identifier) link.



ISSN: 2147- 284X  
Year: July 2018  
Volume: 6  
Issue: 4

## CONTENTS

- A. Dumlu and M. R. Yıldırım**; Real-Time Implementation of Continuous Model Based Sliding Mode Control Technique for Trajectory Tracking Control of Mobile Robot. ....211-216
- A. Askarova, S. Bolegenova, V. Maximov, S.Bolegenova, Z. Gabitova, A. Yergaliyeva, A. Nugymanova, M. Beketayeva, Sh. Ospanova**; Application of Overfire Air Technology on an Example of a Steam Boiler PK-39 of the Aksu TPP (Kazakhstan), .....217-223
- B. B. Alagoz, H. Alisoy**; Estimation of Reduced Order Equivalent Circuit Model Parameters of Batteries from Noisy Current and Voltage Measurements, .....224-231
- A. Mukhamedgali and Z. B. Rakisheva**; Design and Simulation of Uniform Magnetic Field, .....232-236
- İ.Kıyak**; Harmonic Analysis of Electrospindle System with Wavelet Packet Transform, .....237-241
- G. B. Nurpeissova, D. V. Panyukova, and A. T. Nurpeissoy**; Smart Techniques' Implementation for Small Entities and Central Power Grid in Almaty, Kazakhstan: Challenges and Possibilities, .....242-246
- N. Onat**; Trends in Power System Protection Researches: A Review of Fundamental Relays, .....247-256
- N. S. Doszhan, G.E. Ibrayev and R.R. Pilpani**; Ultra-High Accurate Attitude Determination and Control of Microsatellite Formation Flight, .....257-261
- S. B. Efe, B. Kocaman and D. Demir Aktaş**; Implementation and Performance Analysis of a Switched Reluctance Motor Fed from Non-Energy Stored PV System, .....262-265
- O. Aydin, B. Samanci and S. Ozoguz**; Characterization and Measurement of Cable Losses Using Fractional-order Circuit Model, .....266-270

## BALKAN JOURNAL OF ELECTRICAL & COMPUTER ENGINEERING

(An International Peer Reviewed, Indexed and Open Access Journal)

**Contact**  
Batman University  
Department of Electrical-Electronics Engineering  
Bati Raman Campus Batman-Turkey

**Web:** <http://dergipark.gov.tr/bajece>  
<http://www.bajece.com>  
**e-mail:** [bajece@hotmail.com](mailto:bajece@hotmail.com)

